Fundamental and Engineering Application Studies of Pressure-Assisted Injection Forging of Thick-Walled Tubular Components

(Volume I)

Yanling Ma

Glasgow, October 2004

Fundamental and Engineering Application Studies of Pressure-Assisted Injection Forging of Thick-Walled Tubular Components

Yanling Ma

This thesis is submitted to the Department of

Design, Manufacture and Engineering Management,

University of Strathclyde,

for the degree of Doctor of Philosophy

Glasgow, October 2004

Dedication:

The author wishes to dedicate the thesis to her father, mother, her husband and son, for the love and support. Without their support and sacrifice, the thesis would not have been completed. The thesis is also dedicated to all members of the author's extended family for their continuous encouragement and tolerance throughout the whole period of the author's study in the UK.

Acknowledgements

The work exhibited herein was carried out in the Department of Design, Manufacture and Engineering Management, the University of Strathclyde, through a full-time study. Financial support provided by the EPSRC and the university is gratefully acknowledged.

The author is grateful to her supervisors, Dr. Y. Qin and Prof. R. Balendra, for their, untiring guidance, inspiring encouragement, invaluable suggestions throughout the research and writing of the thesis as well as meticulous checking of the manuscript.

The author also would like to express her sincere thanks to Dr. M. Rosochowska and Dr. A. Rosochowski for their advice and help during the author's study.

Last but none the least, the author's thanks go to all the laboratory staff for their skilful technique and constant support, throughout the fabrication of experimental device and conduction of experiments.

Abstract

Fundamental issues and engineering application aspects of Pressure-Assisted Injection Forging (PAIF) of thick-walled tubular components were studied experimentally and analytically. Achievements from this study met its pre-defined goals and are demonstrated with the following facts:

Pressurising materials were selected and qualified under six different loading conditions, based on which a simplified configuration for confined compression tests was proposed, and particularly, a unique biaxial testing machine was developed and used satisfactorily. The test data were subsequently used to establish constitutive descriptions of the materials and to facilitate the FE modelling to simulate the forming processes.

An upper bound analysis of Pressure-assisted injection forging of thick-walled tubular components with hollow flanges was conducted and formulated solution for the forming process was developed, by which the maximum forming-force for a given component geometry can be predicted with sufficient accuracy.

Failure modes and process range for pressure-assisted injection forging of thick-walled tubular components were studied experimentally and numerically, as a result, eight standard failure forms were categorized and three forming limit diagrams were established, which were validated experimentally and can be used as a guidance for the process design.

By combining above results achieved, an approach for synthesising concurrent design and manufacture of thick-walled tubular components with pressure-assisted injection forging was developed, in which technical details of the process and step by step procedure towards producing sound tubular components were provided. The development represents a significant progress towards engineering and industrial applications of the pressure-assisted injection forging (PAIF) technology.

Using the forming limit diagrams as a design guideline and following the approach for synthesising concurrent design and manufacture, an engineering component – hollow gear shaft was formed successfully.

List of the publications

The following publications were prepared based on, (fully or partially) the work presented in this thesis.

[1] Y. Ma, Y. Qin and R. Balendra, "Experimental and FE investigation of performance of polymers under confined compression conditions by using a simplified configuration", Advances in Manufacturing Technology, XVI, The 18th NCMR, 2002, pp. 203-208.
*** Based on the part of the contents of Chapter 3.

[2] Y. Qin, Y. Ma and R. Balendra, "Performance of pressurising-materials and process design considerations for the forming of thick-walled tubular components", Proc. of the 9th ISPE Conference on Concurrent Engineering (CE2002), July, Granfield, UK, pp. 251-262, 2002.
*** Based on the part of the contents of Chapter 3.

[3] Y. Ma, Y. Qin and R. Balendra, "Clamping design for the biaxial tension test of rubbers", Advances in Manufacturing Technology, XVII, The 1st ICMR and 19th NCMR, 2003, pp. 329-333.
*** Based on the part of the contents of Chapter 4.

[4] Y. Qin, Y. Ma and R. Balendra, "Pressurising materials and process design considerations of the Pressure-assisted Injection Forging of thick-walled tubular components", Journal of Materials Processing Technology, Vol. 150, No. 1-2, pp. 30-39, 2004.
*** Based on the part of the contents of Chapter 3.

[5] Y. Ma, Y. Qin and R. Balendra, "Process ranges of pressure-assisted injection forging of thick-walled tubular components", Advances in Manufacturing Technology, The 2nd ICMR and 20th NCMR, 2004, pp. 25-29.
*** Based on the part of the contents of Chapter 6.

[6] Y. Ma, Y. Qin and R. Balendra, "Concurrent design and manufacture in pressure-assisted injection forging of tubular components", Advances in Manufacturing Technology, The 2nd ICMR and 20th NCMR, 2004, pp. 139-144.

*** Based on the part of the contents of Chapter 3, 4 and 5.

[7] Y. Qin, Y. Ma and R. Balendra, "Mechanics of Pressure-assisted Injection Forging of tubular components", Proc. Instn Mech. Engrs. Vol. 218 Part C: J. Mechanical Engineering Science, 2004, pp. 1-18.

*** Based on the part of the contents of Chapter 3, 4 and 6.

[8] Y. Ma, Y. Qin and R. Balendra, "Upper Bound analysis of Pressure-assisted Injection Forging of Thick-Walled Tubular Components with Hollow Flanges", submitted.

*** Based on the part of the contents of Chapter 5.

Contents of Volume I

Contents of Volume II

Chapter 1

Introduction

In this chapter, following a brief review of the background of the research in **Section 1.1**, definition of the project, including objectives achieved, methodology used and programmes planned, is described in **Section 1.2**. Scope of the thesis and references used in this chapter are given in **Sections 1.3** and **1.4**, respectively.

1.1 Background

Developing manufacturing technologies, by which tubular components can be manufactured in a manner that they are light in weight and strong in structure, has been a target for the automotive and aerospace industries over the last century. As a result, manufacturing of tubular components has taken a firm root with manufacturing industries.

During the last few decades, a lot of work have been published, with regard to the development of process configurations, extension of process limitations and optimisation of process parameters etc. in metal forming, which contributed a lot to the development of manufacturing technologies. However, development of methods and technologies for manufacturing tubular components with high strength to weight ratios, and high cost-effectiveness is still insufficient. For example, to date, the manufacture of tubular components for the NASA space shuttle, which would require the highest degree of the perfection and reliability to withstand excessive forces, still involved multiple processes, such as bending, curving and forging of the tube separately first, then the complex shapes could only be achieved by the subsequent welding or other assembling processes. Obviously, such a manufacturing approach not only costs too much, but also takes longer time. On the other hand, these shapes and performance requirements of the parts reflect the demands on the effectiveness of the manufacturing and provide the new opportunities/directions to develop manufacturing processes to meet these challenges.

To-date, research and applications in the forming of tubular components have concentrated on the forming of thin-walled tubes. These components are usually unable to sustain heavy working-loads. Under such circumstances, industry still largely uses solid components, which are of low strength-to-weight-ratios. Thick-walled tubular components would be an ideal option to provide a balance between the strength and the weight of the component-structure. Manufacture of this type of components is currently effected largely by forging, cross rolling, rotary

swaging/radial forging or cold extrusion plus welding. These processes, however, either require complex machinery or increased numbers of operations. An alternative to the processes named above for manufacturing thick-walled, tubular components was, therefore, proposed and proven to be a more efficient means to produce this type of tubular components [1-3]. The process is so called Pressure-assisted Injection Forging (PAIF).

It is clear that PAIF is the latest development of injection forging with many new areas to be explored. Fundamental studies and engineering application aspects of pressure-assisted injection forging of thick-walled tubular components were, therefore, planned. As it will be introduced in the following **Chapters 3** to **7**, respectively, the studies include: (1) selection of pressurising materials (P-Ms) for PAIF; (2) qualification of mechanical properties of the selected P-Ms for PAIF; (3) development of analysis methods for PAIF; (4) definition of the failure modes and forming limit diagrams for PAIF and (5) forming of engineering components with PAIF.

1.2 Definition of the Project

1.2.1 Objectives

The overall objective of the proposed study is to establish systematic theory and technical details of Pressure-assisted Injection forging (PAIF) of thick-walled tubular components. Based on the analysis of insufficiencies of previous research and technology development of PAIF, the following measurable objectives have been defined for this project:

(1) Evaluation of aspects of the engineering of the PAIF with reference to pressurising materials (P-Ms).

(2) Qualification of mechanical properties of P-Ms, and development of new constitutive-descriptions of these materials.

(3) Development of new methods, including upper bound solution, FE and experimental procedures for the analysis of PAIF.

(4) Definition of the process ranges of PAIF as a function of forming sequences, P-Ms and work-materials (W-Ms).

(5) Testing methods and procedures to form an engineering component.

1.2.2 Methodology

By combining fundamental research in mechanical properties of pressurising materials (P-Ms), forming experiments with FE simulation, research was conducted to analyse the feasibility of P-Ms, define application-ranges of PAIF and develop an approach for synthesising concurrent "design and manufacturing" of engineering components.

Initially, a wider range of investigation on the polymers as possible P-Ms was carried out, which was followed by initial tests on the all possible P-Ms (available from the market) under different confined pressures, with a view to qualifying the feasibility of the materials as the P-Ms for PAIF. Subsequently, mechanical properties of the selected P-Ms were qualified with five types of the tests i.e., uniaxial tension, uniaxial compression, planar tension, planar compression and bi-axial tension tests. Based on the above tests, mechanical properties of the selected P-Ms were defined using the known constitutive models. The FE modelling was initiated based on the measured material-constants. The developed FE simulation models were further conditioned with forming experiments. In addition, an upper bound solution for PAIF was also developed with a view to delivering a quick tool for process analysis. By combining experiments, FE simulations and analytical calculations, with reference to the stability of tubular billet and initiation of forming defects, the process range was defined as a function of forming sequences, P-Ms and W-Ms. Based on these exercises, a general approach for design and manufacture was defined. Using this approach, tubular components with secondary elements - hollow-gear-shafts were formed.

1.2.3 Programmes

The PhD study was planned to cover the research in four major areas:

Qualification of pressurising materials

P-Ms were selected from all possible sources. These were subjected to initial tests under confined pressures to establish their feasibility as a P-M for PAIF, for which a simplified configuration for testing was developed. Three selected P-Ms were subjected to further tests to establish descriptions of their mechanical properties with reference to confined pressures.

Design, construction and trials of research equipment

In order to carry out the further qualification of mechanical properties of the selected P-Ms under biaxial tension conditions, a biaxial tension test machine was needed. The development included design review, patent search, concept development and detailed design. Test trials were carried out before the construction was finalised.

Development of analysis methods

FE Modelling and analytical procedures were defined for PAIF. Both numerical and analytical models were then verified experimentally. With respect to the forming of hollow flanges, the conditioned FE models were used for two groups of analyses: (a) to examine material deformation, strain and stress distributions for variations of die-cavity geometries, and (b) to compare different pressurising and injection schemes for each combination of the selected P-Ms and W-Ms. The analytical model -upper bound solution, was used to predict the maximum forming load and to analyse the process parameters for PAIF. Based on the analysis-results, a synthesis algorithm for deriving forming-sequences for complex component-forms was developed.

Forming experiments

Different lubrication schemes were studied with a view to establishing an "optimal" lubrication scheme for PAIF. With reference to the forming of hollow flanges, further experiments were conducted respectively for: (a) conditioning FE models, (b) examining effectiveness of P-Ms, (c) verifying the process-range defined, and (d) verifying the forming-sequences designed.

1.3 Scope of the Thesis

In this thesis, following the introduction to the PhD study in **Chapter 1**, literatures concerning the relevant work, with regard to the methods, components, formability and defects in the manufacture of tubular components are reviewed in **Chapter 2.** The selection of pressurising materials is described in **Chapter 3.** The experimental equipment, materials and techniques, with reference to the qualification of mechanical properties of the selected pressurising materials, are introduced in **Chapter 4.** Theoretical analysis methods developed for pressure-assisted injection forging are depicted in **Chapter 5.** Based on both, experimental and theoretical analysis results, failure modes and forming limit diagrams for pressure-assisted injection forging of thick-walled tubular components are defined and presented in **Chapter 6.** With the design and manufacture approaches developed in **Chapters 3, 5** and **6,** forming of a gear-shaft was presented in **Chapter 7.** Suggestions to the future work are given in **Chapter 8.**

1.4 References

[1] R. Balendra and Y. Qin, "Pressure-assisted Injection Forging of thick-walled tubes", Int. J. of Mach. Tools Manf., Vol. 35, No. 11, 1995, pp. 1481-1492.

[2] Y Qin and R. Balendra, "Technical evaluation of pressure-assisted injection forging of thick-walled tubes", Advan. In Manuf. Tech. IX, London, 1995, pp62-66.

[3] R. Balendra and Y. Qin, "Technical feasibility and processing limitations of pressure-assisted injection forging of thick-walled tubes", Proc. 5th ICTP, 1996, pp327-330.

Chapter 2

Literature Review

In this chapter, after identification of the demands on tubular components in **Section 2.1**, the development of both methods and technologies of manufacturing tubular components is concisely reviewed in **Section 2.2**. Injection forging process is described in **Section 2.3**, including the latest development of Injection Forging, i.e., Pressure-Assisted Injection Forging (PAIF), which is reviewed in detail with respect to the forming process classifications. Definitions of formability, component defect-forms and extension of process ranges of injection forging are addressed in **Section 2.4**. Following the discussion on the modelling of injection forging processes and testing pressurising materials in **Sections 2.5** and **2.6**, respectively, the main research issues identified during the literature review are summarised in **Section 2.7**. References are given in **Section 2.8**.

Nomenclature

d	diameter of billet
w	wallthickness of tube
t	thickness of flange or free-gap height of pdz
r	exit-radius of injection chamber
l	length of billet
p	punch pressure component
L	specific length of billet, l/d_o
D	specific flange diameter d_l/d_o
T	specific flange thickness or aspect ratio of pdz, t/d_o
R	specific exit-radius, r/d_o
P	total punch pressure
σ	stress/strength
ε	strain
μ	coefficient of friction

Subscripts

o	original/outer
l	current
i	injection
a	applied (at the punch/billet interface)
b	transmitted (at the injection-chamber/die-cavity interface)

2.1 Demands on Tubular Components

Tubular components are those products having a hollow section with or without secondary elements (flanges etc.). The use of this type of components can not only save the engineering materials, but also reduce the weight of the structures and/or, at the same time meet some specific requirements. It is well known that tubular components are among the variety of the products of manufacturing technologies, by which one or more than one raw material can be converted into products to serve and satisfy our society and people's increased demands. The start of such manufacturing technologies can be dated back to the 5000 to 4000 BC with the production of variety of articles made of either metallic or non-metallic materials [1-2]. The subsequent development of manufacturing technologies has historically influenced the civilization of every human society and improved people's daily life greatly. Their products have, therefore, been firmly bounded with us and widely used in many areas. As described by Kalpakjian "A ballpoint pen, for example, consists of about a dozen parts, a lawnmower about 300 parts, a grand piano12, 000 parts, a typical automobile 15,000 parts, a C-5A transport plane more than 4 million parts, and a Boeing 747-400 about 6 million parts." [1]. Tubular components as one family of the many products of these manufacturing technologies are, of course, not exceptional. Tubular components had been manufactured 200 years ago by the basic extrusion process. The first hydraulic press was used to produce lead pipes to meet people's requirement at that time [2]. Nowadays, tubular components are used in almost everywhere, from house hold utilities (such as central heating pipes, wire covers and daylight lamp tubes) to industrial applications (such as tubular drive shafts, tubular steering columns and tubular stabilizer bars manufactured by cold extrusion, radial forging or swaging) for vehicles etc. [3-5]. In addition, many hydroformed tubular components, as those shown in Figs. 2.1 to 2.3 [6-14], are also successfully used by industries.

Automotive and aerospace industries are, however, still under pressures to produce environmentally friendly cars and airplanes. It means that these vehicles should be

lighter in weight and less in consumption of fuels, as a result, to reduced the pollution to the environment. To achieve such a goal, more tubular components, which are of high strength to weight ratios, have to be manufactured to replace the still largely used solid components, which are of low strength to weight ratios.

Since capability of manufacturing tubular components is largely prescribed by the levels of the development of the technologies, it is of great interest, for the defined research, to carefully examine what have been achieved in this field during the last decades.

2.2 Methods and Technologies for Manufacturing Tubular Components

In order to carry out a wider range of investigation on the development of the technologies for manufacturing tubular components, a classification of the tubular components is required.

2.2.1 Classification of tubular components

Tubular components can be classified using several different criteria, such as by component feature (seamless or seamed), by its use (for structural materials or for transportation of radio signals) and by its special quality (precision forged or not) etc. [15]. According to their geometric axis, tubular components also can be classified into two types of the tubular components with straight axes and the tubular components with bent axes [9]. Based on the different materials used, the tubular components can also be divided into metallic and non-metallic tubular components, etc.

In this thesis, attention is paid to the tubular components made of metallic materials by means of tube forming. Further to the several classifications made by Dohmann

and Avitzur [9, 15] for tubular components, a systematic classification of the tubular components has been developed, which is presented in Fig 2.4. This classification takes into account the dimensions of the tubular components (i.e., from thin-walled to thick-walled), shapes of the tubular components (i.e., from the simplest form, a plain tube, to the complex form, the tube with hollow flange), as well as suitable forming methods (i.e., from the ancient tube extrusion to the newest PAIF).

2.2.2 Methods and technologies for manufacture of tubular components

As shown in Figure 2.4, the methods and technologies of manufacturing (forming in particular herein) tubular components are well related to their dimensions and shapes. For example, for a thin-walled T tube, shown as component-form (1), it can be manufactured by either tube hydroforming [8-10] or tube rubber-forming [16-19]. The component-form (2) is a thin-walled tube with bent axis (sub-frame for Ford Mondeo), which is preferably manufactured by tube hydroforming [8-9, 12, 14]. The component-form (3) is a thick-walled bend, which can be formed by three tube bending methods (stretching bending, draw bending and compression bending). The component-form (4) is a thick-walled plain tube, which can be produced by more than three tube forming methods (rotary tube-piercing, tube extrusion and tube drawing/sinking). The component-form (5) is a thick-walled tube with locally wall-thicken profile, which can be manufactured by tube spinning. The component-form (6) is a thick-walled tube with local or end portion reductions in diameters of the tube, which can be formed by tube swaging or tube rotary swaging. The component-form (7) is a thick-walled tube with both inward and outward solid flanges, which can be produced by two different methods (injection forging with the support of mandrel and combined radial with axial forging. The component-form (8) is a thick-walled tube with hollow flange which may only be manufactured by pressure-assisted injection forging (PAIF). All of these tube forming methods and technologies are described in the following, **Sections 2.2.2.1** to **2.2.2.8**, respectively.

2.2.2.1 Tube hydroforming

Tube hydroforming is one of the relatively new metal-forming processes. "About 30 years ago, the first hydroformed parts, fabricated by expanding a straight or pre-bent tube, were manifold elements and components of similar geometry for sanitary use." [9, 20]. Nowadays, it is gradually gaining more importance as its potentials and benefits are being realised by industries [8-14, 21]. In tube hydroforming, the tubular billet or pre-bent tubular billet is placed between the desired top, bottom and movable side forming dies first. Then one end of the tube is sealed by a punch and the other end may be connected to a hydraulic horizontal cylinder. When the cylinder pumps the liquid into the tubular billet, it is pressurised. As a result, the tubular billet deforms gradually and locally within the expected zones, as the movable die over the selected zone is moved away radially from the original shape of tubular billet. During such a tube hydroforming process, no axial compressive force is applied to feed in the tubular billets into the deformation zone and the tubular billets are mainly subjected to a radial internal pressure applied by the pumped liquid. Hence, the forming of tubular billets is mainly accompanied by thinning the thickness of the tubular billet radially and locally. Fig. 2.5 illustrates such a similar process in which a side movable die is not involved [12].

Although such a tube hydroforming process offers several advantages as compared with the conventional manufacturing via stamping and welding [8, 22-25], it also has some drawbacks, such as low cycle time, very expensive equipment and high skill requirement to the operators [8]. It is also only suitable for the manufacturing of the thin-walled tubular components, with a specific wall thickness of $w/d_o<0.13$ [8-10, 26].

2.2.2.2 Tube rubber forming

As Thiruvarudchelvan pointed out [18], "Rubber-forming had its beginnings in the latter part of the 19^{th} century. Rubber was used over metal dies to eliminate scratching of the sheet-metal surfaces during blanking or forming. In the early part of

the 20th century, rubber pads were used to bulge metal barrels. By 1925 many possibilities of rubber forming such as shearing, forming, bulging and embossing, had been explored" [18]. In the second quarter of the 20th century, several rubber-forming processes were used industrially. One of these processes is the Guerin process [27-28], which was used during the Second World War (1939-1945) for the forming of aircraft panels. The development of the polymer-industry since the 1960s [29-30] has promoted the research and development work of the techniques of rubber forming (flexible-tool-forming) worldwide over the last four decades [18]. The process of rubber-forming tubular components is, in principle, similar to the tube hydroforming, except that the radial forming load is applied by the internally filled and compressed rubber, rather than by liquid. Since the drawback of the leakage accompanied with tube hydroforming can be avoided in rubber-forming, the tooling and equipment used for rubber tube forming cost less than those for hydroforming. However, tubular components that can be formed by rubber forming technique is even thinner (with a specific wall thickness of $w/d_o \leq 0.083$) than those (with a specific wall thickness of $w/d_o < 0.13$) by the tube hydroforming [16-19, 26, 31].

2.2.2.3 Tube bending

There are three tube bending methods, i.e., stretch bending, draw bending and compression bending as shown in Fig. 2.6 [1-2], that can be used to produce component-form (3) in Fig 2.4 and the similar components. In stretch bending, the form block (die) is fixed and two chucks are used to apply the forming load to bend the tube into the desired shape. In draw bending, the form block is rotational. A pressure bar and a clamp are used to effect the bending process. In compression bending, the form block similar to that used in stretch bending is fixed. A wiper shoe and a block are used to carry out the work. Although these three tube bending processes are somewhat different from each other and the tooling is specialised individually, they are characterised by two common features. One is that the tubular billets for all three tube bending processes have to be prepared in a same manner prior to the bending processes. Another is that the components produced after the bending processes have the same diameters as originally. In other words, all the

tubular billets prepared to be bent are equally and internally packed with some loose materials or flexible mandrels to prevent the collapse and buckling of the tubes inwardly during the bending processes. All the tubular components produced after these tube bending processes have only changed the geometrical axis shapes from straight lines into curved ones. But it doesn't alter the outside diameters of the tubular billets after bending processes, due to the constant tooling conditions. Therefore, the methods of tube bending might be only used in the circumstance, where the geometric shape of tubular billets need to be altered but without the change of their outside diameters.

2.2.2.4 Tube rotary-piercing, extrusion and drawing/sinking

In order to produce thick-walled tubular components similar to the component-form (4) as shown in Fig 2.4, three forming technologies, rotary-tube-piercing, tube extrusion and tube drawing/sinking, as shown in Fig. 2.7 (a), (b) and (c), respectively [1-2], may be used. The forebears of these tube-forming technologies plus the tube bending, spinning and swaging technologies can be traced back to the Neolithic, in Mesopotamia and other areas around the Mediterranean. When gold was found by early man, it was in relatively pure form in nature and could be hammered into shape [2], which evoked the subsequent evolution and development of metal forming technologies throughout human history. "The rotary-tube-piercing process (the Mannesmann process, developed in 1880s) is carried out by an arrangement of rotating rolls [1]", as shown in Fig. 2.7 (a), where two rolls and a mandrel are used. This process is based on the principle that when the solid rod is subjected to cycling compressive stresses, a cavity begins to form at the centre of the rod. It is a hot-working process starting from a solid billet and it is suitable for producing long, thick-walled, plain and seamless tubes. "Extrusion as an industrial process was invented around 1800 in England during the Industrial Revolution when that country was leading the world in technological innovations. The invention consisted of the first hydraulic press for extruding lead pipes." [2]. In tube extrusion process, a container and a ram with a mandrel (for direct extrusion) or with a punch/die (for indirect extrusion) of a tube are normally used Fig. 2.7 (b). Indirect extrusion is also

called backward extrusion or reverse extrusion. According to different working temperature of the work-piece, tube extrusion can also be divided into hot, warm and cold extrusion. When cold extrusion is conducted at a high speed, the process is also called impact extrusion. Extrusion process can start either from a tubular billet or a solid billet, and can be used to produce not only the circular tubes, but also the other components with hollow or semi-hollow cross sections, as well as the solid cross sections. The PhD study is mainly focussed on the extrusion of the circular tubes. In tube drawing process Fig. 2.7 (c), a die and a mandrel are involved. When the tube drawing, sometimes, is conducted without the use of a mandrel, the process is also called tube sinking. This process begins from a tubular billet produced originally by some other processes, such as tube extrusion and rotary-tube-piercing, and can be used to reduce the diameters or wall thicknesses of the seamless and plain tubes.

2.2.2.5 Tube spinning

The manufacture of thick-walled tubular components with locally wall-thicken profiles, similar to the component-form (5) as shown in Figure 2.4, is related to the use of tube spinning. Similar to tube drawing, tube spinning process starts with a tubular billet produced by either tube extrusion or rotary-tube-piercing. In tube spinning, a roller tool and a mandrel (to support the inside wall of the tube for external spinning) or a die (to surround the tube for internal spinning) are used (Fig. 2.7 (d)). This process can be used to reduce the wall thickness and increase the length of a tube by means of the roller tool applied to the work-piece over the cylindrical mandrel or die. Unlike injection forging with the support of mandrel, both inward and outward local wall thicken profiles can not be formed simultaneously in a single tube spinning process. In other words, the products produced by the tube spinning can only have either an inward wall thicken profile (by internal spinning) or an outward wall thicken profile (by external spinning) after a single spinning process.

2.2.2.6 Tube swaging/rotary swaging

Tubular components similar to the component-form (6), as shown in Fig. 2.4, normally have local or end portion reduction in diameters of the tube and can be manufactured by tube swaging [1-3]. Tube swaging is also known as tube rotary swaging, as shown in Fig. 2.7 (e). In this process, a mandrel and a set of rollers as the rotational forming tools caged are usually used. When the rotation of the rollers (dies) is instead with the rotation of work-piece to feed it into the hammering dies, this process is also called rotary forging or rotary forming [2-5]. Similar to tube drawing and spinning, it starts with a tubular billet and can be used to reduce the diameter of a tube locally or at the end of the tube to create a tapered section. By taking advantage of the specially shaped mandrels, such as longitudinal or spiral grooves on them, both internally and externally shaped tubes can be swaged. In addition, without using the internal mandrel, this process also can be used to reduce the diameter of a solid stock. The process for swaging tubular billet is, however, usually limited to the manufacturing of the tubular components whose diameter is less than 50mm and whose length is smaller than that of the mandrels used in the process. Although the products produced by swaging have improved mechanical properties and good dimensional accuracy, the tooling and machinery used in this process are quite complex and expensive.

2.2.2.7 Injection forging with the support of mandrel and combined radial with axial forging

The thick-walled tubular components with solid flanges (inward, outward or both) ,similar to the component-form (7) in Fig 2.4, may be formed with two different methods starting with tubular billets. One is the process which combines radial forging with axial forging [5], whose tooling and machinery costs are very high. Another is the radial extrusion process plus an inner support provided by a mandrel to prevent the tubular billet from collapse [32-34]. Although the latter is cheaper than the former, neither of the two tube forming technologies can be used to produce the

thick-walled tubular components with hollow flanges, similar to the component-form (8) as shown in Fig 2.4.

2.2.2.8 Injection forging with the support of the pressurising material (PAIF)

Considering the deficiencies with the above methods and technologies of manufacturing tubular components, many efforts were devoted to the development of new methods and technologies to manufacture the tubular components, similar to the component-form (8) in Fig. 2.4. Early attempts showed that injection forging with the support of a pressurising medium may be a solution for producing thick-walled tubular components efficiently [35-37]. It is, therefore, necessary to review the research and engineering applications of the injection forging of engineering components.

2.3 Injection Forging Process Configurations and Applications

Although earlier interests in injection forging were generated in the early 1960s [38-40], as a new configuration was proposed to achieve a nett-shape definition for complex component-forms, further development of this concept was somewhat restrained until the 1970's [41-43]. Such a delay was caused by the insufficient development of tool-materials (particularly cold-forged steels), work-materials, lubrication procedures and tool construction techniques. The significant progresses in this technology were only made during the 1980's when some complex component-forms, such as cruciforms for universal joints [44-45] were produced successfully with this processing option. Although forming of these component-forms has since breached the conventional formability limits and extended the ranges of nett-shape manufacture, to date, injection forging of tubular components is still a relatively new process [46-47]. There are several names, such as injection forming, injection upsetting, radial extrusion, side extrusion, transverse extrusion and lateral extrusion

used to describe the similar process configurations [48-52]. The name of injection forging is used throughout this thesis.

2.3.1 Definition of injection forging

Injection forging is a process being recognised as an efficient method to produce engineering components with low cost in machinery and tooling, high quality in component-performance and dimensional accuracy among the other metal forming technologies [41]. Injection forging is, usually, defined as a nett-shape or near nett-shape manufacturing process, in which work-material is contained in an injection chamber and injected into a die-cavity to form a desired engineering component-form. A simplified process model of injection forging is shown in Fig. 2.8. The work-material-flow in this process is characterised by the simultaneous movement of work-material along both radial and axial directions to fill the die-cavity which is largely prescribed by the exit-geometry [53-54]. When injection forging is conducted without the use of the flange-ring-die, refer to Fig. 2.8, it is, alternatively, called injection upsetting. When injection forging is combined with other metal forming processes, such as backward or forward can extrusion, it is also called combined can with radial extrusion, and so on [55].

2.3.2 Configurations of injection forgoing

As mentioned previously in **Section 2.3**, injection forging has been developed significantly over the last three decades. Ultimate goal is to achieve the nett-shape or near-nett-shape components without the post-processing. For example, in addition to the development of cold and warm forging technologies with this objective in mind [56-63], configurations of injection forging processes have been developed gradually from the injection of solid billets to the injection of tubular billets [32-41]. Three popularly used configurations of injection forging are shown in Fig. 2.9, which respectively uses a solid billet, a tubular billet with a mandrel and a tubular billet with a pressurising medium [64].

2.3.2.1 Injection of solid billets

Early development of injection forging was mainly in the forming of solid components. In 1963, Cogan [38] attempted to produce solid flanges from solid billets by injection forging. For the similar configuration, other attempts, such as those reported by Pugh in 1964 [65], Alexander in 1965 [39], and Parsons in 1973 [66], were conducted by applying an active counter-pressure, which was being achieved using fluids and matrix materials, with a view to preventing the initiation of fractures on the front edge of the flanges. The fundamentals of these developed configurations were based on the assumption that the superimposed hydrostatic pressure would extend the threshold of formability of the flanges. As a result, a multi-axial extrusion configuration of a solid billet was attempted in 1974, in which the billet contained in a closed die was extruded along several axes to produce solid or hollow branched components in a single operation [67]. Following this process configuration, the L, T and X-shape component-forms were cold-extruded from cylindrical aluminum billets on a special testing machine [64].

With reference to die-structure-forms and component-forms produced, injection forging of solid billets was further divided into four groups [44], i.e., solid radial extrusion, tubular radial extrusion, radial can extrusion and radial extrusion of a flange, as shown in Fig. 2.10. With reference to tool-kinematics, another classification was made by Aliev [50], shown in Fig. 2.11, from which, deformation mechanisms and forming forces associated with different configurations were initially compared. A more detailed classification of injection forging solid billets was conducted with respect to the direction of work-material-flow relative to tool-movement, loading arrangement and the type of products produced [68] and it was suggested that radial extrusion can be applied to open-die, semi-open-die and closed-die extrusions.

2.3.2.2 Injection of tubular billets with mandrels

Although engineering components are usually manufactured from solid billets, because of the well developed processing technologies, many engineering products

may also be produced from tubular raw material to meet all the performance requirements in such a manner that the specific energy consumption is reduced and the work-material utilization efficiency is improved. With this intention, research in the injection forging of tubular billets was initiated in 1977 [43] with a view to investigating the failure-forms and energy requirements. In this investigation, a solid-mandrel was used (similar to Fig 2.9 (b)), by which either the entire length or the length contained by the injection chamber of the tubular billet could be supported to either prevent the inward flow or allow the inward flow of the work-material respectively during the process.

Another effort was made to classify the failure-forms and define the process-ranges for similar process configurations [32-33, 43, 51, 69], with reference to the number of injection punches used, constraints to the tubular billets and flow-directions of the work-materials [32, 69]. Fig. 2.12 shows such a classification [32] by which the forming of solid annular flanges from tubular billets was addressed. In this classification, the terms of "one end constraint" and "both end constraint" were used. The former is for the free-ended injection and the latter is for end-constrained or double-ended injection forging. The mandrel-forms of both a plain rod and a rod with locally reduced diameter were also used as a criterion to allow the sub-division of the process into the outward-flow-forming, inward-flow-forming and free-flow forming (Fig. 2.12).

In the later 1980's, injection forging of tubular billets was progressed to produce solid-flanged-tubular-components with axially varied geometries, as shown in Fig. 2.13. In this process configuration, the combination of the radial extrusion and the axial extrusion of the tubular billets was conducted simultaneously. The results obtained demonstrated the feasibility of using a single-stage injection forging to replace a multi-stage forming of a similar engineering component [47]. The ratio of work-material-flow in the radial direction and that in axial direction at any stage of the forming was controlled by the die-cavity geometry and friction conditions between the work-material and the die-surfaces.

In 1993, another effort was made to combine the radial extrusion with inside ironing process with a view to preventing the non-uniform diameters of the tubular components [70]. In this process, radial-extrusion was conducted at a point along the length of a tubular billet, while a punch was used to iron the billet, by which the forming of components from thin-walled tubes was addressed. Using this configuration in the forming of thick-walled tubes may prove to be more difficult due to the unacceptable high pressure produced at work-material and die-surfaces.

2.3.2.3 Injection of tubular billets with a pressurising medium

Although some of the engineering components (thin-walled) might have been successfully injection forged from the thin walled tubular billets with the support of a pressurising medium, injection forging of thick-walled tubular billets into the thick-walled engineering components with the support of a pressurising medium, to date, was not well explored. More attention will, therefore, be paid to the injection of thick-walled tubular billets with the support of a pressurising medium, in the following **Section 2.3.2.3.1**.

2.3.2.3.1 Configuration and development of injection of thick-walled tubular billets with the support of a pressurising medium

Injection forging of thick-walled tubular billets, with the support of a pressurising medium is the latest development of the technologies. It is developed with a view to producing the tubular components similar to the component-form (8) (Fig. 2.4) and (Fig. 2.9 (c)). In this process, pressurising medium is inserted into the tubular billet and the compound billet is then contained in the injection chamber before being injected into the die-cavity. The injection chamber provides additional stability to the compound billet and larger amount of both work-material and pressurising-material can, therefore, be injected into the die-cavity by the forces applied by both injection and pressurising punches. Hence, thick-walled tubular components with hollow flanges can be produced. The principle of using the pressurising medium can be

traced back to the early of 1960s, when metal-forming had been conducted with the assistance of fluids [71] and elastomers (polyurethane) [72]. More recent progresses in this process have been made since 1985 when more complex tubular components, like tee-forms, have been formed by elastomers [16-19] (Fig. 2.14 (b)). In this process, the T-piece was formed using a number of urethane plugs [16, 18], a stepped punch as well as a tubular billet, which was pre-chamfered at each of the two ends of the billet and following a designed forming sequence of the operation. These configurations may be regarded as injection forging, since the process configuration was characterised by the simultaneous injection of the tubular billet and radial bulging of the tubular billet to form hollow flanges [18]. These successful examples have encouraged the research in the field of metal forming technologies to introduce the pressurising media into injection forging to form thick-walled and hollow flanged tubular components, which used to be considered being unachievable, with the conventional metal forming technologies. In the latest process configuration, two concentric punches may be required and independently controlled in order to apply much higher pressures to both work-and pressurising-materials [35-37].

2.3.2.3.2 Forming processes and classifications

As mentioned in **Section 2.2.2.8**, pressure assisted injection forging (PAIF) was proven to be a feasible solution for producing thick-walled tubular components with hollow flanges. Such component-forms can not only overcome the drawbacks with either thin-walled tubes, which are unable to sustain heavy working load or solid components, which are sometimes material-wasteful, but also provide a balance between the strength and the weight of the components. This process configuration, however, may involve different forming sequences and parameters to those which are used in the forming of thin-walled tubes, since bulk flow of the work-material is inevitable in the forming of thick-walled tubes. The success of this process would, therefore, largely depend on the understanding of the technical details, such as forming process classifications, formability, and component defect-forms of the process, etc. Efforts were, therefore, devoted to address these issues subsequently.

Actually, there are many metal forming processes, such as rolling, bending and so on, for which many classifications were proposed, such as those proposed by Lange, Kalpakjian and Mikell [1-2, 73], respectively. For example, using the predominant stresses of forming processes as the criterion, Lange classified metal forming processes into five groups, i.e., compressive forming, tensile forming, combined tensile and compressive forming, forming by bending and forming by shearing [73]. Other efforts were also devoted to further classify forming processes for more specific metal forming fields, such as radial extrusion and injection forging. For instance, with reference to the number of the punches, movement of the dies and mandrel-forms, radial extrusion was further classified into radial extrusion, radial extrusion combined with die movement and upsetting [32]. According to billet forms, configurations of injection forging were also further divided into injection forging of solid billets and tubular billets, respectively [74-75]. However, no literature has been found with the attempt to address the process classification of pressure-assisted injection forging (PAIF).

According to different pressurising media used, processes of pressure-assisted injection forging of engineering tubular components may be further classified into tube injection-hydroforming [8-10, 21, 76], tube injection-rubber forming [16-19, 28, 31, 77] and tube pressure-assisted injection forging [35-36]. In tube injection-hydroforming, a liquid pressurising medium is used, which is similar to that used in the tube hydroforming. In the tube injection-rubber forming, a rubber medium, which is similar to the one used in the tube rubber forming, is used. In pressure-assisted injection forging, a polymer medium is preferred. With reference to the different thicknesses of tubular components produced, the processes of pressure-assisted injection forging may also be classified into two groups. One is the pressure-assisted injection forging of thin-walled tubes with the specific wall thicknesses of $w/d_o \leq 0.13$ [16-19, 26, 31]. In this group, the processes of tube injection-hydroforming and tube injection-rubber forming are included.

In the tube injection-hydroforming, tube injection-rubber forming and pressure-

assisted injection forging (PAIF), the work-material flows are characterized by the simultaneous axial injection and radial expansion. Therefore, tube hydroforming may be further classified into tube hydroforming and tube injection-hydroforming. Similarly, tube rubber forming may also be further divided into tube rubber forming and tube injection-rubber forming. The later (both tube injection-hydroforming and tube injection-rubber forming) from both further classifications is treated as the pressure-assisted injection forging, in this thesis.

2.3.2.4 Classification of injection forged component-forms

Injection forging, may be used to manufacture various engineering components in a manner, by which the components produced are of high quality, low cost and complex forms, such as components with symmetric or asymmetric flanges, branches and other secondary elements. Owing to its feasibility to achieve nett-shape or near-nett-shape definition of component-forms [62], it was reported that when a four-pronged cruciform (also called universal joint) was produced by injection forging, the manufacturing cost was two-thirds of the cost by conventional hot-forging [78], mainly due to the reduction of work-material consumption - from 133g to 53g (component-weight reduced by 40%) and the elimination of the post-forming machining requirements. In addition, the combination of injection forging with other forming processes also enables the forming of complex component-forms in a single operation [44, 50, 78-80], rather than multi-stage operations with conventional cold forging to achieve similar component-forms.

2.3.2.4.1 Component-forms with the configuration of injection forging of solid billets

The main component-forms produced by this configuration are the backward-/forward-can-shaped and multi-branched components when this process configuration was combined with other metal forming-processes, such as backward can extrusion, forward can extrusion as well as radial can or rod extrusion [51, 55-56, 79, 81]. Also, when injection upsetting combined with subsequent forward can

extrusion [71, 73-74, 82] and solid back extrusion, a multi-branched and flanged component can also be produced [83]. The sound results from these combinations showed the feasibility of producing complex component-forms and enabled the reduction of intermediate forming operations, the number of tools and, hence, the reduced cost of manufacturing these components.

2.3.2.4.2 Component-forms with the configuration of injection forging of tubular billets with the support of a mandrel

Regarding to this process configuration, the main component-forms produced are the tubular components with solid flanges in a manner of improved work-material utilization and component performance [32-33, 43]. By using different types of mandrels, the flange can be formed inwardly, outwardly and both. According to different die-arrangements, the flange can also be formed at one of the two ends of the tubular billet or away from the end of the tubular billet [32-33, 43, 46, 51, and 84].

2.3.2.4.3 Component-forms with the configuration of pressure-assisted injection forging

Using the configuration of injection forging of thick-walled tubular billets with the support and pressure transmission of the pressurising media, the main component-forms are similar to the component- form (8), as shown in Fig. 2.4 and 2.9 (c) [35-37, 74, 82].

Classification of such a variety of engineering components produced/achievable by injection forging was promoted by two facts: one was the deficiencies with the previous classifications of the component-forms produced by cold forging; another was the dramatic achievements with the injection forging technology its self. For example, Lange [73] classified the cold-forged and only axis-symmetric components without addressing the components produced by injection forging. Later, some components, which were considered to be difficult or impossible to produce by

conventional cold forging, were also grouped by Keller [83]. However, with the development of injection forging technologies, some of them, such as spiders for universal joints [62, 78], bodies for diesel injectors [59], pipe flanges [47], solid flanges with square cross-sections [85], alternator pole parts with claws [80] and staggered branches [86], have already been formed by injection forging or its combination with other metal forming processes. In addition, extruded helical gears without shafts were also reported by King [87]. Some components formed by the Manufacturing Engineering Research Group at the University of Strathclyde, are shown in Fig. 2.15. Among these, forming of hollow-gear-shafts is a latest effort to produce engineering components. With the consideration of all possible variables, such as billet-geometry, tool-constraint, tool-kinematics, and the combination of injection forging with other forming processes, a new and more systematic classification of component-forms, which are formable by injection forging, was proposed, as shown in Fig. 2.16 [74].

2.4 Definition of Formability and Component Defects

There are many metal forming processes [1-2, 73] by which raw work-materials can be converted into various engineering component-forms. The capability of these forming processes is largely prescribed by the factors, such as process configurations, forming tool geometries and work-material properties. Several terms, such as "ductility", "formability" and "workability" are associated with the definition of the capacity of the forming processes [88].

"* *Ductility* is the ability of work material to deform plastically without fracture in a standard test, which is usually expressed by some measure of limiting strain.

* *Formability* is the ability of a material to deform plastically without the occurrence of a defect in a forming process.

* *Workability* is also the ability of a material to deform plasticity without the occurrence of any defect in a bulk forming process."

It is clear that the above three definitions were originally different from each other. For example, the term of "formability" was mainly used for the sheet metal forming [88-89], where localised thinning and wrinkling of the work-material are two major defect-forms, and which were used to define the ability for sheet metal forming. The term of "workability" was largely used for bulk metal forming processes [89]. Although several other similar definitions were discussed by Hosford and Dieter [90-91], the term of "formability" is currently widely used to all forms of work-materials in metal forming analysis.

The formability of a metal forming process is prescribed by the initiation of forming defects, which are invariably influenced by several factors, such as work-material properties, process conditions and process configurations. Regarding the work-material only, the formability usually refers to the initiation of ductile fracture of the work material in bulk forming, which can be determined by the formability test-methods [15, 73, 90-91]. A defect within a component may be further defined as that, due to which, the properties of a component do not conform to the design specifications and makes it less suitable or unsuitable for the purpose for which it was designed [77]. In metal forming, a variety of defect-forms may be developed. In order to classify such defect-forms and define formability, several attempts were made with such objectives in mind. Devedzic, in 1986 [92] proposed some formability limit criteria in which possible defect-forms were classified into seven types as shown in Fig. 2.17. This classification, however, only referred to general defect-forms and did not consider the influences of different characteristics of forming process operations. In order to establish further sub-classifications, which are able to address the differences between forming processes, as was attempted for the forming process classifications [73], classifications of the defects in cold and warm forged components were attempted [88, 93]. In these classifications, the work-material fractures of both internal and external ductile cracks of the components,

surface imperfections (like surface roughening, scratching and laminations), flow imperfections (like dimensional errors, folding, under-filling, non-concentricity, fins, flashes and buckling), and other undesirable changes in physical properties of the work-material were considered. These may be the general inclusions of the defects which may occur in cold and warm forging. In addition, two more detailed classifications were also reported by Kudo and Arentoft [94-95] with reference to either a particular defect-form (similar to the classification of fractures with reference to cold forging [95]), or a particular process (similar to the classification of die-filling flaws with reference to closed-die forging of H-shape profiles [95]).

Definition of a "defect" in a component/workpiece may vary with different processes. Even if within one process, it may also vary with different machine-tools, work-materials and other auxiliary media used. An accurate definition of defects is, therefore, required with reference to either different forming processes or different manufacturing requirements. For example, the term of "accuracy" of a component usually has relative meaning for different processes. A given form-error may be treated as a defect in a nett-shape manufacturing process, but it may not be a defect as for other forming processes.

In one word, many factors could determine the initiation of the defects in a component during a forming process. A forming process may, therefore, be considered as operations conducted in a system, in which the operations are conducted under designed working conditions (such as friction and temperature) [64, 96-98] and for achieving the designed manufacturing requirements. Defects may be initiated due to any undesirable factors in the system, such as equipment, materials and process conditions. The correctness of a procedure, including the preparation of billet and the design of forming sequences for performing an operation, is also another key factor. All the factors, which may influence the formability of the component formed, may be classified as following five groups:

Equipment

Machine and tools: Both static and dynamic behaviors of the machine used would influence the behavior of tooling and consequently the component-quality [98], such as the concentricity of component and dimensional errors. The performance of the tools would directly influence the forming capability of a process and component-quality, in particular, the die-cavity-geometry [53-54], tool material property, tool-surface-quality like coating and wear. With a wider perspective, the formability of a component should also refer to the state of a tool, specifically, any defects, like fracture of the die, because the defects in the forming tool will definitely result in the failure of a forming process and a component-defect [88].

Work-materials

It is clear that, except for billet geometry (including preformed), work material properties, such as its metallurgical property (composition), mechanical and physical properties always have significant influences on the initiation of defects [42]. For instance, when a work material possesses a better ductility, the onset of a defect would be delayed or avoided and the work material would present a better formability during a forming operation than that for a work material possessing a worse ductility [42].

Process conditions

Friction, temperature and velocity: Friction always influences material flow and tool deflections. Some times it facilitates a metal forming operation and the component-quality, such as using friction to improve the stability of the work-piece during upsetting or injection upsetting [96-97]. Some times, it, reversely, undermines a forming process' efficiency, such as extra applied force is required to overcome the friction losses and more commonly the damage of the work-piece surface due to friction [64, 96]. Temperature also influences material deformation and tool deflections in such a manner that when a proper temperature range is set, mechanical properties of the work material will be improved and component form-errors will be reduced [97]. The deformation of a rate-dependent material would also be

significantly influenced by the velocity of the loading on the work material [99].

Process operations

Preparation of the billets and forming procedure: one of the process operations is to prepare the billets including design, manufacture, billet lubrication and relative location of the billets [40]. Another one is the design of the forming procedures in which forming sequences of the work material, number of forming stages and the nature of each of the stages [35, 82, 98], e.g., the loading and unloading which may be involved in each stage of the forming operation. Any incorrect step would result in the initiation of the component-defects [35, 82 and 98].

Pressurising-materials

Liquid, rubber or polymers: Factors mentioned above which could influence the onset of component-defects, may be applicable to any metal forming operations. Factors of this group of influencing the onset of component-defects herein may only be applicable for the pressurising-medium-assisted forming processes, such as tube injection-hydroforming, tube injection-rubber forming and pressure-assisted injection forging (PAIF). The proper timing and amplitude of the pressurisations in pressurising-medium-assisted forming would result in the defect free components. For the processes of using rubbers or polymers as the pressurising media, their mechanical properties also have a direct influence on the initiation of component-defects. For example, when the pressurising material could perform effectively beyond certain levels of the radial strains [35-37, 75] (refer to Fig. 2.9 (c)), the corresponding hollow flanged components would be formed without defects. Otherwise, diameter of the hollow flange must be restricted or the result in of the defects within the components [75].

Obviously, information on the formability is essential to the design of any metal forming processes. In this thesis, much attention was paid to injection forging, for which past work on the definition of the formability, component failure forms and

process ranges is reviewed in the following **Sections 2.4.1** to **2.4.2**

2.4.1 Classification of formability and component defects of injection forging

With reference to different process configurations i.e., injection forging of solid billets, injection forging of tubular billets and pressure-assisted injection forging of thick-walled tubular billets (Fig. 2.9), efforts have been devoted to identify failure-forms of the components and define the process ranges.

2.4.1.1 Injection forging of solid billets

With respect to injection forging of solid billets (bulk work-materials), three types of component defect-forms, i.e., folding, fracture and θ-shear, were well examined. For example, earlier efforts could be traced back to the 1960s, when some early experiments illustrated several kinds of the defect-forms for larger aspect ratios ((die cavity gap/flange) height/billet diameter, i.e., $T=t/d_o$) of the primary deformation zone (pdz) as shown in Fig. 2.8 [40, 42, 48, 100-101], from which, a predominant cause of the component defect-forms was found to be the instability of the free length of the solid billets. The critical aspect ratios for the development of the component defects were also defined to be the range of T=1.5-1.64 [42, 50, 81, 101]. Such an understanding of the process, however, didn't address the influence of the variation of process conditions, with the aspect ratios of the pdz. Subsequent experimental and FE simulation results on the injection forging of solid billets revealed that geometrical, metallurgical and interfacial conditions would either individually or combinationally influence the stability of the free-standing solid billets and, therefore, the stable process ranges [64, 102-103]. The FE simulation results showed that when the interface friction condition between billet and anvil was similar to that for conventional forging, instability of solid billet initiated, when aspect ratio beyond a certain value of T>1.64 for injection upsetting. When injection upsetting was conducted on a smooth anvil (μ<0.03), instability (lateral sliding of the base of the solid billet) was always occurred and resulting in the asymmetric deformation of the billet. In addition, with the increases of the radius of the exit-

geometry of the injection chamber, the instability of the billet increased accordingly. The dimension of the exit-geometry of the injection chamber was, therefore, another factor influencing the instability of the billet. Other research also showed that an annular folding occurred when the aspect ratio beyond T=1.4 during double-ended injection forging [104-105]. More recent research revealed that even under stable condition, folding could occur as well, due to the simultaneous rotation of the work material issuing from the injection chamber and radial expansion of the base of the billet. Due to which, the stable pdz aspect ratios were further reduced to T=1.2-1.3 [75, 106-107].

For injection forging of solid billets, another component defect-form is fracture associated with the injection forging of flanged components, due to the high tensile stresses imposed on the front edge of the issuing flange [40, 50, 75, 101, 105]. The onset of this component defect-form imposes a limit on the dimensions of the flanges, i.e., D=2.0-3.0. The value of D is a function of pdz aspect ratios, flange geometries and the characteristics of the work materials [42, 100-101, 54, 108]. Experimental investigation was also conducted to compare the fractures and deformation profiles for aluminum, pure lead, and plasticine [109]. Small exit radii and poor friction conditions also cause the initiation of the fracture of the work material at the exit of the injection chamber [54-55].

The intermittent θ-shear surface is the incidence-occurrence of which is dependent on the severity of the exit geometry of the die cavity and the subsequent die-filling constraints [53-54]. During closed-die injection forging, more than one intermittent θ shear surfaces may initiate [53-54], due to the lateral constraints to the flow of the issuing work-material and the development of the folds on the free surface [107]. In addition, "Macrographic examination of test specimens revealed that the shear is of relatively high intensity in comparison to that which occurs in the remaining shear zones: the severity of shear would work-harden the material to a level at which the performance of the injection-forged product could be impaired; however, hardness tests conducted along the path of the θ-surface and FE analysis did not confirm

these observations." [75].

Based on all the studies [40, 42, 48, 50-51, 53-55, 64, 81, 100-109], with respect to different component defect-forms, a forming failure diagram for injection forging of solid billets was proposed which is shown in Fig. 2.18.

2.4.1.2 Injection forging of tubular billets with the support of mandrel

Component defect-forms were studied through years regarding this process configuration [32, 43, 50-51, 79]. Research results showed that work-material folding was one of the major component defect-forms. Particularly when the specific wall thickness T (free gap height of the die-cavity/wall-thickness of the tubular billet) was bigger than double of the wall-thickness of the tubular billet, a folding defect was most likely to initiate [51, 79]. With the decrease of the free gap heights of the die-cavity, the initiation of this type of component defect-forms was delayed but unavoidable. When the free gap height gets further smaller (t<<w), other component defect-forms-local reduction and fracture would occur at the front edge of the flange. Investigations on the component defect-forms for the free-ended and constrained forming processes also showed the similar results [33, 110-111]. These results concluded that the main limitations to the radial extrusion of tubular components resulted from the tendency of the work-material to develop convolution defect-forms. The studies also revealed that a major factor which limited the application of this technology was the reduction of the flange thickness. Because these component defect-forms reported originally referred only to the free injection upsetting of tubular billets, it was, therefore, suggested that a further injection forging of the work-material may help to eliminate some of the defined defect-forms, such as irregular peripheral surfaces, irregular plane surfaces and non-uniform flange thickness, but at the expense of a higher die-surface stresses [75]. The nature of the folding in the issuing work-material also has been studied. The results illustrated that several mixed process parameters, such as inner diameter of the tubular billet, inner diameter of the flange, thickness of the flange and the extent of injected work-material, influenced the nature of the defect-form of folding [32, 46, 69, 112-113].

The results also showed that during injection forging, the tendency of work-material folding was reduced with the increases of the inward flow of the work-material. Owing to the further development of FE simulation, engineering and physical modeling techniques, the forming limit diagrams with reference to different defect-forms for this process configuration were defined [32, 46, 69, 112-113], from which an upper threshold ratio (t/w =1.6-1.8) for the flawless injection forging of tubular components was determined. One of the formability limit diagrams for this process configuration is shown in Fig. 2. 19.

2.4.1.3 Injection forging of tubular billets with the support of pressurising materials

The formability for the forming of thin-walled tubular components by PAIF was studied [31, 114-115]. Results showed that the tendency of the work-material to collapse was the main limitation to the process. The component defect–forms with the forming of thick-walled tubular components by PAIF are different from that with the forming of thin-walled tubes [36-37]. Component defect-forms of folding, buckling, necking, thinning and weakened sections may occur, with reference to different forming sequences, pressuring materials and aspect ratios. For example, when an incorrect forming sequence was used, defect-forms of necking, thinning or work-material accumulated might occur [35, 64]. If a pressurising material had a low capability to produce enough diametrical strains, force transmission efficiency of the process could be reduced [36, 75]. When either a too small ($T<0.5$) or a too big ($T>1.64$) aspect ratio of pdz was used, defect-forms of either fracture/folding or buckling might occur, respectively [35-37, 64, 75, 102-103].

2.4.2 Extension of formability and process ranges

2.4.2.1 Extension of formability of injection forging of solid billets

To date, many efforts have been made to study the formability of injection forging processes and to classify the component defect-forms, with a view to extending the formability and process ranges. Back to the 1960s, in order to eliminate the major

component defect-forms of fracture with cold extrusion of solid billet to form solid flanges, a hydraulic compensating pressure was applied to the leading-edge of the flange to prevent the initiation of the fracture, and hence, to extend the process formability. This concept was attempted with a number of experiments. The method proposed and the experiments conducted were based on a good understanding of the mechanism of the initiation of the fracture, i.e., the excessive tensile stress promoted the onset of the fracture on the circumference of the flange [39]. In the 1970s, in order to overcome the limitation (fracture initiated in the periphery of the issuing work-material) with single ended injection forging, a multi-axial tooling configuration was used and a branched component was formed. Due to the refined control of the tool movement in both axial and radial directions during this process, billet instability and particularly fracture on the periphery of the issuing work-material was suppressed, and therefore extending the process range [67]. A similar effort was made by changing the forming-tool kinematics (relative movement between forming-dies, punches and work-piece) to regulate the work-material deformation and the force parameters, from which the formability of the process was extended [50]. The principle of the approach may be interpreted by the follows. When the process begins with a small aspect ratio of the pdz, the stability of the billet could obviously be improved. With the progresses of the process, the aspect ratio of the pdz could be increased progressively by the relative retraction of the injection chamber from the forming die. A component with large flange-thickness could therefore be formed under a more stable condition of the billet throughout the forming process [50, 75]. The research also reported that, based on an extra cost for the use of double ended tooling, formability of the process could also be improved [50]. In 1988, another attempt was made to eliminate the fracture in the leading edge of the flange by using a "truncated-conical" forming-die to replace the use of hydrostatic pressure on the rim of the issuing flange [108]. This attempt was conducted based on the understanding of the relationship between the component defect-form (fracture), die-cavity geometry as well as work-material flow state [108]. In 1993, some shaped anvils, such as anvils with radial grooves or concentric steps, were used to prevent both the instability of the billet and the initiation of the fracture

in the rim of the issuing flange. This alternative approach demonstrated the feasibility of the improvement of formability of the process [52, 116]. Recently, based on further understanding of the process (free-ended injection forging of solid billet), i.e., even if under a stable work-material flow condition, component defect-form of folding was initiated due to the combination of work-material rotation in the die cavity and the radial expansion of the billet base, approaches of using either a pre-shaped billet or a two-stage forming sequences were proposed and used to extend the formability of the process [107, 117-118]. For instance, using the approaches proposed, the process range of injection forging of solid billet could be extended from T=1.2-1.3 to T=1.4-1.5 using pre-shaped billets and to T=1.5-1.64 using preformed billets [117-118], as shown in Fig. 2. 20.

2.4.2.2 Extension of formability of injection forging of tubular billets

In addition to the attempts made to extend the formability for injection forging of solid billets, efforts were also devoted to the extension of the process ranges of injection forging of tubular billets. For example, based on the experimental and FE simulation results for quantifying the forming limit of injection forging of tubular billets with the support of the mandrels, a two-stage forming procedure was proposed to extend the formability of the process [112-113, 119]. Design rules for the pre-forms of the flawless forming flanged tubular components were established. That is, the mandrel was designed with a conical re-entrant geometry by which the work-material inward flow was allowed when a pre-forming ring was used to restrict the outward flow of the work-material during the pre-forming stage. After filling the conical die-cavity around the mandrel, the pre-forming ring was removed and the flange was formed by the subsequent injection of the work-material. It was reported that, using this process configuration/procedure, tubular components with large-flange-thickness were produced successfully, e.g., the limiting ratio of t/w was successfully extended from 1.8 up to 3.6 [75, 113] as shown in Fig. 2.21.

2.5 Process Modelling

Metal forming processes may be modelled using several different methods, such as experimental and physical modelling, analytical and numerical methods.

2.5.1 Experimental and physical modelling

Experimental modelling method may be referred to physical modeling method, by which the work-material deformation was simulated [120]. Subsequently, in order to investigate the initiation of component defect-forms for radial extrusion of tubular billets with the support of mandrels, modelling materials (waxes) were used to simulate the process. The results showed good agreement with metal forming experiments [32, 69], as shown in Fig. 2.22. Physical modelling method might also have the capability to simulate more complex component-forms, for which either analytical or numerical methods might be difficult or impossible to deal with at the present [121].

2.5.2 Analytical modelling

Analytical methods include Slab, Slip-line field and upper bound methods. Slab method was used to analyse the approximate stress of radial extrusion [122], in which, the work-material was assumed to be rigid-plastic; the Tresca's yield criterion was used and that the friction in both injection chamber and die-cavity was considered using a constant friction factor. The work-material was divided into four zones that were analysed using equilibrium-equations, respectively. Slip-line field method is mostly suitable for investigating sheet metal forming processes, such as sheet drawing, extrusion, rolling and forging. A number of applications of this theory are shown in [123]. It also was used in the analysis of injection forging/upsetting processes [39, 49], as shown in Fig. 2.23. The upper bound method seems to be the quite popular one to be used in the analysis of injection forging processes over the past few decades. Tracing back to the 1960s, the initial application of upper bound theorem was the analysis of a hydrodynamic compression forging of a flange. During

this analysis the flange was treated as an expanded thick-walled tube and the power requirement due to the plastic deformation of the work material was defined [38]. Other early theoretical models for analysing injection upsetting were also developed based on some assumptions, i.e., both the work-material flow within the die cavity was in a steady state and the friction losses along the injection chamber were insignificant, throughout the injection processes [39, 49]. Further effort was made with a view to extending the previous upper bound solutions [39, 49] in the following two aspects: one was to take into account the friction losses along the tool-workpiece interfaces; another was the incorporation of the velocity discontinuities along the internal shear surfaces, i.e., the interface between any two of the adjacent zones of the work-material divided. From this modelling, the maximum force requirement for the injection upsetting of a solid flange against a hydrostatic pressure was derived, although the external hydrostatic pressure was ignored in this analysis [124]. Other applications of the upper bound method can also be found in the prediction of maximum forming loads for extrusion of solid flanged tubular components and forming of multi-branched components [69, 111]. One of the analytical models using upper bound theorem is shown in Fig. 2.24. Forming of rotationally asymmetric segmented flanges was also analysed using an upper bound method to study the effect of the segment angle on the load characteristic of the process. It was found that with the increase of the segment angle, the extrusion load was decreased dramatically [85]. Based on two different velocity fields assumed for radial extrusion of a same component, after the comparison of the difference between the maximum forming loads for the two corresponding velocity fields, the optimal upper bound solution for this process was derived [125]. Also, in order to develop a simple and reliable analytical model for the heading of engineering material processes, experimental data, lower bound solution and upper bound solution were used to predict the free surface profiles, strain-stress histories and fractures initiated at the equatorial-free surface [100].

2.5.3 FE modelling

Finite element method (FEM) is one of the most powerful numerical methods [73,

88, 126-130] for engineering analysis. Although the use of the method may rely heavily on the expensive software and also may be time-consuming for some complex-3D analysis, finite element techniques have been used to simulate bulk metal forming since the early 1970s. For example, FEM was used to simulate the injection forging of engineering components (flanges), with a view to predicting the injection forging pressure under the process conditions of D=1.4, T=0.2 and a flange compensation pressure of 154 MPa [131]. The predicted pressure was within 6% of the results obtained from the earlier experimental study [38]. Another process of the combined radial with forward can extrusion was simulated using a rigid-plastic FE code of PLADAN [55]. In this simulation, work-material flow patterns and tool stresses were defined for small aspect ratios of pdz (T<0.5) and large radii of the injection chamber exit. In the early 1990s, FEM began to be used in the simulation of the development of component defect-forms for injection forging of tubular billets [32], through which the drawbacks with the existing modelling methods were revealed. In order to overcome the deficiencies with the previous research [32], a PC-based FE simulation package was subsequently developed for the analysis of the injection forging of tubular components when a rigid-plastic work-material description was adopted [112-113]. These efforts enabled the simulation of the development of component defect-forms with injection forging of tubular billets, that were observed experimentally but failed to simulate by previous research [32]. Using this FE code, a two-stage forging process of pre-forming plus subsequent forming was simulated [112-113, 119, 132-133] in which the pre-forming stage was designed to eliminate the initiation of component-defects. Furthermore, from the significant differences between experimental and FE simulation results in punch-force-histories for long billets and small exit-geometries, the fact that traditional descriptions of friction may no longer be suitable for the friction conditions at the billet and injection chamber interface was recognised [134]. As a whole, based on the progresses of FEM being able to consider multi-factors, such as friction conditions on the anvil, aspect ratios of the pdz, exit-geometry of the injection chamber and inhomogenity of the work-material, the initiation of different types of component defect-forms during injection forging either solid or tubular components was simulated using ABAQUS

[64, 82, 102-103, 107, 117-118, 134]. Some of the FE simulation results are shown in Fig. 2.25 [75]. As a result, with the improvement of FE simulation techniques, not only more realistic patterns of work-material flow were modelled, but also the qualification of work-material flow patterns for different process conditions was conducted. Moreover, the improved FE techniques also enabled the preform-designs for extending the formability limits of injection forging as well as to design the optimal forming sequences for pressure-assisted injection forging of thick-walled tubular components [82, 107, 113, 117-118].

It is clearly that FE simulation has been widely used to analyse the bulk metal forming processes successfully. Simulation of the development of component defect-forms, particularly the defect-forms with pressure-assisted injection forging of thick-walled tubular components was, however, not fully explored.

2.6 Testing of Pressurising Materials

Efficiency of pressure-assisted injection forging of thick-walled tubular components is largely prescribed by the performance of pressurising material used. Since, unlike forming thin-walled tubes, in the forming of thick-walled tubes, bulk metal flow within the work material and much higher pressurisation within the pressurising material are inevitable. Therefore, a fine control on the deformation of both work- and pressurising materials are required. In other words, a quantitative understanding of the mechanisms of controlling both work and pressurising material flow is essential to the process (PAIF) to be used successfully and industrially. Obviously, only a wider range of investigation on the mechanical properties of the pressurising materials (for PAIF) would be helpful to achieve this goal. The investigation should include the examinations of the selected pressurising materials under not only uniaxial tension/compression and planar tension/compression conditions, but also confined compression and biaxial tension conditions.

In order to carry out the initial examination on the selected pressurising materials under confined compression condition experimentally for PAIF, an investigation on the relevant experimental methods and techniques was conducted. During the last few years, some efforts have been devoted to the development of experimental techniques and facilities to study the mechanical properties of either metallic or non-metallic material under tri-axial loading states [135-138]. An electromechanical tri-axial testing facility was developed to test composite materials [135]. It mainly comprises three primary subsystems-the reaction frame, test fixture and the computer control system. It was successfully used to perform the biaxial and tri-axial tests. However, this facility was only suitable for a thin cruciform shape specimen and its maximum bearing capacity is only 94kN which is far less than that the forming force -300 to 450 kN required by the author's study. Another method for dynamically proportional, multi-axial compression tests on RTV630 silicon rubber was also reported [136]; a split Hopkinson pressure bar (SHPB) [136-137] was used to generate a uniaxial compressive pulse and a standard hydraulic pressure vessel used to supply lateral force for a thin rubber disc specimen. In addition, another experimental set-up was also introduced [137] for imposing dynamic multi-axial compression on a brittle material-ceramic by using a shrink-fit metal sleeve to supply the lateral force on the ceramic specimen. All these approaches are, however, not suitable for examining materials under larger scale deformations.

Another investigation was also conducted with a view to finding a suitable machine to conduct the biaxial tension tests of the selected pressurising materials for PAIF. Several attempts were reported regarding the development of equipment and methods in the qualification of mechanical properties of several non-metallic materials under biaxial tensile loading conditions [139-140]. For example, four pairs of pulleys and eight pairs of ropes were used as a stretcher to pull a biological material specimen [139], which was sutured by the ropes separately along each loading direction. By this design, loads may not be evenly applied along the clamping area of the specimen. Particularly, the clamps used are not suitable for a high level stress test, because the tearing failure may occur at the sutured points,

even before the material at the tested area reaches its ultimate strength. A square loading-frame and two notched aluminium-plates were also used to test composite panel specimens under the biaxial loading conditions (either biaxial compression or combined compression with tension along the different loading directions) successfully [140]. The device is, unfortunately, unable to carry out biaxial tension tests. Also Buet-Gautier and Boisse' s device consisted two cross-placed deformable parallelograms and four clamps made up of a solid plate with three cap screws for each of them, which were used to hold each side of the cross-shaped woven specimen [141]. More closely, a biaxial stretcher designed as an attachment for an Instron tensile test machine was used to stretch polymer (PVC) sheet effectively with a maximum draw ratio of 4*4 by Hitt and Gilbert [142], which is, unfortunately, much more smaller than the draw ratio of 10*10 which the rubber may undergo in the author's study. Moreover, the complex clamps used in their stretcher are not effective enough for holding rubber specimens. As a result, a suitable machine for testing rubber like materials, which may undergo large-scale deformations under the biaxial tensile loading conditions, for the author's PhD study was not found within the UK.

2.7 Summary Comments from the Literature Review

Injection forging has been developed dramatically over the last few decades due to the following facts. Development of physical, analytical and particularly the numerical modeling techniques has contributed a lot to the prediction of the processing requirements, to the profound understanding of the mechanisms of controlling work-material deformations and to the production of the sound engineering components. More importantly, the potential advantages of injection forging have encouraged and facilitated the development of the technology itself. First of all, injection forging as a nett-shape or near-nett-shape manufacturing process, has lower work-material consumption and less secondary processing

requirements than conventional forging (e.g., intermediate bulk metal-removal is not needed for the injection forged components, the amount of the scrap metal can, therefore, be reduced). Secondly, energy requirement for injection forging to convert the work-material into a component is less than that required for conventional forging, particularly for the forming of tubular components. Thirdly, more complex component-forms can be achieved by injection forging than that by conventional forging, with reduced process-chains.

Pressure-assisted injection forging (PAIF) is the latest development of injection forging. This process configuration possesses not only the above outstanding advantages as the other injection forging processes have, but also the feasibility to produce thick-walled tubular components with hollow flanges, like the component-form (8) in Fig. 2.4 and 2.9 (c), which used to be considered as unachievable by conventional forming processes. The successful manufacture of this type of components by PAIF would not only breach the formability of the existing forming processes, but also provide an ideal balance between the strength and the weight of the component structure. However, the engineering application of PAIF is still largely limited by the lack of the technical details and the systematic process design procedures. Deficiencies of the previous research development regarding this process may be summarized as follows:

2.7.1 Opportunities and challenges

Although numerous engineering tubular components were produced successfully by either forging/extrusion or conventional tube-forming methods over the last few decades, industries, particularly automotive and aerospace industries, are still under pressure to produce these components more efficiently, with a view to reducing the costs. Demands, on the further extensive use of tubular components, which are of high strength to weight ratios to replace the still largely used solid components, which are of low strength to weight ratios, provide the opportunities and challenges to the research and development in the field of injection forging.

2.7.2 Development of injection forging

Injection forging is recognized being one of the most efficient forming processes. Configurations of the process have been developed from the injection of solid billets to the injection of tubular billets. The corresponding component-forms were achieved from the solid components to tubular components successfully. Thick-walled tubular components with hollow flanges and flanges with secondary elements, unfortunately, have not been tested by industries, due to the insufficiencies of the development with this technology, referred to **Section 2.3**.

2.7.3 Development of pressure-assisted injection forging (PAIF)

The previous research suggested that pressure-assisted injection forging (PAIF) might be a solution for producing this type of tubular components economically and efficiently. The successful application of this process to industries would rely largely on the understanding of the process and its mechanics. To date, process classifications for the conventional forging have been found from a number of sources. A classification for PAIF was, however, not found yet. The similar case was also found, for the definition of formability and component defects for PAIF, i.e., formability and component defects for injection forging of solid billets and injection forging of tubular billets with the support of mandrels were well studied, however, limited sources were found on addressing these issues for PAIF. Formability and process ranges for injection forging of both solid and tubular billets were extended with several different methods, such as using compensating pressures, preformed billets, two-stage forming, etc. Nothing has been found for PAIF, on these issues.

2.7.4 Process modelling

Although injection forging of both solid and tubular billets was modeled either physically or numerically, process modelling would still need to be extended to enable the prediction of the forming limits for more complex component-forms. It has also been revealed that both numerical and physical modelling of the forming of complex component-forms may face some difficulties due to the limitations of

currently available FE codes in the modelling of hybrid materials, like in PAIF. However, further to the previous physical and numerical modelling, analytical modelling seems to be another option for the analysis of injection forging, for industrial applications. Analytical modelling, particularly upper bound method, was used to analyse injection forging of both solid and tubular billets through years for predicting the maximum forming loads. No upper bound solution was found for pressure-assisted injection forging (PAIF) of thick-walled tubular components with hollow flanges.

2.7.5 Forming of engineering components

Separated gears from the shafts may be manufactured by several different means, i.e., machining, cold/warm/hot forging and pre-pieced forging, successfully. These are, however, based on not only a huge cost for machinery, tooling and heat treatment for manufacturing individual components, but also the subsequent assembly by welding or keyway-assembly. A method by which an engineering component, i.e., a hollow gear-shaft could be formed as one integral part and with a single stroke would be desirable. Injection forging, particularly PAIF, could be a solution to achieve this goal.

2.7.6 Testing of pressurising materials

Over the last few years, many efforts have been made on the development of experimental methods and techniques for testing either metallic or non-metallic materials under tri-axial compression conditions. For example, a cylindrical ceramic specimen was tested, with a shrink-fit metal sleeve (supplying lateral forces) successfully; a thin circular (ϕ=19mm*3.15mm/6.35mm) rubber specimen was examined with a fluid-filled pressure vessel and a split Hopkinson pressure bar (applying axial load) efficiently; and a thin cruciform shaped specimen was evaluated with an electromechanical testing facility (applying both lateral and axial forces) sufficiently. However, none of these techniques are suitable for the testing of rubber like materials under larger scale deformations for PAIF.

Some progresses of developing equipment and technologies of testing non-metallic materials under biaxial loading conditions were also made during the last few years. For instance, a biological material specimen was tested with a biaxial stretcher (consisting of four pairs of pullys and eight pairs of ropes) efficiently. Buckling of a composite panel (specimen) under combined tension and compression loading condition was examined using a square loading frame and two-notched aluminum plates successfully. A polymer (PVC) sheet was also evaluated with another biaxial stretcher (an attachment of an Instrom tensile test machine) satisfactorily. None of these facilities are able to qualify the mechanical properties of the selected pressurisng materials under biaxial tensile loading conditions for PAIF.

2.8 References

[1] S. Kalpakjian and S. R. Shmid, "Manufacturing Processes for Engineering Materials", Fourth Edition, Prentice Hall, 2003, pp1-24, 300-368.

[2] Mikell P. Groover, "Fundamentals of Modern Manufacturing", Second Edition, John Wiley & Sons, INC., 2002, pp1-21, 429-471.

[3] F. Schmieder and P. Kettner, "Manufacturing of hollow transmission shafts via bulk-metal forging", Journal of Materials Processing Technology, Vol. 71, 1997, pp. 113-118.

[4] E. Rauschnabel and V. Schmidt, "Modern applications of radial forging and swaging in the automotive industry", Journal of Materials Processing Technology, Vol. 35, 1992, pp.371-383.

[5] D. Schmoeckel and F.-D. Speck, "Axial-Radial Forming of Tubular Components", Annals of the CIRP, Vol. 44, No. 1, 1995, pp235-238.

[6] F. Dohmann and Ch. Hartl, "Hydroforming-a method to manufacture lightweight parts", Journal of Materials Processing Technology, Vol. 60, 1996, pp.669-676.

[7] B. Viehweger, "With water to the shape", Blech Rohr Profile, 2, (1), 1996.

[8] M. Ahmetoglu and T. Altan, "Tube hydroforming: state-of-the-art and future trends", Journal of Materials Processing Technology, Vol. 98, 2000, pp.25-33.

[9] F. Dohmann and Ch. Hartl, "Tube hydroforming-research and practical application", Journal of Materials Processing Technology, Vol. 71, 1997, pp.174-186.

[10] M. Ahmetoglu, K. Sutter, X.J. Li and T. Altan, "Tube hydroforming: current research, applications and need for training", Journal of Materials Processing Technology, Vol. 98, 2000, pp.224-231.

[11] T. Nakagawa, K. Nakamura and H. Amino, "Various applications of hydraulic counter-pressure deep drawing", Journal of Materials Processing Technology, Vol. 71, 1997, pp.160-167.

[12] F. Dohmann and Ch. Hartl, "Hydroforming-applications of Coherent FE-Simulations to the Development of Products and Processes", Journal of Materials Processing Technology, Vol. 150, 2000, No. 1-2, 2004, pp.18-24.

[13] S. Tiruvarudchelvan and H. Wang, "Investigations into the hydraulic-pressure augmented deep drawing process", Journal of Materials Processing Technology, Vol. 105, 2000, pp.161-175.

[14] Ch. Hartl, H.-U. Lücke and T. Abbey, "Hydroforming" J. Mater. Process. Technol. Vol. 115, 2001, pp87-91.

[15] B. Avitzur, "Handbook of Metal-forming processes", John Wiley & sons, Inc., USA, 1983, Chapter 9, pp457-458.

[16] L.A. Moreira Filho and H.A. Al-Qureshi, "Unconventional tee forming on metal tubes", Sensors and controls for automated forming, The ASME , 1985, pp.123-135.

[17] T. Wang, S. Sun and D. Mo, "The research of tube bulging using polyurethane under compound external forces and its application", Proc. 4th ICTP, 1993, pp494-499.

[18] S. Thiruvarudchelvan, "Elastomers in metal forming: a review", J. of Material Processing Technology, Vol. 39, 1993, pp. 55-82.

[19] L.A. Moreira Filho, J.C. Menezes and H.A. Al-Qureshi, "Analysis of unconventional tee forming on metal tubes", J. of Mater. Process. Technol., Vol. 45, 1994, pp383-388.

[20] T. Ueda and T. Ogura, "Liquid bulge forming", Metalworking Prod., 24 April 1968, pp. 73-81.

[21] Y. Qin and R. Balendra, "Design considerations for hydromechanical deep drawing of sheet components with concave features", J. of Mater. Process. Technol., Vol. 145, 2004, pp163-170.

[22] K. Brewster, K. Sutter, M.A. Ahmetoglu and T. Altan, "Hydroforming tube", The tube and pipe quarterly, Vol. 7, No. 4, 1996, pp34-40.

[23] K. Dengler, "Exploring internal high-pressure forming of metal", The Fabricator 7 and 8, 1996.

[24] S. Shah and C. Bruggemann, "Hydroforming products and process requirements and implementation", Proc. 2nd Annual Automotive Tube Conference, Dearborn, Michigan, 13-14 May 1997, pp85.

[25] F. Horton, "Using forming simulation in development of complex hydroformed shapes", Proc. 2nd Annual Automotive Tube Conference, Dearborn, Michigan, 13-14 May 1997, pp173

[26] F. Dohmann, A. Böhm and K.-U. Dudziak, "The shaping of hollow shaft-shaped workpieces by liquid bulge forming" Advanced Technology of Plasticity, Proc. 4th ICTP, 1993, pp447-452.

[27] E.W. Pleines, "Rubber forming processes", Werkstattstechn. Maschinenbau, 40, 1950, pp405-409.

[28] H. Hermans and F.H.R.F. Vermulen, "Metal forming with flexible tools". Met. Work. Prod., 1961, pp69-72.

[29] C.A. Harper, "Modern Plastics Handbook", Published by The McGraw-Hill Companies, 1999, p3.1-3.52, A1-C60

[30] J. Brandrup, E.H. Immerdut and E.A. Grulke, "Polymer Handbook", Fourth Edition, Published by John Wiley & Sons, 1999, pVII 688-VIII 24.

[31] S. Thiruvarudchelvan and F.W. Travis, "Tube bulging with a urethane rod", Journal of Materials Processing Technology, Vol. 23, 1990, pp195-209.

[32] B. Andersen and C.B. Andersen, "Radial extrusion of tubular components" (M.Sc. dissertation), Technical University of Denmark and University of Strathclyde, 1991.

[33] B. Lengyel, S.A. Shahmoradi, "Forming flanged components by upsetting", Proc. of the 27th Int. MATADOR Conf., 1988, pp. 313-319.

[34] B. Lengyel, S. A. Shahmoradi and I. A. Chaudhry, "Cold Extrusion of Flanges on Cylindrical Hollows", 30th Int. MATADOR Conference, 1993, pp227-234.

[35] R. Balendra and Y. Qin, "Pressure-assisted Injection Forging of thick-walled tubes", Int. J. of Mach. Tools Manf., Vol. 35, No. 11, 1995, pp. 1481-1492.

[36] Y Qin and R. Balendra, "Technical evaluation of pressure-assisted injection forging of thick-walled tubes", Advan. In Manuf. Tech. IX, London, 1995, pp62-66.

[37] R. Balendra and Y. Qin, "Technical feasibility and processing limitations of pressure-assisted injection forging of thick-walled tubes", Proc. 5th ICTP, 1996, pp327-330.

[38] R. M. Cogan, "Hydrodynamic Compression Forging", General Electric Company, ASD Report 7-890 (111), 1963.

[39] J. M. Alexander and B. Lengyel, "On the cold extrusion of Flanges Against High Hydrostatic Pressure", Journal of the Institute of Metals, Vol. 93, 1965, pp137-145.

[40] "Some aspects of the cold extrusion of steel", NEL Report 196, Staff of Plasticity Division, Department of Industry, UK, 1965.

[41] R. Balendra and Y. Qin, "Nett-form manufacturing by injection forging", Proceedings of 14th Intern. Conf. on Computer Aided Product. Eng., Tokyo, Sep.8-9, 1998, pp301-306.

[42] J.C. Henry, "An investigation of the injection upsetting of six steels", NEL Report 494, Department of Industry, UK, 1971.

[43] J. C. Hendry and M. T. Watkins, "The Production of Hollow Flanged Components from Bar Stock by Upsetting and Extrusion", NEL Report, No. 628, 1977.

[44] R. Geiger, "Near-nett Shape Forming by Radial Extrusion" Proc. 7th Int. cold Forging Cong., Birmingham. UK, 1985, pp29-38.

[45] R. Balendra, "Review of Injection Forming", Proc. Of the 9th brazilian Congress of Mech. Eng. 1987, pp1077-1081.

[46] M. Arentoft, S.B. Petersen, J.M.C. Rodrigues, P.A.F. Martins, R. Balendra and T. Wanheim, "Review of research into the injection forging of tubular materials", Journal of Materials Processing Technology, Vol. 52, 1995, pp.460-471.

[47] A.C. Okafor and R. Balendra, "Stress and energy distributions in injection forming of a complex shaped component", Proc. 7th Int. Cold Forging Congress, 24-26th, April, Birmingham, UK, 1985, pp. 79-86.

[48] R. Balendra, "Studies of injection forming", Research report, University of Strathclyde, UK, 1971.

[49] P.R. Milner, "The injection upsetting process", Ph.D. Thesis, Leeds University, UK, 1971.

[50] I.S. Aliev, "Radial extrusion process", Sov. Forg. Met. Stamping Technology, Part 3, 1988, pp. 54-61.

[51] W. Osen, "Variation of the transverse impact extrusion process", Wire, Vol. 35, Part 3, 1985, pp.109-113.

[52] M. Motomura and K. Inoue, "Improvement of limit deformability of aluminium disc by lateral extrusion method (Part I)", Light Metal, Vol. 43, No. 12, 1993, pp. 678-682.

[53] R. Balendra, "Injection-chamber to die-cavity interface for Injection

Forming", Int. J. Mach. Tools Manufact., Vol.33, No 6, 1993, pp 753 - 760.

[54] R. Balendra, "Exit-geometry for injection forming", 4th Int. Conf. on Manufg. Eng., Brisbane, Australia, 1988, pp. 11 - 17.

[55] W. Osen, "Possibilities and limitations of cold extrusion processes combined with radial extrusion", Advanced Technology of Plasticity, Vol. 1, 1986, pp. 575-582.

[56] K . Lange, "Cold forging - today and tomorrow", Proc. 7th Int. Cold Forging Congress, 24-26th, April, Birmingham, UK, 1985, pp. 3-14.

[57] R. Geiger, "State of the art and development trends in cold forging technology", Proc. of the 2nd ICTP, 1987, pp. 469-477.

[58] J. A. Pale and R. Shivpuri and T. Altan, "Recent developments in tooling, machines and research in cold forming of complex parts", J. of Mater. Process. Technol., Vol. 33, 1992, pp. 1-29.

[59] T.A. Dean, "Progress in net-shape forging", Adv. Tech. of Plasticity, Vol. 2, 1993, pp. 1031-1040.

[60] K. Lange, "some aspects of the economic production of complex bulk components by cold forging and machining", Adv. Tech. of Plasticity, Vol. 2, 1993, pp. 1144-1156.

[61] T.A. Dean, "A profile of the market for cold forging", Proc. of the 9th Int. Cold Forging Congress, Solihull, UK, 22-26 May, 1995, pp. 17-27.

[62] R. Geiger, "From near-net-shape to net-shape cold forging - State of the art", Proc. of the 9th Cold Forging Congress, 22-26 May, UK, 1995, pp. 59-75.

[63] Y. Qin and R. Balendra, "Computer-aided design and assessment of tools and components for nett-shape manufacturing", IMechE Conference Transaction 1995-3 (11th Int. Conf. on CAPE, Sept., London, UK), 1995, pp.35-40.

[64] Y. Qin, "FE and Experimental analysis of injection forging", PhD Thesis, Chapter 1, 4, 6, The University of Strathclyde, 1997, pp1-21.

[65] H.L.D. Pugh, "The mechanical properties and deformation characteristics of metals and alloys under pressure", NEL Report 142, UK Department of Industry, 1964.

[66] B. Parsons, P.R. Milner and B.N. Cole, "Study of the injection upsetting of

metals", J. Mech. Engng. Sci., Vol. 15, No. 6, 1973, pp. 410-421.

[67] H. Kudo and K. Shinozaki, "Investigation into multiaxial extrusion process to form branched parts", Proc. of the Int. Conf. Prod. Eng., Tokyo, Part I, 1974, pp. 314-319.

[68] S.I. Rozhkov and K.A. Kirsanov, "One- and two-directional extrusion of parts with one branched rod element", Soviet Forging and Sheet Metal Forming Stamping Technology, No. 3, 1988, pp. 5-9.

[69] C. Enghave, "Tvaerflydepresning af roerflanger (in Danish)", Procesteknisk Institut, DtH, MM-rapport ny. (91.08), 1991.

[70] J. Pipan, "Radial extrusion combined with inside ironing of tube", UMFORMTECHNIK, 27/4, 1993, pp. 262-267.

[71] J.L. Remmerswaal and A. Verkaik, "Use of compensating forces and stresses in difficult metalforming operations", Proc. Int. Conf. Mfg. Technology, ASTME, 1967, pp. 1171-1180.

[72] H.A. Al-Qureshi, "Factors affecting the strain distribution of thin walled tubes using polyurethane rod", Int. J. Mech. Sci. Vol. 13, 1971, pp.403-413.

[73] K. Lange, “Handbook of metal forming”, Mcgraw-Hill, New York, 1985, pp2.1-2.23.

[74] Y. Qin and R.Balendra, “Computer-aided design of nett-forming by injection forging of engineering components”, J. Mater. Proces. Technology, Vol. 76, 1998, pp62-68.

[75] R. Balendra and Y. Qin, “Injection forging: engineering and research”, J. of Mater. Process. Technol., Vol. 145, 2004, pp. 189-206.

[76] T. Sokolowski, K. Gerke, M. Ahmetoglu and T. Altan, “Evaluation of tube formability and material characteristics: hydraulic bulge testing of tubes”, J. of Mater. Process. Technol., Vol. 98, 2000, pp. 34-40.

[77] S. Thiruvarudchelvan, “A theory for the bulging of aluminium tubes using a urethane rod”, J. of Mater. Process. Technol., Vol. 41, 1994, pp. 311-330.

[78] T. Nakano, "Modern applications of complex forging and multi-action forming in cold forging", J. of Mater. Process. Technol., Vol. 46, 1994, pp. 201-226.

[79] W. Osen and K. Lange, "Deformation pattern, forces and process limits in combined radial and backward can extrusion", Steel Research, Vol. 56, No. 4, 1985, pp.211-214.

[80] V. Krusic and K. Kuzman, "Cold radial extrusion in automotive industry", 26th ICFG Plenary Meeting, Osaka, 1993.

[81] W. Osen and W. Schatzle, "Chances and limits of radial extrusion", Proc. 7th Int. Cold Forging Congress, 24-26th, April, Birmingham, UK, 1985, pp.178-187.

[82] Y. Qin and R.Balendra, "Simulation of forming sequence of Pressure-assisted injection forging of thick-walled tubes", Trans. NAMRI/SME, Vol. XXIII, 1995, pp27-32.

[83] J. Keller, "Optimierung der Fertigungsfolge Kaltmassivumformen und spanen", Neu. Entwicklungen in der Massivumformung, 1989, pp. 8/1 - 8/3.

[84] D. Colla, S.B. Pertersen, R. Balendra and P.A.F. Martins, "Injection Forging of industrial components from thick-walled tubes", J. Manufacturing. Science and Engineering, Vol. 119, 1997, pp537-541.

[85] M. Plancak, A. Bramley and F. Osman, "Non-conventional cold extrusion", J. of Mater. Process. Technol., Vol. 34, 1992, pp. 465-472.

[86] K. Shinozaki, "Further investigation of cold lateral extrusion to form staggered branches from a cylindrical billet", Annals of the CIRP Vol. 38/1, 1989, pp. 253-256.

[87] W. King, J.A. Fan and D. Seibert, "Recent developments in the extrusion of helical gears", Int. J. of Mach. Tools. Manufact. Vol. 33, No. 4, 1993, pp.599-614.

[88] B. Dodd and A. A. Konieczny, "Limit phenomena in cold forging", Proc. of the 9th Int. Cold Forging Congress, May, 22-26th, Solihull, UK, 1995, pp. 259-268.

[89] E. M. Mielnik, "Metalworking science and engineering", Mcgraw-Hill, New York, 1991.

[90] W. F. Hosford and R. M. Caddell, "Metal forming - Mechanics and Metallurgy", Prentice-Hall, Englewood Cliffs, USA, 1983.

[91] G. E. Dieter, "Mechanical Metalllurgy", McGraw-Hill, London, 1988.

[92] B. Devedzic, "Evaluation of the plastic workability of metals - possible approaches and specific problems", Proc. of the 26th Int. Mach. Tool Design and Res. Conf. (ed. by B. J. Davies), Macmillan Ltd., 1986, pp. 443-451.

[93] B. Dodd, "Defects in cold forging", Plenary Meeting of ICFG, Osaka, 1993.

[94] H. Kudo, "Material fracture in cold forging - systematic classification of working methods and types of cracking in cold forging", The Sumitomo Search, No. 9, May, Sumitomo metal Industries, Osaka, Japan, 1973.

[95] M. Arentoft, P. Henningsen, N. Bay and T. Wanheim, "Simulation of defects in metal forming - an example", J. of Mater. Process. Technol., Vol. 45, 1994, pp. 527-532.

[96] Y. Qin and R. Balendra, "Optimisation of the lubrication for the extrusion of solid and tubular components by injection forging", J. of Mater. Process. Technol., Vol. 135, 2003, pp. 219-227.

[97] Y. Qin, R. Balendra and K. Chodnikiewicz, "Analysis of temperature and component form-error variation with the manufacturing cycle during the forward extrusion of components", J. of Mater. Process. Technol., Vol. 145, 2004, pp. 171-179.

[98] Y. Qin and R. Balendra, "Development of a methodology of analysis and compensation of component-form errors for high-precision forming", IMechE Conference Trans. 2000-5, 2000, pp. 363-372.

[99] P.S. Bate, "Strain path change effects in the local necking of aluminium sheet and in the tension of internally pressurised tubes", Metallurgical transactions A, Vol. 24A, 1993, pp2691-2699.

[100] P. Bariani, "Free surface profiles and workability limits in heading process", Annals of the CIRP, Vol. 31/1, 1982, pp. 185-189.

[101] R. Balendra, "Process mechanics of injection upsetting", International Journal of Machine Tools Manufacture, Vol. 25 (1), 1985, pp63-73.

[102] R. Balendra and Y. Qin, "FE simulation of the development of flaws during injection forging", Int. J. Mach. Tools Manuf. Vol. 34 (8), 1994, pp1091-1101.

[103] Y. Qin and R. Balendra, "Development of the flaws during injection forging", Proc. 10th NCMR, Loughborough, UK, 1994, pp587-591.

[104] W. Schatzle, "Transverse extrusion of acollar on solid steel bodies", Wirc, Vol. 34 (2), 1984, pp71-74.

[105] W. Schatzle, "Radial extrusion of flanges on steel cylindrical work-piece", Technical report 93, Institute of metal forming, university of Stuttgart, Springer, Berlin, 1987.

[106] Y. Qin and R. Balendra, " The limiting aspect ratio of the PDZ in injection forging", Proc. 32nd Int. MATADOR Conf. Manchester, UK, 1997, pp349-354.

[107] R. Balendra and Y. Qin, "Material-flow considerations for the design of injection forging", Trans. ASME, J. Manuf. Sci. Eng. Vol. 119, 1997, pp350-357.

[108] J. Richert, "Stability conditions of metal flow in radial extrusion", Z. Metallkde., Bd. 79, H. 4, 1988, pp. 248-251.

[109] G.W. Vickers, A. Plumtree, R. Sowerby and J.L. Duncan, "Simulation of the heading process", J. Eng. Mat. Technol. Vol. 97, 1975, pp126-135.

[110] K. Dieterle, "Formation of folds during upsetting of hollow bodies", Proc. Of the NAMRC, 1975, pp 179-190.

[111] B. Lengyel, S. A. Shahmoradi and I. A. Chaudhry, "Cold Extrusion of Flanges on Cylindrical Hollows", 30th Int. MATADOR Conference, 1993, pp227-234.

[112] S.B. Peterson, J.M.C. Rodrigues and P.A.F. Martins, "Production of tubular components by radial extrusion-a finite element analysis", J. of Mater. Process. Technol., Vol. 45, 1994, pp. 87-92.

[113] S.B. Peterson, J.M.C. Rodrigues and P.A.F. Martins, "Extended formability limits for tubular components through combined injection forming/upsetting-a finite element analysis", Proc. Inst. Mech. Eng., Part B 209 (B2), 1995,pp107-114.

[114] W.J. Sauer, A. Gotera, F. Robb and P. Huang, "Free bulge forming of tubes under internal pressure and axial compression", Proc. 5th North America

Metalworking Research Conference, SME, Florida, 1978, pp. 228-235.

[115] J. Pipan, "Bulging process of tubes loaded by inside pressure and axial pressure force", PhD. Thesis, University of Ljubljana, Slovenia, 1993.

[116] M. Motomura and K. Inoue, "Deformations pattern of unaxisymmetrical flat aluminium products by lateral extrusion method (Part II)", Light Metal, Vol. 43, No. 12, 1993, pp. 683-687.

[117] Y. Qin and R. Balendra, "Preform design for eliminating folding defects during injection forging of engineering components", Proc. 14th International conference on CAPE, Tokyo, 1998, pp. 307-312.

[118] Y. Qin and R. Balendra, "An approach for the forming of large-thickness-flange components by injection forging", J. of Mater. Process. Technol., Vol. 145, 2004, pp. 153-162.

[119] S.B. Petersen, R. Balendra, J.M.C. Rodrigues and P.A.F. Martins, "Avoid defects in radially extruded parts by performing", J. of Mater. Process. Technol., Vol. 69 (1-3), 1997, pp. 155-161.

[120] T. Wanheim, V. Maegaard and J. Dankert, "The physical modelling of plastic working processes", Keynote paper, 1st ICTP, Tokyo, 1984.

[121] S. Glibbery and T. Wanheim, "Geometrical analysis of 3-D bulk-forming processes by physical simulation", Annals of the CIRP Vol. 39, (1), 1990, pp. 223-226.

[122] T.P. Ghosh and D.K. Tripathy, "Approximate stress analysis of radial extrusion", J. Inst. Eng. India, Vol. 63, Part ME 2, 1982, pp. 75-79.

[123] W. M. Johnson, "Engineering plasticity", Chapter 12, Van nostrand, 1973 (1975), pp. 381-414.

[124] W. A. Gordon and C.J. Van Tyne, "Injection upsetting - an upper bound analysis", Proc. of 15th NAMRC, Vol. 2, 1987, pp. 278-284.

[125] T.P. Ghosh and D.K. Tripathy, "Upper-bound analysis of radial extrusion", J. Inst. Eng. India, Vol. 63, Part ME 6, 1982, pp. 218-221.

[126] B. Avitzur, "Metal forming and processes", McGraw-Hill, New York, 1968.

[127] R. H. Wagoner and Jean-Loup Chenot, "Fundamentals of metal forming", John Wiley & Sons, New York, 1997.

[128] S. Kobayashi, S. Oh and T. Altan, "Metal forming and the finite-element method", Oxford University Press, 1989.

[129] Rowe, G. W., "Principles of industrial metalworking processes", Edward Arnold, London, 1977.

[130] Altan, T., Oh, S. I.,and Gegel, H., "Metal forming: fundamentals and applications", American Society for Metals, Metals Park, Ohio, 1983.

[131] A. S. Wifi, "Large strain elastoplastic analysis of some hydrostatic pressure-aided deformation processes", Proc. of Int. Conf. Numerical Methods in Ind. Forming Processes, 12-16, July, Swansea, UK, 1982, pp. 135-144.

[132] R. Balendra, D. Colla and S.B. Petersen "Simulation of preform design for injection forging of tubes", Proc. 11th NCMR, Leicester, UK, 1995, pp. 82-86.

[133] R. Balendra, S.B. Petersen and D. Colla, "Preforming considerations for the injection forging of tubes", Proc. 11th CAPE Conference, London, UK, 1995, pp. 79-84.

[134] Y. Qin and R. Balendra, "Friction and numerical modelling in injection forging", Proc. 13th NCMR, Glasgow, UK, September, 1997, pp. 470-475.

[135] J. S. Welsh and D. F. Adams, "Development of an Electromechanical Triaxial Test Facility for Composite Materials", Int. J. experimental mechanics, 40, No. 3, 2000, pp312-320.

[136] W. Chen and F. Lu, "A Technique for Dynamic Proportional Multiaxial Compression on Soft Materials", Int. J. experimental mechanics, 40, No. 2, 2000, pp226-230.

[137] W. Chen and G. Ravichandran, "An Experimental Technique for Imposing Dynamic Multiaxial-compression with Mechanical Confinement", Int. J. experimental mechanics, 36, No. 2, 1996, pp155-158.

[138] W. Chen and X. Zhang, "Dynamic Response of Epon 828/T-403 Under Multiaxial Loading at Various Temperatures", Transactions of the ASME, Journal of Engineering Materials and Technology, 119, 1997, pp305-308.

[139] Michael S. Sacks, "Biaxial Mechanical Evaluation of Planar Biological Materials", Journal of Elasticity, vol. 61, 2000, p199-246.

[140] M. Tuttle, P. Singhatanadgid and G. Hinds, "Buckling of Composite Panels Subjected to Biaxial Loading", Proceedings of the Society for Experimental Mechanics, INC. Vol. LVI, p191-201, 2000.

[141] K. Buet-Gautier and P. Boisse, "Experimental Analysis and Modeling of Biaxial Mechanical Behavior of Woven Composite Reinforcements", Proceedings of the Society for Experimental Mechanics, INC. Vol. 41, No. 3, 2002, p260-269.

[142] D. J. Hitt and M. Gilbert, "A Machine for the Biaxial Stretching of Polymers", Journal of Polymer Testing, Vol. 13, No. 3, 1994, pp219-237.

Chapter 3

Selection of Pressurising Materials

In this chapter, following an introduction to the deficiencies of both the selection and evaluation of the performance of pressurising materials for PAIF with the previous research in **Section 3.1,** materials selected and equipment involved are described in **Section 3.2.** The procedures used are explained in **Section 3.3.** The results are shown in **Section 3.4.** Discussion on the results is conducted/presented in **Section 3.5.** Conclusions and references are given in **Section 3.6** and **Section 3.7,** respectively.

Nomenclature

r_i inner radius of the tubular billet

r_o outer radius of the tubular billet

t_f thickness of the tubular billet $t_f = r_o - r_i$

d_i inner diameter of the tubular billet

d_o outer diameter of the tubular billet

r_f final flange radius of the component

d_f final flange diameter of the component

d specific flange diameter of component $d=d_f/d_o$

d_r diameter of the polymer rods

p_i forming pressure applied by injection punch

p_p forming pressure applied by pressurising punch

h_f thickness of flange or free-gap height of die-cavity (pdz)

P force for compression of compound cylinder

D1 diameter of polymer rod

D2 outer diameter of compound cylinder

H height of compound cylinder

σ_{op} flow stress/yield strength of pressurising material

3.1 Introduction

Pressure-assisted injection forging (*PAIF*) has been proven to be an efficient means to produce thick-walled tubular components with hollow flanges [1-3]. The configuration of the process is shown in Fig. 3.1, in which both the beginning and the final stage of PAIF of a thick-walled tubular component are depicted. Clearly, during this process, the thick-walled tube needs to be not only externally contained by the injection chamber, to provide additional stability to the tube, but also internally supported by the pressurising material, to prevent the tube from inward collapse, and more importantly, to transmit the forming force from the pressurising punch to the work-material to produce a sound thick-walled tubular component.

However, previous research revealed that besides for the friction in the injection chamber, which significantly prescribes the process limit [4], efficiency of the pressure-assisted process is also largely prescribed by the performance of the pressurising material used. Polymers may have advantages over hydraulic media: avoiding problems such as sealing, only requiring simple tools, machinery and controls [5]. Forming of thick-walled tubes, however, invariably requires fine control on the deformation of both, the pressurising-material and the work-material, development of the proposed technology [1-3] would require wider ranges of investigation on the performance of the polymers as the pressurising media for the process [6]. Depending on the component-form to be produced and the work-material used, the type of the pressurising material to be used will have to be determined with reference to the forming processes [6]. Although a few initial examinations on the pressurising-materials were conducted with reference to different forming sequences previously, from which feasibility of PAIF was originally defined and the relatively better pressurising-material (Polyethylene) was identified [1-3], only a small range of pressurising-materials were tested. The method used in the previous research may also be timing-consuming, since the full-scale experiments were carried out to examine the feasibility of the pressurising materials

for PAIF, particularly, when a large number of polymers (like the research presented in this chapter) need to be qualified.

In this study, based on the evaluation of the engineering aspects of PAIF applications and the definition of criteria of selecting pressurising-materials for PAIF, all possible pressurising-materials were selected and tested. Particularly, a simplified configuration for testing pressuring-materials (rubber-like materials) under larger scale deformations and nearly confined compression conditions for PAIF was proposed and used to replace the previous expensive one. The experimental results (compression of compound cylinders) were validated by tube forming experiments and FE simulation results. The findings from this study on the issues of concerning the selection, performance of the pressurising materials and the process design considerations for the Pressure-assisted injection forging of thick-walled, tubular components with hollow flanges are reported.

3.2 Materials and Equipment

3.2.1 Engineering aspects of PAIF applications

Engineering application of PAIF successfully will no doubtfully contribute a lot to the increased use of tubular components, to replace the still largely used solid components in automotive and aerospace industries. Therefore, the overall weight of the vehicles, consumption of the fuels and the pollution caused by the use of vehicles can, obviously, be reduced.

The research, conducted previously and in this PhD study, has identified three principal factors, which significantly prescribe the engineering applications of the technology (*PAIF*). One of these is friction in the injection chamber, and hence, forming-pressure requirements were studied experimentally, numerically and analytically in the previous research [4], as well as in this PhD study (refer to

Chapters 5 and **6**). Another are the mechanical properties and performances of the pressurising-materials used, and hence, evaluation of the feasibility to form sound component-forms and qualification of mechanical properties of P-Ms were addressed in the study (refer to **Chapters 3** and **4**, respectively). The third factor is forming sequence, and hence, the requirements on machine/tool control were determined in the study as well (refer to **Chapters 3** and **6**, respectively). In one word, due to all the three factors, which largely prescribe the process limitations and its engineering applications, the research was, therefore, conducted to address those three issues through years [1-4, 6-8]. Based on these practices, engineering components – pre-form of hollow-gear-shafts, was carried out, from which feasibility of engineering applications of PAIF was verified.

In this chapter, the work done concerning the selection and examination of the pressurising materials (factor 2) for PAIF is described in the following sections.

3.2.2 Requirements on the properties and criteria for selecting pressurising materials

3.2.2.1 Requirements

As shown in Figs. 3.1 and 3.2, during PAIF of thick-walled tubular components, the pressurising materials are under confined compression conditions, which may be several orders higher than their yield strength, particularly, during the final stage of the process. For instance, such a ratio of $p_p / \sigma_{op} = 4.19$ was needed for a specific component geometry (model B, when an upper bound solution developed was used, refer to **Chapter 5**). Therefore, the pressurising material must be able to transmit such a high pressure from the pressurising punch to the work material effectively and without damage (cracks) during the loading phase. Also, the pressurising materials should have good thermal properties to sustain the rising temperature from 20^0C to about 300^0C (surrounding media). Ideally, after the completion of the final stage die

filling, the pressurising materials should also be able to return to their original dimensions and shapes during the unloading phase. So that the pressurising materials could be reusable and the separation of the pressurising materials from the components could be done easily.

3.2.2.2 Criteria

The criteria for the selection of the pressurising materials, therefore, should be that the selected pressurising materials should have larger elongation, good elasticity, lower strength, smaller compressibility and better thermal properties to meet the above working conditions and performance requirements for PAIF. The availability in a-rod-form from the market and the cost-implication of the application should also be taken into account.

3.2.3 Selection of Pressurising Materials

3.2.3.1 Review of the use of polymers

In order to select all possible pressurising materials for testing for PAIF, a wider range of investigation on the use of polymers was conducted. The investigation results demonstrated that the development of the polymer industry has reached a high level of commercial importance, involving many new products, industrial participants, and a large number of strong academic research groups. In fact, various products, such as constructive materials, automotive components and household utensils made of polymers, are more and more widely used nowadays [9]. Moreover, the use of polymers in metal forming [5] has brought a great deal of benefits, such as reducing the use of the expensive tool steels, the cost of the die making and improving the quality of work-pieces in sheet metal forming and thin-walled tube forming.

3.2.3.2 Materials selected for PAIF

Among a variety of the polymer products, however, not every type of the polymer products can be a pressurising material for PAIF. In other words, priority and favourite were only given to those with good elasticity, larger elongation, lower strength, smaller compressibility, etc., as well as availability in a rod-form, and cost-implication of the application. Based on these criteria, seven types of polymer products, as shown in Table 3.1, were selected for testing; all of these are available from the market, in a rod-form. Six groups of polymer specimens, in-a-rod-form, are shown in Fig. 3.2. They are Natural Nylon 66, Red Qsash (Ether Purod), PTFE, Natural HDPE (Polyethylene), Solid Nitrile642 (rubber) and Neo Sponge.

Work-materials (tubular cylinders) selected for the testing are also shown in Table 3.1. Two types of tubular materials were used in this study: one was low carbon steel which had a flow characteristics of $\sigma=715(0.001+\varepsilon)^{0.18}$ MPa [10]; another was pure aluminium (E1CM) which had a following flow characteristics of $\sigma=135(0.07+\varepsilon)^{0.33}$MPa. One group of the assembled specimens - compound cylinders (low carbon steel with Red Qsash (Ether Purod)) are shown in Fig. 3.3.

In addition, the aluminium tubular material and the selected, best P-Ms (Solid Nitrile/rubber and HDPE/Polyethylene) as well as the worst P-M (Red Qsash/Ether Purod) identified by the initial compression tests were further used to form the hollow flanges with a view to validating the compression test results. Some of the specimens prepared for the forming of hollow flanges are shown in Fig. 3.4.

3.2.4 Equipment

A 90 tones TINIUS OLSEN universal test machine as shown in Fig. 3.5 was used for both the compression of compound cylinder tests and the tube forming experiments for validating the compression test results; it mainly consists of a motor driven

mechanical leads-screw press, a dial gauge control panel, a XY plotter and a PC based data-log. The force and displacement for the analysis of compression of the compound cylinder tests were recorded using a built-in load cell and a PT-101-0010 Wire wound transducer, respectively. Both the load cell and the transducer were connected to the PC for automatic data acquisition.

To carry out the forming of hollow flanges experimentally, an additional independently-controlled hydraulic ram mounted against the mechanical platen (cross head) of the above universal test machine was used, as shown in Fig 3.6. Two sets of tools were also developed for the tube forming tests as described in **Chapter 5**: one was a set of dies that enabled the forming of hollow flanges and another was a set of hydraulic/mechanical punches that enabled pressurisation onto the pressurising medium, as shown in Fig. 3.7. The die-cavity was designed for the production of a circular, hollow flange. The total forming pressure and corresponding injection punch's displacement were recorded automatically with testing machine (attached load cell and transducer) during the whole process of the compression of compound cylinder tests. The pressure levels within the pressurising material and the displacement of the pressurising punch were recorded using a 808-141 dial Hydraulic pressure gauge attached to the hydraulic system and a DCT1000A LVDT transducer attached to the crosshead (mechanical platen) of the testing machine, respectively (Fig. 3.6.).

In addition, an FE Code of ABAQUS [11] and a Silicon Graphics Workstation were also used to conduct FE simulations for both the compression of compound cylinders and the forming of hollow flanges. The software provides an option on the formulas of the strain energy function for modelling hyperelastic materials, like rubbers.

3.3 Procedures

Studies of the configuration shown in the Fig. 3.1 and development of the corresponding process design procedures have included not only the selection of the pressurising materials, but also the testing of these materials, conducting forming simulations and experiments.

3.3.1 Simplified configuration for the confined-compression tests of compound cylinders

As mentioned in **Section 2.7**, many efforts were devoted to the development of experimental methods and techniques, with a view to testing either metallic or non-metallic materials under tri-axial compression (loading) conditions. However, none of these is suitable for examining the rubber like pressurising materials, under confined conditions and particularly under larger scale deformations (for PAIF).

A simplified configuration that can be used to create a nearly confined compression condition was, therefore, proposed to examine the performance of the selected pressurising materials which would undergo larger deformations. The configuration of the simplified test is shown in Fig. 3.8. The specimen design and testing considerations to ensure the functional performance of the tests are described in the following sections.

3.3.2 Specimen design and testing considerations

3.3.2.1 Specimen design

To enable the creation of a nearly confined compression condition while the materials still can undergo a larger deformation, compound cylinders were used for the compression tests. A compound cylinder is an assembly of the pressurising-material (polymer rod) and the work-material (tubular billet), refer to Fig. 3.3. The

pressurising material which is in a-rod-form (Fig. 3.2) was inserted into the tubular cylinder (Fig. 3.3) which was made of either low carbon steel or pure aluminium, refer to Table 3.1. All aluminium specimens were machined from a 38mm diameter E1CM pure aluminium bar to the required external and internal dimensions of 35mm and 14.9mm, respectively (Table 3.1). All the low carbon steel specimens were also machined from a 36mm diameter standard carbon steel bar to the required outer and inner diameters of 35mm and 12.25mm to 16.10mm, respectively, for different pressurising materials (Table 3.1). The pressurising materials were simply cut from the standard bar sizes to the required length of 35mm (Table 3.1). The internal diameters of the tubes were determined by considering 0.1mm clearance between the tube and the polymer rod to provide a light push fit and to apply the lubricants for most of them. The external diameter and height of the tubes were determined based on the supporting information from the initial FE simulation with a view to ensuring the model to produce a mainly radial expansion under the axial compression.

To verify the compression test results with the forming of hollow flanges, eight groups of pure aluminium tubes with the inserted rod-form pressurising materials were also designed, which referred to five different pressurising materials and two different tube lengths refer to Fig 3.4 and Table 3.2. Clearances of the specimens between the aluminium tube and the polymer rod were determined to use the same value (0.1mm) as that for the compound cylinders. Two different lengths of 230mm and 160mm of the specimens were designed with a view to producing the hollow flanges with different diameters, in this case d_f=85mm and 60mm, respectively. Dimensions of the tube forming specimens are shown in Table 3.2. Both billet/die and polymer/work-material interfaces were lubricated with the identified optimal lubrication scheme, as for some of the compression of compound cylinder tests, to reduce the forming force-requirement and to ease sliding of the work material and polymer along the die and inner surface of the tubular billet.

3.3.2.2 Testing considerations

Since friction over a contact interface prescribes the tube forming process significantly, an optimal lubrication scheme, which was identified previously [4] was, therefore, used for this simplified configuration-compression of the compound cylinders. Previous research results showed that friction at a contact interface was greatly reduced by the combined use of Zinc Stearate powder with, either Molybdenum Disulphide grease or Teflon grease. The use of the improved lubrication procedure in this test would allow the ease of sliding of the polymer along the inner surface of the cylinder, and hence, allowed to better examine spring-back performance of the polymer after unloading.

By carefully designing the specimen geometry and using the optimal lubrication scheme - a hybrid lubrication procedure [4], uneven bulging of the specimen under axial compression could be avoided and each section of the specimen would be mainly radially expanded. Under such a circumstance, it may be assumed that the stress within the pressurising material is nearly hydrostatic, which was confirmed by the FE simulation results as shown in Fig. 3.9. Using this configuration, performance of the pressurising materials under a high pressure level can be examined (stress, strain, compressibility, etc.). Spring-back of the material after unloading (the ram retracts) and the damage of the material can also be assessed. In addition, using different types of work-materials, tube-thicknesses and different scales of the deformation of the specimens, different pressure levels within the pressurising materials can be achieved. The relationship of the performance of the pressurising material with its inside pressure level can, therefore, be established.

In this study, apart from the seven groups of well lubricated specimens, two groups of three specimens in each group with the lubricant of zinc powder only and another two groups without lubricant were also used for the tests. Therefore, the performances of the selected pressurising materials were examined under different friction conditions, different work materials, pressurising materials and different

thicknesses of the tubular cylinders with the compression of compound cylinder tests.

3.3.3 Experiments

Compression tests on the compound cylinders (Fig. 3.3) were conducted to assess the performance of the polymers, which may be suitable for functioning as a pressurising medium for the PAIF application. The experimental set-up is shown in Fig. 3.10.

Compound cylinders from each group were compressed to different heights, i.e., from 35mm (original height of the compound cylinders) compressed down to 25mm, 15mm and 5mm, respectively, to show the sequence of the deformation and to study the influence of different deformation scales to the performance of both the work- and pressurising-material. Two groups of the specimens produced by the compression tests are shown in Fig. 3.11. Performance of the polymers was assessed with reference to the pressurisation, spring-back and damage of the pressurising materials, as well as deformation of the tubes. Influence of the friction condition at the tube/pressurising-material interface was also investigated, which referred to the use of different lubricants.

In addition, the forming of hollow flanges was also performed experimentally with the same universal testing machine as that for the compression of compound cylinders, apart from an additional independently-controlled hydraulic ram mounted against its mechanical platen (cross head), as shown in Fig 3.6. The injection and pressurisation were effected by tubular injection punch and rod pressurising punch, respectively. Under the actions of both punch pressures, the cylinder specimens with the height of 230mm were compressed down about 145mm and deformed into the thick-walled and hollow flanged tubular components with a diameter of 85mm, as shown in Fig. 3.12 (a). The cylinder specimens with the height of 160mm were compressed down about 60mm and deformed into the thick-walled and hollow flanged tubular components with a diameter of 60mm, as shown in Fig. 3.12 (b).

Performance of the polymers was, therefore, further examined using these tube forming experiments.

3.3.4 FE simulations

FE simulation of compression of the compound cylinders was initially conducted with a view to providing the supporting information. Based on the supporting information, an "optimal" specimen-geometry which referred to the establishment of a nearly-confined compression conditions was established. The model and the results are shown in Fig 3.9. The cylinder was designed to achieve nearly-parallel expansion (radially) of the tubular billet, under axial compression. Under such a circumstance, it may be assumed that the pressuring medium is under a nearly confined condition. Performance of the pressurising material was assessed under such a condition, which is similar to the working condition that would occur during the forming of an engineering tubular component (Fig. 3.1). Such an arrangement significantly simplifies traditional setup of the experiment for testing materials under confined conditions which either used a hydraulic chamber or three axis's compression test machine/apparatus [12-14].

During the FE simulation, rubber-like pressurising materials-Solid Nitriles were modelled using hyperelastic material-models provided in ABAQUS [11]. The rest of polymers, (such as Natural Nylon 66, PTFE and Natural HDPE/Polyethylene) were modelled using elastic-plastic models. The work materials (low carbon steel and aluminium tubes) were also modelled using the elastic-plastic model. Since the rubber-like pressurising materials are highly confined during both, compression (Fig. 3.9) and particularly during the tube forming (Fig. 3.13), the models were tested and compared to enable a correct modelling on the compressibility of the materials. The rubbers (Solid Nitriles), which are preferable for the use in PAIF should have very little compressibility. At the same time, these materials, normally, have certain shear flexibility. Such a combination creates particular problems in modelling the materials under a highly confined condition. In ABAQUS, a hyperelastic material is described

in terms of a "strain energy potential" [11], which defines the strain energy stored in the material per unit of reference volume (the volume in the initial configuration) as a function of the strain at that point in the material. Three strain-energy-function forms provided in ABAQUS - Mooney-Rivlin form, Ogden form, Polynomial form, were tested, respectively, for both configurations - compression of the compound cylinders and forming of the hollow flanges. The Ogden form was eventually used for the simulations due to a good numerical convergence obtained during the simulations. The stress strain data of the selected pressurising materials were obtained from the uni-axial, bi-axial, planar tensile and compressive tests conducted in **Chapter 4** for the simulations. The models were further compared with reference to numerical stability, solution convergence as well as experimental results.

3.4 Results

Seven groups of the compound cylinders with the optimal lubrication scheme and two groups of the compound cylinders with zinc powder only or without lubricant were tested; two groups of the tube forming experiments were also conducted. Some of the experimental results for both the compression of compound cylinders and the tube forming are shown in Figs. 3.11 and 3.12, respectively.

In addition, selected pressurising materials were further assessed using FE simulation by analysing pressure and stress distributions in the materials, for which FE-result output locations were defined as shown in Fig. 3.14. Four locations (A-D) across the middle section of the specimen (horizontal) were defined for the output, for both, compression of the compound cylinders and the forming of the hollow flanges. Five locations (E-I) along the central axis (longitudinal) of the hollow flanged component were also chosen for output (Fig. 3.14 (b)). Fig. 3.15 shows Pressure/Mises stress histories in the two types of pressurising materials - Rubber (Solid Nitrile) and Polyethylene (HDPE), at four locations, respectively. Low carbon steel was the work-material in both cases. Subsequent to investigation on the performance of the

pressuring materials subjected to compression, FE simulations were conducted to examine feasibility of the polymers functioning as a pressurising medium for pressure-assisted injection forging applications. A rubber which was fully incompressible and one with a small compressibility were tested - deformations and pressure distributions are shown in Fig. 3.16. Punch-force/time histories were also examined for three types of materials, as well as two different hyperelastic models as shown in Fig. 3.17. Further, deformations and stresses in a rubber material, under both, the loading (forming) and unloading (punch retracts) conditions during the forming of the hollow flange were also investigated; the results are shown in Figs. 3.18 and 3.19 for locations A-D and E-I, respectively.

3.5 Discussion

3.5.1 Selection of the pressurising materials

Pressurising materials which were used in metal forming were, previously, largely hydraulic media. Elastomers, such as urethane, natural rubber and polyethylene, are now widely used because these render some particular merits for manufacture. Applications of these materials have been seen largely in the forming of sheet metals or thin-walled tubes as mentioned in **Section 3.2.3**. The configuration developed for the forming of thick-walled tubes (Fig. 3.1) requires much higher working-pressures than that involved in the forming of a sheet metal or a thin-walled tube. Performance of the pressurising material under a high working-pressure, therefore, needed to be examined, with a view to defining an "optimal" combination – between the pressurising medium, work-material type and the component-form to be produced.

As mentioned in **Section 3.2.3**, pressurising materials for this study were selected by taking following several factors into account - good elasticity, larger elongation, lower strength, better thermal properties and commercial availability of the products, particularly, compressibility of the materials. If the volume loss (Fig. 3.16 (b)) of the

pressurising material due to its compressibility could be sufficiently compensated at the beginning of the process, using a step punch and under a reasonable pressure level, which should be roughly same as the pressure level designed for the forming sequence, there might be a possibility to use a simplified process configuration (a single step punch may be used) for PAIF as shown in Fig. 3.20 to replace the configuration developed previously (two punches were used) for PAIF of thick-walled tubular components, as shown in Fig. 3.1. Such a simplification would allow the process to be carried out on a general-purpose press without the subsystem to control the pressurising punch. In other words, the effectiveness of the process simplification for PAIF would be largely dependent on the compressibility of the pressurising material in supporting the work-material and transmitting the force from pressurising punch to the work material, which was proven to be the case by the FE simulation (Fig. 3.16). In addition, it seems that the use of a pressurising material in PAIF would mean that the pressurising material may have to remain to be inside the component, if the tube undergoes a larger or complex plastic deformation. The experimental results derived recently also showed that it is unlikely for the pressurising material to be fully "cleaned" out by its self after unloading. A subsequent ejection process may be able to eject the pressurising material out of the tubular component. However, the pressurising material would not be reusable in this case. If the existence of the pressurising material within the tubular component would not affect its applications, they may be left inside after the manufacture. Therefore, a material which is able to fully spring back to the original shape after the punch retracts would be an ideal pressurising medium for PAIF applications. How such types of the materials may behave during the PAIF of thick-walled tubes was not known yet. This was a reason that such materials have been bought for testing.

Hence, it would have included more pressurising materials for testing if such materials were available in a rod-form, from the market. The pressurising material, which was identified to be "optimal" for the PAIF application in this study, therefore only represents a relatively optimal solution among currently available pressurising materials.

3.5.2 Design of the experiment

Upsetting of the compound cylinders was conducted to examine performance of the pressurising materials under the nearly-confined conditions. The configuration (Fig. 3.8) was used rather than that traditionally used for the confined pressurising tests (such as use of hydraulic chambers or applying pressures by tri-axial mechanical loading). By properly designing dimensions of the cylinder and applying friction at the material/punch and material/anvil interfaces, certain pressure-levels can be achieved within the polymer. Pressures and Mises stresses presented in the Fig. 3.15 shows no significant differences in these values, among the four locations examined. Although the material undergoes radial expansion, it may still be treated as a nearly-confined condition. The configuration is unable to generate a fully confined condition, the condition created by this configuration is, however, closer to a real working-condition of a pressurising medium during PAIF, as shown in the Figs. 3.1, 3.13 and 3.16.

One of the advantages of using the configuration shown in the Fig. 3.8 is that the pressure level generated within the material (polymer) to be tested can be pre-determined by properly designing the geometry (e.g. the wall thickness of the cylinder), selecting the work-material (e.g. steel, aluminium, etc.), applying certain friction conditions, and controlling the scale of the deformation (punch displacement). It, therefore, renders flexibility to study mechanical properties of the pressurising media (solid polymers) for PAIF applications. At a similar pressure level to that required to form an engineering component, feasibility of a polymer functioning as a pressurising medium may be, initially, determined by conducting a compression test of the compound cylinder. Such a test is much simpler than an actual forming experiment of producing an engineering component and, therefore, reduces the cost of the tests.

3.5.3 Performance of the pressurising materials

3.5.3.1 Under the conditions of compression of compound cylinders

Although mechanical properties of the selected pressurising materials (polymers) (Table 3.1) had been well defined under general conditions, their performance under very high and confined pressures (> 100 MPa, refer to Fig. 3.15) as well as subsequently being subjected to unloading (Fig. 3.8 (b)) was not studied sufficiently. The experimental results of compression of compound cylinders in this study suggested that rubbers (Solid Nitriles) might be the better materials to function well as a pressurising medium for PAIF applications, due to their high elasticity, less compressibility and certain strength. For instance, both Solid Nitrile 641 and 642 showed excellent ability to transmit pressure onto the inner surface of the work-material, while they can still almost fully spring back after the unloading (Fig. 3.11 (a)). Among the rest five types of polymers (Natural Nylon 66, Ether Purod/Red Qsash, PTFE, Natural HDPE/Polyethylene and Neo sponge), Neo sponge showed the biggest compressibility and therefore was defined to be unusable for PAIF. Ether Purod/Red Qsash showed the best elasticity but the worst ability to achieve enough radial expansion (radial strain) for PAIF, therefore, the polymer of Ether Purod/Red Qsash was also classified to be not suitable for PAIF. Natural Nylon 66 and PTFE showed good pressure-transmission ability but limited radial expansion ability and small elastic working ranges, therefore they may be suitable to form the hollow flange with relatively small diameters. Natural HDPE/Polyethylene demonstrated good pressure-transmission ability, larger radial expansion ability (suitable for forming hollow flange with relatively larger diameter), but small elastic working range, therefore, plastic deformations within this material during the forming of hollow flanges will be inevitable. Occurrence of permanent deformation, which was also indicated by the Mises stress distribution in the Fig. 3.15 (b) for a Natural HDPE/Polyethylene (pressurising material), suggests that the pressurising material may remain inside the work-piece, after unloading. As mentioned before, if the existence of the pressurising medium within the component would not affect its

applications in engineering, these materials may be left inside the component after the manufacture. Also the polymers with a lower elasticity normally suffered some damages, such as cracks after unloading. The development of such cracks within these materials after unloading was observed from the specimens. The reason may be due to that the change of stress state within the pressurising materials during unloading, i.e., the confined condition no longer existed and the shearing stresses developed simultaneously.

To achieve a large strain within the work-material during PAIF, rubbers (similar to Solid Nitriles) may be used. Under the confined conditions, the rubber (Solid Nitrile) functions almost like a liquid-type medium, due to its high elasticity and very low strength (Fig. 3.15 (a)). The stress state can, therefore, be approximately treated as hydro-static for a simplified analysis.

From above analysis, it can be summarized; Solid Nitrile642 and 641 are the best ones to be the pressurising materials for PAIF. Natural HDPE/Polyethylene is the second best. Natural Nylon 66 and PTFE are ranked the third position. The worst ones are Neo sponge and Ether Purod/Red Qsash.

3.5.3.2 Under the conditions of forming of the hollow flanges

As mentioned in **Section 3.3.3**, forming of hollow flanges was further conducted experimentally and computationally with two objectives in mind. One was verifying the above testing results, i.e., using the simplified configuration - compression of compound cylinders. Another was confirming the importance of mechanical properties of a pressurising medium in the support of the work-material during the forming of hollow flanges with PAIF.

3.5.3.2.1 Forming of the hollow flanges experimentally

In PAIF, the pressurising material was inserted into the tube to prevent the tube from collapse; the compound tube was then contained in the injection chamber before being injected into the die-cavity. Since the injection chamber can provide additional stability to the compound tube during injection forging, larger volume of both pressurising-material and work-material can be injected into the die cavity by forces applied by both injection and pressurising punches, respectively. And more importantly, due to the use of the separately controlled pressurising punch, a much higher pressurisation can be effected, hence, thick-walled tubular components with hollow flanges can be formed. Correspondingly, performance of the pressurising materials identified by the compression tests can, therefore, be further examined with these forming experiments.

With reference to different pressurising materials and different diameters of the hollow flanges formed, the experimental results in sectioned views are shown in Fig. 3.21. As can be seen, the hollow flange formed with Solid Nitrile (642 or 641) demonstrated the best die filling, even wall thickness and the best spring back (though not fully) ability (Fig. 3.21 (a) and (e)) after unloading. The component formed with HDPE/Polyethylene (Fig. 3.21 (b) and (f)) showed the second best result, i.e., compared with Solid Nitrile, only the spring back ability after unloading was worse than that of using Solid Nitrile. Hollow flanges formed with Nylon 66 and PTFE (Fig. 3.21 (d)) represented the worse die filling ability, than Solid Nitrile and HDPE, uneven wall-thickness and similar spring back ability to that of HDPE/Polyethylene. This was because these polymers possessed the less radial expansion ability as observed in the compression of compound cylinder tests. Similar tubular component produced with Ether Purod/Red Qsash (Fig. 3.21 (c) and (g)) showed the worst die filling ability, uneven wall-thickness, though the best spring back ability after unloading. Due to its worst radial expansion ability and its largest elastic instability (twist of the polymer rod) during tube forming, such undesired results were obtained for forming either large diameters (85mm) or small diameters (60mm) of the hollow flanges.

It is clear that the results of forming of hollow flanges verified the test results of compression of compound cylinders. Namely, Solid Nitrile and HDPE are the best pressurising materials for PAIF of thick-walled tubes; Ether Purod/Red Qsash and the Neo sponge are the worst ones (useless) for PAIF; Nylon 66 and PTFE are ranked between the best and the worst ones.

3.5.3.2.2 FE simulation of the forming of the hollow flanges

The further FE simulation of the forming of a hollow flange with PAIF was also conducted, which confirmed the importance of mechanical properties of a pressurising medium in the supporting of the work-material during the tube forming process. It is evident that a fully incompressible pressurising material (similar to Solid Nitrile and HDPE which have small compressibility) will be able to effect a successful forming of the components (Figs. 3.16 (a)). The FE result also showed good agreement with the experimental results (Fig. 3.21 (a), (b), (e) and (f)). The process will fail to produce a sound hollow flange, if the pressurising material is compressible (like Neo Sponge) or unable to produce enough radial expansion (like Ether Purod/Red Qsash in the experiment) as shown in Figs. 3.16 (b). These also agreed well with the experiments (Fig. 3.21 (c), (d) and (g)). Collapse of the tube to form a fold at the flange will, therefore, terminate the forming process. For the pressurising material which has small compressibility, initial pressurisation onto it may help to compensate the volume loss of the pressurising material. This may be effected using a stepped punch as shown in Fig. 3.20. The stepped geometry may be pre-determined through FE simulation. Iteration may also be required to finalise the tool design. Using a stepped punch to effect initial pressurisation rather than using two separately controlled punches - the pressurising punch and the injection punch, as used currently in this research, would significantly simplify requirements on the machinery and tooling if the concept is feasible.

FE simulations of forming of an aluminium hollow flange with different pressurising materials were also conducted. The results showed that for forming a same hollow

flange, using a rubber as the pressurising medium would result in a lower forming force requirement (about 30% reduction) than that for using aluminium as the pressurising material, as shown in Fig. 3.17, since using an aluminium as a pressuring medium seems represented the feature of the forming of a solid bar. The results presented in the Fig. 3.17 also suggest that there will be no significant differences in the forming force requirement between the processes using the rubber (Solid Nitrile) and that using Polyethylene (HDPE). Polyethylene may, therefore, be equally used as a pressuring medium in PAIF as a rubber-like material. Except that its spring back ability is worse than rubber (Solid Nitrile) (Fig. 3.21 (a), (b), (e) and (f)). FE simulation results showed that if a pressurising material (rubber/polymer) possesses both a full incompressibility and large radial expansion ability, it will be no doubt to function well as the pressurising medium for PAIF of thick-walled hollow flanges. One of such examples is shown in Fig. 3.13, which was already confirmed by the experimental results of forming hollow flanges (Fig. 3.21 (a), (b), (e) and (f)).

FE simulation results shown in Figs. 3.18 (a) and 3.19 (a) show that the pressure distributions within the rubber are almost uniform; only small Mises stresses are generated. These results may suggest that the damage would not occur within the rubber, during the forming. During the unloading (Figs. 3.18 (b) and 3.19 (b)), only rubber at the two ends of the component had sprung back. High pressures sustained in the middle sections of the rubber after the punch retracts also indicates that due to non-uniform contraction of the tube during the unloading and friction between the rubber and the work-piece the rubber may not be able to freely spring back, as it was expected. This was also confirmed by the forming (hollow flange) experiments (Fig. 3.21.

3.5.4 Concurrent design and manufacture

It is evident that the forming process is largely prescribed by the type of the pressurising materials used, i.e., using a pressurising material, which has small

compressibility and large radial expansion ability, a sound hollow flange with either small (d<1.71) or large specific diameter (1.71<d<2.43) can be formed. While using a pressurising material, which has limited radial expansion ability, a hollow flange with a samll specific diameter (d<1.71) may only be formed, but it is impossible for the forming of a similar component with large specific diameter (1.71<d<2.43). Therefore, a forming process design would have to be carried out with reference to the selection of the pressurising materials. Iterations, which would include qualification of mecahanical and physical properties of the pressurising material, design of the punch geometry, and conducting forming-simulations, would be invariably needed to determine the forming die geometry and process parameters. A general procedure to effect concurrent design and manufacture of the engineering components has been developed which includes the following steps:

(a) Studying the component-form to be produced to determine material deformations required (the scale of the deformation and extent of the ease of the material flow) .

(b) Conducting FE simulation to predict the pressure-levels to be involved during the forming of the component.

(c) Selecting pressurising materials for testing and designing the geometry of the "compound cylinders".

(d) Testing the pressurising materials by conducting compression tests on the "compound cylinders" to examine their performance under the certain pressure-levels.

(e) Designing tool/punch geometry by taking compressibility of the pressurising material into account.

(f) Conducting FE simulation to examine deformation sequences of both, the pressurising material and the work-material, and stress/strain distributions.

(g) Evaluating the process and the "component-form" simulated. Going back to the step (a) or (c) or (e), if necessary.

(h) Detailed tool-design, tool manufacturing and manufacturing tryout. Going back to the step (a) or (c) or (e), if necessary.

(i) Component manufacturing and inspection.

Further to this general procedure, a detailed approach for the synthesizing concurrent design and manufacture of sound engineering tubular components was subsequently proposed and illustrated in Fig. 3.22 by which the major factors which have siginificant effects on the design and manufacture of tubular components with PAIF are synthesized. To enable this approach, several supporting analysises, testing methods and corresponding algorithms/models, such as simplified configuration for the confined-compression tests, coupled FE modelling of PAIF, qualification of mechanical properties of pressurising materials using the unique bi-axial tension testing machine and upper bound analysis of PAIF were developed. These supporting methods/algorithms/models are described in this **Chapter 3, Chapter 4 and Chapter 5,** respectively.

3.6 Conclusions

From the study of the selection of pressurising materials and the development of process design considerations for Pressure-assisted injection forging of thick-walled tubular components, following conclusions may be drawn:

(1) Polymers may be tested using a simplified configuration - upsetting of the compound cylinders, for PAIF applications.

(2) Solid Nitriles are the best pressurising materials for PAIF among those tested; HDPE (Polyethylene) is the second best for PAIF; performances of Natural Nylon 66 and PTFE are worse than the HDPE does; Neo Sponge and Ether Purod/Red Qsash almost can not be used as a pressurising medium for PAIF.

(3) Solid Nitriles and HDPE can be used to produce hollow flanges with either small (d<1.71) or large (1.71<d<2.43) diameters due to their large radial expansion ability. Natural Nylon 66 and PTFE can only be used to produce hollow flanges with small diameters (d<1.71), because of their limited radial expansion ability.

(4) For the forming of hollow flange-type components, it is unlikely a rubber can fully spring back after the punch retracts, due to non-uniform contraction of the work-piece and friction between the rubber and the work-piece.

(5) A pressurising material which is fully incompressible and is able to fully spring back after unloading has not been identified yet.

3.7 References

[1] R. Balendra and Y. Qin, "Pressure-assisted Injection Forging of thick-walled tubes", Int. J. of Mach. Tools Manf., Vol. 35, No. 11, pp. 1481-1492, 1995.

[2] Y. Qin and R. Balendra, "Technical evaluation of pressure-assisted Injection Forging of thick-walled tubes", Advances in Manufacturing Technology IX, edited by D. Stockton and C. Wainwright, Taylor & Francis, London, pp. 62-66, 1995.

[3] R. Balendra and Y. Qin, "Feasibility and limitations of pressure-assisted Injection Forging of thick-walled tubes", Proc. of 5th ICTP in Ohio, 7-10th October, pp. 327-330, 1996.

[4] Y. Qin and R. Balendra, "Optimisation of the lubrication for the extrusion of solid and tubular components by Injection Forging", to appear in the Journal of Materials Processing Technology, 2002.

[5] S. Thiruvarudchelvan, "Elastomers in metal forming: a review". Journal of Material Processing Technology, Vol. 39. pp 55-82, 1995.

[6] Y. Qin, Y. Ma and R. Balendra, "Performance of pressurising-materials and process design considerations for the forming of thick-walled tubular components", Proc. of the 9th ISPE CE2002, July, Granfield, UK, pp. 251-262, 2002.

[7] Y. Qin, Y. Ma and R. Balendra, "Pressurising materials and process design considerations of the Pressure-assisted Injection Forging of thick-walled tubular components", Journal of Materials Processing Technology, Vol. 150, No. 1-2, pp. 30-39, 2004.

[8] Y. Ma, Y. Qin and R. Balendra, "Experimental and FE investigation of performance of polymers under confined compression conditions by using a simplified configuration", Advances in Manufacturing Technology, XVI, The 18th NCMR, 2002, pp. 203-208.

[9] G. Holden, N. R. Legge and et al., "Thermoplastic Elastomers", 2nd Edition, Hanser Publishers, 1996.

[10] A. Rosochowski and L. Olejnik, "Parameter selection in rotary forging", Proc. Of the 11th NCMR, Leicester, Sept. UK, pp. 37-41.

[11] Hibbitt, Karlsson & Sorensen Inc. 2003. ABAQUS User Manuals.

[12] J. S. Welsh and D. F. Adams, "Development of an Electromechanical Triaxial Test Facility for Composite Materials", Int. J. experimental mechanics, 40, No. 3, 2000, pp312-320.

[13] W. Chen and F. Lu, "A Technique for Dynamic Proportional Multiaxial Compression on Soft Materials", Int. J. experimental mechanics, 40, No. 2, 2000, pp226-230.

[14] C. Wang, Z. Guo and X. Zhang, "Experimental Investigation of biaxial and triaxial compressive concrete strength", ACI Materials Journal, 84-M11, 1987, pp 92-100.

Table. 3.1 Materials selected for testing

Material No.	Pressurising Material(Rod)		Work materials(Tubular Cylinder)			
	Name	d mm)	Name	(mm)	(mm)	Height (mm)
1	Natural Nylon 66	15.55	Low carbon steel	15.65	35	35
2	Red Qsash	13.70	Low carbon steel	13.80	35	35
3	PTFE	14.62	Low carbon steel	14.72	35	35
4	Natural HDPE	16.00	Low carbon steel	16.10	35	35
5	Solid Nitrile 642	12.15	Low carbon steel	12.25	35	35
6	Neo Sponge	12.21	Low carbon steel	12.31	35	35
7	Solid Nitrile 641	14.80	Aluminium	14.90	35	35

Table. 3.2 Dimensions of pressurising material rods and tubular billets

Pressurising material No.	Pressurising materials		Work materials(Aluminium)		
	Names of polymer rods	Diameter ϕ (mm)	(mm)	(mm)	Height (mm)
1	Natural Nylon 66	15.55	15.65	35	230
2	Red Qsash	13.70	13.80	35	230/160
3	PTFE	14.62	14.72	35	230
4	Natural HDPE	16.04	16.10	35	230/160
5	Solid Nitrile 642	12.15	12.25	35	230/160

Chapter 4

Qualification of Mechanical Properties of Pressurising Materials

In this chapter, after the necessity of qualification of mechanical properties of the selected pressurising materials for PAIF, is revealed in **Section 4.1**, the materials tested and, particularly, the equipment developed, as well as used for the tests, are depicted in **Section 4.2.** Procedures of conducting five types of tests, on the selected pressurising materials, are described in **Section 4.3**. Test results are presented in **Section 4.4,** prior to the discussion in **Section 4.5.** Conclusions and references are given in **Sections 4.6** and **4.7,** respectively.

Nomenclature

d	inner diameter of the bearing
D	out diameter of the bearing
W	width of the bearing
F_a	applied axial load of the bearing
F_r	applied radial load of the bearing
P_o	the load to bear with the bearings
X_o	radial load factor
Y_o	axial load factor
C_o	maximum basic static load rating
BT	biaxial tension
PT	planar tension
PC	planar compression
UT	uniaxial tension
UC	uniaxial compression

4.1 Introduction

As mentioned in **Section 2.7** and **Chapter 3**, efficiency of the proposed technology, (pressure-assisted injection forging of thick-walled tubular components), is largely prescribed by the performance of the pressurising materials (P-Ms) used. A further detailed investigation, on the mechanical properties of the selected pressurising materials, under various loading conditions (tension and compression) for PAIF would, therefore, be necessary and essential. Furthermore, the subsequent finite element simulation and forming process design also can not be carried out without sufficient material data, concerning the mechanical properties of the selected P-Ms, under different loading conditions.

To date, some improvements have been made to the proposed technology (PAIF) [1-2], by which technical feasibility and processing limitations were defined; an optimal forming sequence for PAIF was also established [3-5], with a view to producing flawless and uniform wall-thickness components with PAIF, in which the pressurising material was treated as a hydrostatic pressure, due to the lack of such test data; further to the previous examinations on the limited numbers of the P-Ms for PAIF, with tube forming procedure [3-5], the simplified configuration was attempted [6-8] in **Chapter 3** as well, in which all possible pressurising materials (available from market) for PAIF, were initially examined, under the nearly confined compression conditions. However, no efforts were made in qualifying the mechanical properties of the pressurising materials under different loading conditions, and therefore, no such technical/test data were available for the previous research.

In this chapter, further to both the initial tests (compression of the compound cylinders) and the validation tests (with forming of hollow flanges) described in **Chapter 3**, the identified pressurising materials (Solid Nitrile641 and Solid Nitrile642), were further qualified under different loading conditions, including uniaxial tension, uniaxial compression, planar tension, planar compression and

biaxial tension, respectively, to determine their mechanical properties and to establish the constitutive descriptions of the pressurising materials for PAIF.

4.2 Materials and Equipment

4.2.1 Materials

Materials tested in this research were Solid Nitrile641, Solid Nitrile642 and Neo Sponge. Although Neo sponge was identified to be unsuitable as a pressurising material for PAIF due to its larger compressibility, some of the tests were conducted on it, with a view to comparing the mechanical properties between Neo sponge and the Solid Nitriles.

4.2.2 Equipment and development

Three existing universal testing machines, i.e., a hydraulic driven one and two motor driven ones, were used; a biaxial testing machine, which was newly developed, was also used, to qualify the mechanical properties of the selected pressurising materials, namely, Solid Nitrile641, Solid Nitrile642 and Neo Sponge, under different loading conditions. The applications of the existing universal testing machines and the development of the new biaxial testing machine for the tests are described in the following **Sections 4.2.2.1** to **4.2.2.2**, respectively.

4.2.2.1 Equipment for uniaxial compression, uniaxial and planar tension tests

Uniaxial compression tests on all the materials were conducted on the hydraulic driven universal testing machine (Zwick rel 2061 MOW41), as shown in Fig. 4.1, with a maximum capacity of 50 kN and a maximum stroke of 100mm. It is well facilitated with a Strain Sert Fatigue Rated Flat load cell, mounted against the hydraulic ram, and a displacement transducer. Both load cell and displacement transducer are connected to a PC based data log for automatic data acquisition. Uniaxial and planar tensions of Neo Sponge were also conducted using the same machine as that for the uniaxial compression tests.

Due to the limited stroke, 100mm with above testing machine (Zwick rel 2061 MOW41), uniaxial and planar tension of the Solid Nitriles641 and 642, which usually have larger elongations than sponge does, were performed with one of the motor driven universal testing machines, as shown in Fig. 4.2, with a maximum capacity of 10 kN and a maximum stroke of 1000mm. The load and displacement were recorded using a built in load cell, a displacement against time transducer as well as an X-Y plot attached to the machine.

It should be pointed out that, although the maximum capacity (10kN) of the motor driven testing machine fully covers the possible maximum load with Neo Sponge specimens, its maximum stroke of 1000mm may be too large to measure the accurate test data that Neo Sponge can produce, which is usually much smaller than the Solid Nitriles. Hence, uniaxial and planar tensions of Neo Sponge were still performed, with the hydraulic driven testing machine.

Planar compression tests on all the materials were carried out using the other motor driven universal testing machine (900kN TINOUS OLSEN), which is same as that for the compression of compound cylinders in **Chapter 3** (Fig. 3.5).

4.2.2.2 Equipment for biaxial tension tests

As mentioned in **Section 4.1**, in order to establish constitutive descriptions of the rubber like pressurising materials and further to initiate elastic-plastic analysis as well as FE modelling for PAIF, apart from the above four types of tests (uniaxial and planar tension/compression), biaxial tension tests on the selected pressurising materials were required. Initial investigation was, therefore, conducted **(Section 2.7)**. Many progresses were made in the development of the equipment and facilities, to study mechanical properties of several non-metallic materials, under biaxial loading conditions [9-12]. A suitable machine for testing the issued materials and under the issued loading conditions (biaxial tension), for this study was, unfortunately, not available in the UK.

It was, therefore, decided to develop a new biaxial testing machine, which should allow the rubber specimens undergo larger scale deformations. The design considerations, conceptual design, detailed design and the fabrication of the biaxial testing machine are described in the following **Sections, 4.2.2.2.1** to **4.2.2.2.4**, respectively.

4.2.2.2.1 Design considerations of the biaxial testing machine

In order to carry out the essential tests on the selected pressurising materials for PAIF with the testing machine to be developed, prior to the detailed design of the machine, following considerations were taken into account:

(1) Considering the criteria of selecting pressuring materials for PAIF applications and the previous examination results ([6-8] and **Chapter 3**) on the possible pressurising materials, i.e., Solid Nitrile641 and Solid Nitrile642 were identified as two of the better pressurising materials, due to their good elasticity, smaller compressibility and larger, achievable elongations. The specimens made of such materials are, however, very difficult to hold with the conventional clamps during the tests, since the specimen very easily tends to slide out of the clamps, as the thinning of the specimen develops. This phenomenon will invariably occur during the testing of a highly elastic material (like Solid Nitriles) and under the issued (biaxial tensile) loading conditions. The machine should, therefore, have a maximum stroke by which all the highly elastic rubber specimens are able to reach their maximum elongation of about 10 times of their original length, along each of the loading directions. Simultaneously, the clamps should grip the rubber specimens firmly during the course of the testing.

(2) The machine should also have a capacity, which would allow not only testing rubber like materials under biaxial loading conditions, but also extending its applications to other materials, such as testing thin metal sheets.

(3) To ensure the precision and accuracy of the test results with the machine to be designed, the machine frames must have sufficient stiffness, and an accurate

data acquisition system should also be attached to it, to effect the proper measurement and recording of the forces and displacements.

(4) In order to eliminate the influence of loading rate on the mechanical properties of the tested materials, the loading state applied by the machine should be nearly static.

(5) For the safety reason, the machine should have automatic overloading protection as well as maximum motion protection.

(6) Finally, the machine should also have flexibility in its operations, i.e., to enable both manual and automatic loading and unloading.

4.2.2.2.2 Conceptual design of the biaxial testing machine

Several concepts of the biaxial testing machine were proposed initially, with a view to choosing the final design concept and ensuring the best functional performance of the machine. These concepts are shown in Figs. 4.3 to 4.7, respectively.

Fig. 4.3 shows a concept of the machine in which four screw-rods, clamps and hand-wheels may be used. It could be manually operated only. Though this concept seems simple and economic for the manufacture, it may not be able to fully ensure the precision and accuracy of the test results, since it is almost impossible to manually and separately control the four clamps' movements and displacements simultaneously and equally (through four hand-wheels and screw-rods).

Another concept of the machine shown in Fig. 4.4 uses four rotating pulleys fixed on a square loading frame, four pieces of ropes as well as a rope reel to effect its loading. However, due to the soft and flexibility of the ropes and the weight of the clamps may have, it may be difficult to locate such a machine and to avoid the influence of the clamp-weight to the test results. Also, using such a machine is impossible to perform the tests under compression loading conditions.

The third concept of the machine depicted in Fig. 4.5 may be driven by a hydraulic system to perform either tensile or compressive tests on the issued materials.

Dimensions of the machine, however, may be excessive big, since the stroke of each of the four hydraulic cylinders needs to be big enough to allow the rubber specimen to reach its maximum elongation (about 10 times of its original length) along each of the loading directions. Complex hydraulic system and leakage problems may also be accompanied with this concept.

Concept four of the machine described in Fig. 4.6 may use four spur gears, eight pairs of bearings, as well as two loading frames to achieve its functional requirements. Dimensions of the machine in this concept may be smaller than those in concept three and the leakage problem can be avoided herein. Accumulated transmission error of the machine may, unfortunately, be high, when the spur gears are arranged in such a way. Particularly, the manufacturing accuracy for both frames needs to be very high to ensure the co-axial accuracy along each of the loading directions.

In order to overcome the drawbacks with above concepts, concept five of the machine was proposed and presented in Fig. 4.7. In this concept, a gear box may be used to replace the four spur gears and only one loading frame is needed, rather than two in the concept four for the machine.

4.2.2.2.3 Detailed design of the biaxial testing machine

After the comparison of all the concepts proposed, the concept five (Fig. 4.7) was finally chosen to be designed in details. The detailed design of the machine was conducted in two stages. One was the system design, which concerned meeting the functional requirements, such as maximum stroke, capacity, frame stiffness, data acquisition system, loading state, over loading protection, operation system and clamping design of the machine. Another was the individual components/parts design, which dealt with each component/part's details, such as dimensions, tolerances and deviations.

System design of the machine

(a) Maximum stroke

Based on the investigation on the dimensions of the Reduction gearbox (EK60-1) available from the market, refer to Table 4.1, a suitable test area of about 40mm*40mm was planned. Correspondingly, the maximum stroke of about 210mm for the machine was designed to allow all the rubber specimens with a testing area of ≤40mm*40mm to reach their maximum elongation of 10 times of their original length along each of the loading directions (under biaxial tensile loading conditions).

(b) Clamping design

Due to the particular difficulties, i.e., thinning of the rubber sheets significantly under biaxial tensile loading conditions, clamps for holding such materials effectively for the tests are the next key factors. To deal with the issues properly, an investigation on the testing machine and clamping design for the biaxial loading conditions was conducted, as mentioned in **Section 2.7** and **Section 4.2.2.2**, in which several clamps were reported [9-12]. However, none of these clamping designs [9-12] is effective enough for holding rubber-like specimens to undergo larger scale deformations.

A novel set of the clamps that can be used to hold the rubber-like specimens, which may undergo larger scale deformations, under the biaxial tensile loading conditions was, therefore, developed. The principle of the clamping design is illustrated in Fig. 4.8. They should be able to apply not only the compressive loads to the specimen along Z direction (Pz), but also the evenly distributed pulling-forces to the specimen along X and Y directions (Pxy), respectively, so that the specimen's holding areas could be evenly loaded and firmly held by the clamps.

Several clamp-designs were tried, with a view to achieving the above goals. Different test results with different clamp-designs are compared in Fig. 4.9, from which the best design was finally identified (Fig. 4.9 (c)). Components involved in the use of the optimal clamps, and detailed design of the clamps, are shown in Fig. 4.10 [13], that is, a set of the clamps including a flat plate, a slot plate and a small fixing-plate for each clamp. Holes with a diameter of ϕ13mm (Fig. 4.10 (a)), on the flat plate and slot plate were designed, to connect the clamp to the clamp-frame fixed onto the carriage, which was further fixed onto the lead-screw shaft of the testing machine. Also, another group of holes with a diameter of ϕ10mm (Fig. 4.10 (a)), on each of the three plates were designed, by which, the holding area of the specimen was firmly fastened by using four screws, four nuts, eight washers and eight spring washers, as shown in Fig. 4.11. The 5mm*65mm (Fig. 4.10 (a)) slot on the slot plate allowed the holding area of the specimen, refer to **Section 4.3.3**, to go through and then to be folded to the other side of the plate. The small plate was used to press the folded part of the specimen to apply the even pulling force to each holding area of the specimens. Together with the other two plates, the specimen was firmly sandwiched and fastened. In order to increase the friction between two larger plates, a number of ϕ2mm to ϕ3mm blind holes and several ring-grooves were made on these plates before applying the sandpaper onto these plates.

(c) Maximum capacity

Maximum capacity of 20kN of the testing machine was designed to cover all the issued materials – both rubber and thin sheet metal materials. This was guaranteed following an investigation on the maximum capacity and dimensions of both electrical motor (PM4CWS, output torque 74Nm) and double directional action bearings (Four point contact ball bearing QJ303,) available from the market (Table 4.1).

(d) Selection of the bearings

Considering the requirements of maximum bearing capacity-20kN, functioning as both tensile and compressive test machine as well as dimensional suitability, four pairs of back-to-back arrangement of Four point/Angular contact ball bearings (QJ303) were finally chosen, after comparing with several other types of bearings (Table 4.2). There were four considerations for making this choice:

(1) Dimensions of the bearings (d=17mm, D=47mm and W=14mm) were well suitable for the design of the machine;

(2) Under maximum axial loading conditions (F_a=2 tons), the induced maximum load to bear with the bearings was $P_o=X_oF_r+Y_oF_a$=13600N, which is smaller than the maximum basic static load rating (C_o), i.e., P_o=13600N<C_o=13700N, and hence it is safe to use (Table 4.2);

(3) It also could accommodate limited misalignment;

(4) The back-to-back arrangement of the bearings ensured that the bearings could carry axial loads in both directions (for tension and compression tests).

(e) Frame stiffness design

Regarding to the design of the machine frames, several concepts were also proposed initially, with a view to achieving the maximum stiffness. Numerical calculations were conducted, with reference to the deflections of the frames with different cross-sections, under the maximum loading conditions, as shown in Table 4.3. When material consumption for four frames (with different cross-sections) is identical (78.83Kg), frame with a rectangular cross-section would result in a maximum deflection of 2.8mm and a very poor stiffness. Though frame with an I-beam cross-section would be much better than the rectangular cross-section-frame, it still caused a maximum deflection of 0.17mm and poor stiffness. Frame made of channel steel was even better than the previous two (rectangular and I-beam cross-section frames), since a maximum deflection of 0.059mm and a good stiffness were obtained. However, only the hollow-section

frame gave the smallest deflection of 0.036mm and the excellent stiffness. The frame section for this machine was, therefore, determined to be the hollow section, which would ensure the precision and accuracy of the testing.

(f) Data acquisition system of the machine

To ensure the test accuracy and equip the unique testing machine, a data acquisition system has been created. Components involved by the data acquisition system are shown in Fig 4.12. It includes a WA200 inductive displacement transducer with the maximum stroke of 200mm, load cells (designed by the author) with the maximum capacities of 1 ton and 2 tons, respectively, a ME50 signal conditioner and amplifier for the inductive displacement transducer. It also includes a set of National Instrument products, such as a SCXI 1321 Terminal block, a SCXI 1121 module, a SCXI 1000 chassis, a MIO-16E Data acquisition board and a PC. Particularly, a Lab VIEW program was created for this biaxial tension tests to record the loads and displacements for analysis; the front panel and diagram of the program are shown in Figs 4.13 to 4.14, respectively.

(g) Loading design

In order to avoid the influence of high rate loading on the test results, a static loading state was required. The motor (PM4CWS) with an rpm=1 was, therefore, selected for the machine. By the combined use of the motor and the lead-screw shaft, with a pitch of 6mm used in the machine, a speed of 6mm/min was created, which could be considered as a near static loading condition. Actually, the loading state can also be changed, if an adjustable motor-switch is used.

(h) Overloading/motion protection

Following the investigation on several SPDT Micro-switches and DPDT insulated switches, an electrical circuit was designed, as shown in Fig. 4.15, with a view to equipping an automatic overloading protection system to the machine.

So that whenever the machine reaches its maximum stroke, the motor-power will be cut off automatically to prevent the machine from overloading and over movement. Safety of the machine could, therefore, be secured.

(i) Manual and automatic operations

The circuit designed in Fig. 4.15 not only prevents the machine from overloading for safety, but also allowed the machine to be operated automatically. To let the machine render its full flexibility and convenience in its operations, a sliding clutch, between the motor and the machine, was also designed, as shown in Fig. 4.16, which added the excellent feature to the machine to allow operating it manually as well.

Component design in details

Based on the above considerations in **Section 4.2.2.2.1** and the system design of the machine in details in **Section 4.2.2.2.3**, all components, as listed in Fig. 4.17, (i.e., the 47 different types of components with different quantities for each type of the components) to be involved by the machine, were further considered carefully. For example, among these components, apart from a number of standard components, which were bought from the market, the other 77 non-standard ones were further designed in details. All the detailed designs (drawings), for addressing each of the individual components, are presented in **Appendix 4.1** and Figs. 4.1.1 to 4.1.28, respectively.

Two of the similar drawings, for concerning the assembled views of the machine in drawing, are also depicted in Figs. 4.17 and 4.18, for the overall top view of the machine assembled and the assembled front (side) view of the machine, respectively. As shown in the Fig. 4.17, the overall dimensions of the machine are given and all the components used by the machine are listed. In Fig. 4.18, some of the inside structures and the overall height of the machine are depicted as well. From the Fig. 4.17, it also can be seen that, though 47 different types of components with different

quantities, were used by the machine, it mainly includes a gearbox, four lead-screw shafts, four clamp carriages, four sets of clamps and a motor. It can be driven either manually or electrically.

4.2.2.2.4 Construction of the biaxial testing machine

Construction of the biaxial testing machine was conducted based on the standard components bought from the market, non-standard components fabricated herein, and following a two-stage-assembly (initial assembly and final assembly) procedure. Some of the details, regarding these aspects, are described in **Appendix 4.2** and Figs. 4.2.1 to 4.2.21, respectively.

Creation of the data acquisition system

To create the data acquisition system, two types of basic components were needed: one was the sensor (load cell) for recording the load; another was the inductive transducer for measuring the displacement. The load cell, in this case, was designed by the author. The inductive displacement transducer and other related devices, (signal conditioner and amplifier) to facilitate the data acquisition, were bought from the market, as mentioned in **Section 4.2.2.2.3.**

(a) Design and calibration of the load cell

Two load cells, with the capacities of 1 ton and 2 tons, respectively, were designed and fabricated at the University of Strathclyde, as shown in Fig. 4.19 to measure the load applied during the tests. In each of the two load cells, a wheat-stone bridge [14], consisting of four and eight EA-06-120LZ-120 resistors for the 1 ton load cell and 2 tons load cell, respectively, was used.

Both load cells were calibrated at the excitation voltage of 10V, in order to compromise with other related devices' working condition requirement, such as the default settings of the devices - a set of National Instrument and a Hottinger Baldwin Messtechnik (HBM) signal conditioner, respectively. Both calibration results gave

the excellent linear relationships, between the load and out put voltage, which guaranteed the working reliability of the load cells. Fig. 4.20 shows the calibration results of both load cells at the issued excitation voltage value (10V). Also, since the maximum output voltages of both load cells, under this excitation voltage value, were much close to the maximum scale/capacity of the other devices' (National Instruments') working range (10V), the possible smallest reading error would, therefore, be resulted in, with such features possessed by the load cells. Hence, when they were used with the issued other devices, both load cells worked well, throughout the tests, under the excitation voltage of 10V.

(b) Other units involved by the data acquisition system

As shown in Fig. 4.12, apart from the load cells designed and fabricated herein, a WA200 inductive displacement transducer was bought from HBM. A ME50 signal conditioner and amplifier for the inductive displacement transducer and a set of National Instrument products were also involved. Particularly, the Lab VIEW programme (Figs. 4.13 and 4.14), which allowed the direct record of the load and displacement, without any intermediate transferring calculation (from the electrical signal to analogue signal), was created for the biaxial tests, to record the loads and displacements automatically. The programme also adopted the function of bias adjustment, by which the data recorded could always start from zero, and hence, more convenient for the subsequent data processing.

Unique biaxial testing machine

Based on all the exercise conducted, concerning the development of the testing equipment, a unique biaxial testing machine system, which can be used to test either metal or rubber like materials, under either tensile or compressive loading conditions, was, developed and constructed. Although, apart from the uniaxial tension/compression and planar tension/compression tests, only biaxial tension tests on the rubber like materials were further required for the author's PhD study, the unique biaxial testing machine was designed with additional functions for its

potential use. That is the machine not only can be used to test either rubber-like materials or metal sheet materials under biaxial tensile loading conditions, but also can be used to test the both materials under compressive loading conditions. Such a machine is also fully equipped with a PC based data acquisition system to ensure the test accuracy. The machine as well as its data acquisition system is shown in Fig. 4.21.

4.3 Procedures

Based on all the above preparation work, for the qualification of mechanical properties of the selected pressurising materials, the best ones (Solid Nitriles641, 642) and the worst one (Neo Sponge) identified in **Chapter 3**, were further examined and compared, under five different loading conditions, including uniaxial tension, uniaxial compression, planar tension, planar compression and biaxial tension, respectively, for the qualification of their mechanical properties.

4.3.1 Specimen preparation

The specimens used throughout the experimental investigation are summarised in Table 4.4, i.e., five types of specimens with different shapes and dimensions, made from three different types of materials, and with a minimum of three specimens for each material, each thickness and each type of the tests, were designed and fabricated.

The geometries of the specimens shown in Table 4.4, were designed in accordance with the Standard Test Methods for Rubber Property (D 412 – 98a and D395-98) [15] as well as the ABAQUS User Manual [16]. This is for the purposes of the application of the experimental results into the subsequent FE simulation, and the comparison with other's test results. Clamping the specimens into the testing machines was also considered during the determination of the specimen geometries.

The specimens were made from three types of polymers, i.e., Solid Nitrile641, Solid Nitrile642 and Neo Sponge, with a nominal tensile strength of 6MPa, 9MPa and 0.1MPa, respectively. The actual thicknesses of the sheet materials and their suitable applications in the tests were listed in Table 4.5.

All specimens were taken from the same batch of the materials. They were fabricated from the standard sheet products into the shapes of dumbbell, strip, slab and column, as well as the expected dimensions, using either a turning machine/electric wire cutting machine (for the circular specimens) or a hand scalpel/knife (for the straight edges).

4.3.2 Uniaxial tension tests

The experimental set-ups, for uniaxial tension of dumbbell and strip shaped specimens (Table 4.5), are shown in Fig. 4.22. It was performed on both the hydraulic driven press (Fig. 4.1), for the specimens made of Neo Sponge, with the maximum elongations of less than 100mm, and the motor driven press (Fig. 4.2), for the specimens made of Solid Nitriles, with the maximum elongations of greater than 100mm.

Initially, the original thickness and length of each individual specimen were measured and recorded. Two marks were then made on each of the specimens to localize the test areas and to facilitate the setting up of the tests. Subsequently, two ends of each specimen were held by two clamps, which were, in turn, fixed on the hydraulic ram and the cross head of the press, respectively, as shown in Fig. 4.22 (a). During the testing, the load was applied, as the lower clamp was moving downwards, with the hydraulic ram, at a speed of 10mm/min. The applied load and the ram displacement were recorded automatically, by the accompanied data acquisition system (Fig. 4.1).

When uniaxial tension tests were conducted using the motor driven lead-screw press (Fig. 4.2), two ends of each of the specimens were griped by two clamps, which were fixed on the lower stable worktable and the upper moveable beam (cross head) of the press, respectively. The load was applied, as the upper moveable beam was moving up, at the same speed of 10mm/min as that with the hydraulic driven one. In this situation, the load and displacement were recorded by the facilitated time against X-Y plot, as shown in Figs. 4.2 and 4.22 (b).

Since three types of materials, two different shapes and three dimensions (Table 4.4) of the specimens were tested, the influences of these variables on the mechanical properties of the issued materials, under uniaxial tensile loading conditions, were qualified.

4.3.3 Uniaxial compression tests

The hydraulic driven universal testing machine (Fig. 4.1) was also used to conduct the uniaxial compression of the column specimens (Table 4.4). Initially, the original thicknesses and diameters of the specimens were measured and recorded for the subsequent data processing. Then two groups of the specimens made of solid Nitriles641 and 642 respectively, were well lubricated, with the combined use of Zinc Stearate powder and Molybdenum disulphide grease [17], while the other two groups were without any lubricants, with a view to creating different testing conditions, for the uniaxial compression tests. The experimental set-ups are shown in Fig. 4.23.

During testing, each specimen in each group was placed on a base plate, which was pre-put on the ram of the hydraulic press. On the top of the specimen, another plate, with the same surface roughness, was placed and against the upper beam of the press. The load was applied, as the base plate was moving up with the hydraulic ram. The load and displacement were also recorded automatically, by the accompanied data acquisition system (Fig. 4.1).

Therefore, mechanical properties of the different materials, under uniaxial compression loading conditions, as well as under different friction conditions, were studied.

4.3.4 Planar tension tests

Planar tension of the Dumbbell or stripe shaped specimens (Table 4.4), made of Solid Nitriles, was conducted on the motor driven press (Fig 4.2), while hydraulic press (Fig. 4.1) was only used for the testing specimens made of Neo sponge, due to the same reason (limited stroke), as that for the uniaxial tension tests. Two marks were, also initially, made to localise the testing area and to guide the testing set-up. Original thickness and test length were measured and recorded.

Since the tensile stresses and elongations within the planar tension specimens were much larger than those within the uniaxial tension specimens, the existing clamps used for the previous uniaxial tension tests, were no longer suitable for the planar tension tests. Two pairs of new clamps were, therefore, particularly designed with a view to holding the specimens effectively. The geometry and dimensions of the clamps are shown in Fig. 4.24. To increase the friction between the clamp plates and the specimen, sand papers were also applied to the plates, as those used in the clamping design for biaxial tension tests in **Section 4.2.2.2.3**. Then, two ends of each specimen were held by the two clamps, which were in turn fixed on the hydraulic ram and upper beam of the press (Fig. 4.1), respectively, for testing Neo Sponge sheet. These two clamps were also fixed onto the stable worktable and the moveable upper beam of the motor driven press (Fig. 4.2), respectively, for the testing of Solid Nitrile sheet as well. The experimental set-ups are shown in Fig. 4.25.

During the testing, the load was applied, as either the lower clamp was moving downwards, with the hydraulic ram or the upper clamp was moving upwards with the upper movable beam associated with the motor driven press. Similar to the uniaxial tests, the applied load and corresponding displacement were recorded automatically

by either the computer based data acquisition system or the accompanied time against X-Y plot.

The mechanical properties of the different materials, with different specimen geometries, under planar tension loading conditions were, therefore, examined.

4.3.5 Planar compression tests

Planar compression of all the issued materials was conducted with the same, $900\,kN$ TINIUS OLSEN universal testing machine (Fig. 3.5), as that used for the forming of hollow flanges in **Chapter 3**. Initially, the original thickness, width and length of each of the specimens were measured and recorded, with a view to carrying out the final check on the dimensions of the specimens as well as for the subsequent data processing. Then three groups of the specimens, made of three different materials (Solid Nitrile641, Solid Nitrile642 and Neo sponge), were well lubricated with the combined use of Zinc Stearate powder and Teflon grease [17]. The experimental set-up is shown in Fig. 4.26.

During testing, each specimen in each group was placed on a base steel plate, which was pre-settled onto the worktable of the 900kN motor driven lead-screw press (Fig. 3.5). On the top of each of the specimens, another steel plate, with the same surface roughness, was placed and against the cross head (upper beam) of the press. The load was applied, as the cross head (upper beam) was moving downwards. The applied load and corresponding displacement were recorded automatically with both the accompanied data acquisition system and the X-Y plot (Fig. 3.5).

Hence, mechanical properties of Solid Nitriles641, 642 and Neo Sponge were evaluated, under the planar compression loading conditions, as well as the same friction conditions.

4.3.6 Biaxial tension tests

Biaxial tension of the issued materials was performed using the biaxial tension function of the unique biaxial testing machine (Fig. 4.21). Initial thickness, testing area, holding areas as well as fibre direction of each of the specimens, were measured and marked. Some of the specimens prepared are shown in Fig. 4.27. Sixteen ϕ5mm holes were punched and the folding areas were cut into 65mm in width, non-separated strips, before assembling it into the clamps. Each of the specimens was then assembled with the particularly designed clamps (Fig. 4.10), as well as following the designed assembly procedures, which are depicted in Fig. 4.11. That is, each of the specimens was firstly assembled, with the four plates without slots, by using 8 centre holes. Then, four slot-plates were put on and allowed the strip to come out from the slots, and hanged on the strip to the screws by using 8 outside holes of the specimen. Subsequently, the small plates were put above the folded part of the specimen and fastened together by the four screws, as shown in Fig. 4.10 and Fig. 4.11. Next, the assembled specimen and clamps were assembled to the clamp-frames, which were pre-fixed onto the four carriages of the machine. The load cell, (designed by the author), was placed between one of the clamp-frames and the adjacent carriage, with a view to recording the testing load. The inductive displacement transducer (WA-200) was positioned onto one of the machine frames, and its plunger was connected to the nearest carriage, with the intention of measuring the testing displacement. The experimental set-up is shown in Fig. 4.28.

During testing, the load was applied, as the four carriages were moving backward from each other, and along each of the loading directions. The electrical signal (output voltage), produced with the inductive displacement transducer, was conditioned and amplified with the ME50 signal conditioner first. Then the conditioned signal, similar to the output signal from the load cell, as well as output signal from load cell went via a set of National Instrument (a SCXI 1321 terminal block, a SCXI 1121 module and a SCXI 1000 chassis), by which both signal were further conditioned. Subsequently, both signals conditioned were sent to a MIO-16E data acquisition board, which was inserted into a PC. The Lab VIEW programme,

created and shown in Figs 4.13 to 4.14, enabled the instant and direct reading and recording of both of the applied load and the displacement efficiently.

Thereby, performances of Solid Nitriles641 and 642, under biaxial tensile loading conditions, were investigated, which were hardly attempted by other investigators in the past.

4.4 Results

More than five types of specimens (Table 4.4) with different materials as well as different specimen shapes and dimensions were tested. With reference to different loading conditions, the stress and strain curves of all the tested specimens are presented in Figs. 4.29 to 4.51. Where, those under uniaxial tension, uniaxial compression, planar tension, planar compression and biaxial tension are illustrated in Figs. 4.29 to 4.37, 4.38 to 4.41, 4.42 to 4.47, 4.48 to 4.49 and 4.50 to 4.51 respectively.

The corresponding ultimate stresses and ultimate strains of all individual specimens were also computed (as shown in **Appendix 4.3**). Each value of the stress and strain, herein, was determined, by dividing the recorded load and corresponding displacement, of the specimen along its loading direction, by its initial cross sectional area and its initial length, respectively. The ultimate stress and ultimate strain values are equal to the ratios of the maximum applied loads and corresponding displacements of the specimens to their initial areas and original lengths, respectively, when testing specimens were about to fracture in tension, or its strain hardly increase in compression.

The influences of specimen shapes and dimensions, on the stress-strain curves of selected materials, under uniaxial tension and planar tension, are further compared in Figs. 4.52 to 4.54 and Figs. 4.55 to 4.57, respectively.

The effects of lubrication conditions on the material behaviours are presented in Figs. 4.58 and 4.59 for uniaxial compression loading conditions.

The mechanical performances of different materials under each loading condition are, individually, compared in Figs. 4.60 to 4.64, for uniaxial tension, uniaxial compression, planar tension, planar compression and biaxial tension, respectively.

The stress-strain curves of the same material under different loading conditions are also compared in Figs. 4.65 and 4.66, for Solid Nitriles641 and 642, respectively.

It should be pointed out that, in order to simplify the comparison and discussion on the test results, the compressive stress and strain are assumed to be positive, rather than negative in this PhD thesis.

4.5 Discussion

4.5.1 Validation of the test results

As Figs. 4.29 to 4.51 indicate that, for the tested specimens with the identical shapes and dimensions, made from the similar material, and under the similar loading conditions, their stress and strain curves in the same group were hardly varied with specimen numbers. For instance, there are 21 out of 23 figures, such as Figs. 4.30, 4.32 and 4.34, in which the test results of different specimens in the same group are almost identical, though the specimens were different among groups. These indicate that, the selected materials, testing techniques, facilities and procedures adopted in this experimental investigation, have met the anticipated requirements. Hence, overall, the obtained experimental results are believed to be reliable and applicable.

Exceptions happened in the Figs. 4.29 and 4.33, in which the stress and strain curves of different specimens in the same group differ from each other, which may be caused by irregular cuttings along the specimen edges/outlines. Furthermore, Figs.

4.38 to 4.41 and Figs. 4.48 to 4.49, show that the strain-strain curves of different specimens, under both uniaxial and planar compression conditions, always diverse from each other in their later loading phases. This may be mainly due to the variation of the testing sequences and friction conditions, although no evidence could be found to exclude the changes of mechanical properties of material itself at the final stage. Generally, a number of specimens were tested on the same machine in a short period. The first specimen tested might somewhat change the testing conditions, such as surface conditions of the worktable and the crosshead of the testing machine, and therefore further affect the friction conditions of the subsequent specimens.

Although the stress-strain curves of tested specimens were somewhat affected by both the minor irregular hand-cuttings of the specimens and the change of friction conditions, they are still able to represent the mechanical properties of the issued materials, and therefore used throughout the experimental investigation.

Obviously, Figs. 4.29 to 4.66 and the corresponding ultimate strain and strength data (computed in **Appendix 4.3**) can be used to provide the input data, as the constitutive descriptions of the pressuring materials, for finite element simulation of thick-wall tubular components formed with PAIF, which was one of the research objectives for this experimental investigation. In addition, these test data can also be utilised to reveal the mechanical properties of different pressuring materials, under different loading conditions; the influences of specimen shapes, dimensions and friction conditions on the mechanical properties of the selected materials can also be evaluated using these data. For example, Figs. 4.29 to 4.51 show that mechanical properties of the selected pressuring materials mainly vary with loading conditions, and therefore, can be further classified into three different cases, that is, the behaviours of the materials under uniaxial/planar tension, biaxial tension and uniaxial/planar compression, which will be further addressed in the following **Sections 4.5.2** to **4.5.4**, respectively.

4.5.2. Material behaviour under uniaxial/planar tension

4.5.2.1 General behaviour

As shown in Figs. 4.29 to 4.34 and Figs. 4.42 to 4.45, under uniaxial and planar tension conditions, both Solid Nitriles641 and 642 exhibit a similar characteristic. That is, all of their stress-strain curves can be divided into three phases. In the first phase, their stress-strain curves were steep with a great gradient, which indicates that Solid Nitriles641 and 642 are stiff, during the initial tension stage. In other words, a small tension force will not produce a significant elongation within the Solid Nitriles641 and 642 specimens. Once stress exceeded a value of about $0.5\,N/mm^2$, however, the stress-strain curves of Solid Nitriles641 and 642 become more flat, with a small gradient and a small increase of applied load was able to generate sufficient elongation. After the second phase, when the tension strain of specimen were over about 2.0 and 1.0 for uniaxial tension and planar tension, respectively, the stresses of Solid Nitriles641 and 642 were hardened, and their stress strain curves become steeper again with an increasing gradient, until the specimens reached their ultimate strength and broken.

As listed in **Appendix 4.3**, the ultimate strain of Solid Nitriles641 and 642 ranges from 2.86 to 7.72 with an average of 5.02 for uniaxial tension and from 0.86 to 3.56 with an average of 2.25 for planar tension. Hence, through initial stiff, middle softening and later hardening, Solid Nitriles641 and 642 exhibit a greater elongation under uniaxial tension than under planar tension.

In contrast to the Solid Nitriles641 and 642, Neo Sponge shows the different behaviour. For instance, Figs. 4.35 to 4.37 and Figs. 4.46 to 4.47 show that, under uniaxial and planar tension, the stress strain curves of Neo Sponge look like the parabolic curves. As stress or applied load increases, it almost kept softening with its gradient decreasing continuously. In other words, for the same increment of stress, the increment of strain and elongation of the specimen become greater and greater until its fracture. Similar to the Solid Nitriles641 and 642, the ultimate strain of Neo

Sponge ranging from 1.43 to 3.36 with an average of 2.4 in uniaxial tension, which is greater than those from 1.01 to 2.10 with an average of 1.52 in planar tension. Hence, under both uniaxial and planar tension loading conditions, Neo Sponge keeps softening with increases of its elongation, under the same increment of stress values. This is because Neo Sponge possesses the biggest compressibility.

4.5.2.2. Influences of specimen shapes and dimensions on measurement of the material behaviours

Both Figs. 4.52 to 4.54 under uniaxial tension and Figs. 4.55 to 4.57 under planar tension, reveal that, specimen shapes (dumbbell or strip) and dimensions (12mm or 24mm width of the strips for uniaxial tension) of the tested specimens, in deed, affect the stress–strain curves of the selected materials significantly. For the same strain value of 1.00, for instance, the stresses of different specimens made from the similar material are not always equal to each other. Although such differences did exist in the experimental results of both uniaxial and planar tension tests for the three tested materials, no consistent and systematic conclusions could be drawn. For example, under uniaxial tension, the stress-strain curve of 24mm strip specimen of Solid Nitrile641 was above that of 12mm strip one, as shown in Fig. 4.52. For Solid Nitrile642, however, the case was just contrary, as shown in Fig. 4.53. Hence, such differences might be mainly caused by the minor errors during the fabrication of the specimens by hand cutting, rather than the inherent properties of the materials.

In addition to the difference in stresses, the ultimate strains of different specimens made from the similar materials under the similar loading condition also differ from each other. As shown in Figs. 4.52 to 4.54 for uniaxial tension and Figs. 4.55 to 4.57 for planar tension, the ultimate strains of all dumbbell specimens were always less than those of strip specimens. The strip specimens with a width of 24mm were always fractured with larger ultimate strain than those of the strip specimens with a width of 12mm and the dumbbell shaped specimens. Such differences were mainly caused by specimen shapes and dimensions. For the dumbbell shaped specimens,

since their elongations mainly concentrated on their middle narrow testing section, and therefore their ultimate strains were with the smallest values among all the cases. Alternatively, for the strip shaped specimens, since cross sectional area were always same along the entire length of the specimens, thinning and sliding out of the holding sections of the specimens would be easier than those of the dumbbell ones. Some extra elongations, therefore, were added to the ultimate strains of strip shaped specimens.

Hence, when material properties, particularly for rubber like materials, needs to be investigated, the similar specimens, including the similar shape, dimensions, made from the same type of the materials as well as under the identical loading condition, should always be adopted throughout the tests, to exclude the unexpected influences on the material properties.

4.5.2.3. Qualification of the selected materials

Taking dumbbell shaped specimens as a typical example: Mechanical properties of the three types of selected materials under uniaxial and planar tension loading conditions are compared in Figs. 4.60 and 4.62, respectively. It is clear that, under both loading conditions, Solid Nitrile642 exhibits the best mechanical behaviour than those of the Solid Nitrile641 and Neo Sponge. In other words, for the same strain value, stress of Solid Nitrile642 specimen was always greater than those of Solid Nitrile641 and Neo Sponge ones. For example, when a tension strain reached a value of 1.0, the stress within the Solid Nitrile642 specimen, under uniaxial and planar tension were 2.0 and 1.8 N/mm^2, respectively; while those within Solid Nitrile641 and Neo Sponge were only 1.6 and 1.3 N/mm^2 and 0.4 and 0.25 N/mm^2, respectively.

Both ultimate strength and ultimate strain of Solid Nitrile642 were also much larger than those of with both Solid Nitrile641 and Neo Sponge. In addition to the significant differences, as shown in Figs. 4.60 and 4.62, the results listed in

Appendix 4.3 also indicate that, the average values of ultimate stresses and ultimate strains of all groups of specimens made of Solid Nitrile642 specimens were greater than those of Solid Nitrile641 and Neo Sponge. Taking the strip shaped specimen with a width of 24mm, under uniaxial tension as an example, the ultimate stress and ultimate strain values of Solid Nitrile642 were 8.57 N/mm^2 and 6.93, which were much larger than those of 6.20 N/mm^2 and 5.06 for Solid Nitrile641, as well as 0.94 N/mm^2 and 2.88 for Neo Sponge, respectively. Hence, significant evidences show that, from the view of mechanical properties under uniaxial and planar tension loading conditions, Solid Nitrile642 has the best mechanical properties and is ranked to be the most favourable pressurising material for PAIF. Neo Sponge has the worst mechanical properties and is useless for PAIF, while mechanical properties of Solid Nitrile641 are ranked between the best one and the worst one, which is also favourable for the PAIF applications.

4.5.3. Material behaviours under biaxial tension

4.5.3.1 General behaviour

Mechanical properties of further selected pressurising materials, Solid Nitriles641 and 642, are shown in Figs. 4.50 and 4.51, respectively. Compared with those shown in Figs. 4.29 to 4.34 under uniaxial tension, and those shown in Figs. 4.42 to 4.45 under planar tension, Solid Nitriles641 and 642 exhibit the different mechanical behaviours under biaxial tension loading conditions. In stead of initial stiff, middle softening and later hardening under uniaxial and planar tension, both Solid Nitriles641 and 642 under biaxial tension, were initially stiffen with a steeper stress-strain curve, then softened with decreasing gradient, under an increasing tension force and finally kept as a sloping straight stress-strain curves until their fractures. Such difference may be caused by the assumptions that, the particles within the tested materials could be re-arranged, under uniaxial and planar tension, but could not do so under biaxial tension.

Also, as listed and averaged in **Appendix 4.3**, the ultimate stresses and strains, of Solid Nitriles641 and 642 under biaxial tension, are always less than those under uniaxial and planar tensions. Under biaxial tension, for example, specimens made of Solid Nitrile642 fractured with a maximum stress of $2.65\,N/mm^2$ at a maximum strain of 1.96, which are much less than those of $8.57\,N/mm^2$ and 6.93 under uniaxial tension and $6.14\,N/mm^2$ and 3.33 under planar tension, respectively. Hence, tension in biaxial direction decreases both bearing capacity and extension ductility of Solid Nitriles641 and 642.

4.5.3.2. Qualification of selected materials

Mechanical properties of both further selected Solid Nitriles641 and 642 under biaxial tension are compared and shown in Fig. 4.64. It is clear that, under biaxial tension, the stress-strain curves of Solid Nitrile642 were almost over that of for Solid Nitrile641. The results, as listed in **Appendix 4.3**, also revealed the similar facts. For example, when tested specimens fractured, ultimate strength and strain of Solid Nitrile642, were $2.65\,N/mm^2$ and 1.96, which is much greater than those of $1.75\,N/mm^2$ and 1.13 for Solid Nitrile641. Hence, similar to what under uniaxial and planar tension, the mechanical performances of Solid Nitrile642, under biaxial tension, also presented more favourable values than those of with Solid Nitrile641.

4.5.4 Material behaviours under uniaxial and planar compression

4.5.4.1 General behaviours

Figs. 4.38 to 4.41 and Figs. 4.48 to 4.49 show the mechanical properties of all the tested specimens, under uniaxial compression and planar compression loading conditions, respectively. It is clear that overall their stress-strain curves can be divided into three sections, namely, initial straight lines, middle curved lines and later steeper lines. That is, when strain value is less than 0.2 to 0.3 or stress value less than about $1.0\,N/mm^2$, stress-strain curves of all compressed specimens were almost slopping straight lines. In other words, compression deformation of the tested

specimens in loading direction increases linearly with the increases of the applied loads during the first stage/section.

After compression strains exceed the above values, the rate of increases of the compression stresses become greater and greater than that of compression strain, and therefore, stress-strain curves become upward like the concave curves; simultaneously, the materials seem to be hardened. Such hardening may be due to the assumption of re-arrangement of material particles inside the tested specimens. These are also contributed by the transverse friction over two contact interfaces between the specimen surfaces and the testing machine. It is well known that, as specimen was compressed longitudinally, it expanded transversely, which induces corresponding transverse friction. It is the transverse friction that restraints the specimen expansion and therefore promotes an increase of applied stress for a same increment of compression strain.

Once compression strain become extensive and over about 0.55, the effects of end friction condition were strengthened greatly and the micro-gaps between particles inside materials became less and less, which resulted in very steep stress-strain curves. For a very small increment of strain value, compression stress increased dramatically and greatly.

The experimental results show that, even if compression strain exceeds 0.6, tested specimens still didn't show any signs of cracks and faults, as shown in Fig. 4.67, which indicates that the selected pressurising materials were able to well keep its integrity under compression loading conditions.

Such experimental results also suggest that, for tested specimens under uniaxial and planar compression, end lubrication well affect their stress –strain curves, as discussed below.

4.5.4.2 Influences of lubrication conditions

The effect of end lubrication conditions on the mechanical performances of compressed specimens is shown in Figs. 4.58 and 4.59. It is obviously that lubrication conditions well affect mechanical properties (the measured data). For the same type of specimens, made from the same type of materials, stress-strain curves of non-lubricated specimens were always above those of lubricated ones. In other words, for similar compression force, the strain of lubricated specimens was always greater than those of non-lubricated ones, and therefore lubricated specimens deformed more sufficiently than those of non-lubricated ones.

The reason for such differences is just because of the end friction conditions of the tested specimens, as discussed previously. Due to the use of the better lubrication schemes, the transverse frictions over two end surfaces of specimen were reduced greatly, and therefore their influences on material strengths become less.

Figs. 4.58 and 4.59 also indicate that lubrication condition plays an important role in the forming of thick-wall tubular components with Pressuring-assistant Inject Forging. It means that, for the similar forming force, both external and internal surfaces of the tubular billet and polymer rod should be well lubricated, to allow the pressurising materials to flow and deform sufficiently as well as to push the tubular billet to fill in the die cavity significantly, which will be no doubt to facilitate the forming process and to produce the sound tubular components.

4.5.4.3 Qualification of the selected materials

The mechanical properties of three different materials, with the similar lubrication conditions are compared in Figs. 4.61 and 4.63 for uniaxial and planar compressions, respectively. It is evident that under both uniaxial and planar compression conditions, stress-strain curves of Solid Nitrile642 are always above those of for the Solid Nitrile641 and Neo Sponge. For the same value of strain of 0.6, the stress of Solid Nitrile642 were about 6.0 and 4.0 N/mm^2 for uniaxial and planar compression,

respectively, which are greater than those of 4.5 and 2.8 N/mm^2 for Solid Nitrile641 and much greater than those of 0.61 and 0.31 N/mm^2 for Neo Sponge, respectively. Hence, similar to their performances under uniaxial, planar and biaxial tensions, the Solid Nitrile642 also exhibits the best and favourable behaviour, under uniaxial and planar compression conditions.

4.5.5. Material behaviours under different loading conditions

Mechanical properties of the selected materials under different loading condition are also investigated, as shown in Figs. 4.65 and 4.66, for Solid Nitriles641 and 642, respectively.

Obviously, under different loading conditions, even for a same type of the material, stress strain curves are varied significantly, particularly for the tensile and compressive loading conditions. However, some common characteristics of the materials properties can still be seen. That is, generally, they are weak in tension, particularly when they are in planar and biaxial tension, but with a large elongation. As listed in **Appendix 4.3**, for example, under uniaxial, planar and biaxial tension loading conditions, the ultimate strengths of Solid Nitrile642 are 8.41, 3.84 and 2.65 N/mm^2, respectively. Their corresponding ultimate strains are 4.58, 2.67 and 1.96, respectively, where dumbbell shaped specimens for both uniaxial and planar tension tests were considered.

In contrast to the weakness in tension, both Solid Nitriles641 and 642 are strong in compression. In addition to smaller compression strain, they are able to bear a load level of over the stress value of 18.0 N/mm^2, without causing any cracks and faults.

During the forming of thick-walled tubular components with PAIF, the internal pressurising material (polymer rod) is always under compression with a high pressure. It is also anticipated that the internal material may not fail before the forming process completed, which allow it to be able to fill in the die cavity and to

pressurise the tubular billet into the expected form continuously and effectively. Hence, the above experimental results well verified the conclusion that Solid Nitriles641 and 642 are the mostly suitable as a pressurising material for PAIF among the available materials.

4.5.6 Summary of the material properties

As shown in Figs. 4.29 to 4.51, under the similar loading condition, vast majority of stress-strain curves of the different specimens within the same group (similar shapes, dimensions and type of the material), were almost coincident with each other. This indicates that the specimen fabrications, research procedures and testing facilities, including the designed biaxial testing machine used in the tests, are reliable and applicable.

Under uniaxial and planar tension, Solid Nitriles641 and 642 initially stiffened, then softened and finally hardened again, while Neo Sponge kept softened with a decreasing gradient, as the strain increases.

Ultimate strength and strain values of all materials under planar tension are always smaller than those under uniaxial tension.

Mechanical properties, of Solid Nitriles641 and 642 under biaxial tension, differ from those under uniaxial/planar tensions. Instead of the final hardening, their stress-strain curves almost become the slopping straight lines until their fracture. Ultimate strength and strain values of Solid Nitriles641 and 642 under biaxial tension are always less than those under uniaxial and planar tensions.

Under uniaxial and planar compressions, the selected materials initially behave almost elastically, then stress-hardened and finally sharp increase in strength with little increase of compression strain.

Lubrication condition well affects material behaviours, i.e., the measured material data/strength is reduced, under lubricated condition, for a same value of strain. Contrarily, a non-lubricated condition will increase the measured data of the material strength, for the same strain value.

4.6 Conclusions

Form the study of the qualification of the mechanical properties of pressurising materials, following conclusions can be drawn:

(1) Mechanical properties of the selected pressurising materials were further qualified under five types of loading conditions (UT, UC, PT, PC and BT);

(2) Loading conditions, specimen geometries and friction conditions do influence measured values of the mechanical properties of the issued materials;

(3) Solid Nitriles641 and 642 were qualified to be the relatively better pressurising materials for PAIF, among the available materials from the market;

(4) A unique, biaxial testing machine was developed and used successfully, throughout the tests;

(5) More pressurising materials may be tested with a view to finding out the fully elastic and non-compressible pressurising materials for PAIF.

4.7 References

[1] R. Balendra and Y. Qin, "Feasibility and limitations of pressure-assisted Injection Forging of thick-walled tubes", Proc. of 5th ICTP in Ohio, 7-10th

October, pp. 327-330, 1996.

[2] Y. Qin and R. Balendra, "Technical evaluation of pressure-assisted Injection Forging of thick-walled tubes", Advances in Manufacturing Technology IX, edited by D. Stockton and C. Wainwright, Taylor & Francis, London, pp. 62-66, 1995.

[3] Y. Qin and R.Balendra, "Simulation of forming sequence of Pressure-assisted injection forging of thick-walled tubes", Trans. NAMRI/SME, Vol. XXIII, 1995, pp27-32.

[4] R. Balendra and Y. Qin, "Pressure-assisted Injection Forging of thick-walled tubes", Int. J. of Mach. Tools Manf., Vol. 35, No. 11, pp. 1481-1492, 1995.

[5] Y. Qin, "FE and Experimental analysis of injection forging", PhD Thesis, Chapter 1, 4, 6, The University of Strathclyde, 1997, pp1-21.

[6] Y. Qin, Y. Ma and R. Balendra, "Performance of pressurising-materials and process design considerations for the forming of thick-walled tubular components", Proc. of the 9th ISPE CE2002, July, Granfield, UK, pp. 251-262, 2002.

[7] Y. Qin, Y. Ma and R. Balendra, "Pressurising materials and process design considerations of the Pressure-assisted Injection Forging of thick-walled tubular components", Journal of Materials Processing Technology, Vol. 150, No. 1-2, pp. 30-39, 2004.

[8] Y. Ma, Y. Qin and R. Balendra, "Experimental and FE investigation of performance of polymers under confined compression conditions by using a simplified configuration", Advances in Manufacturing Technology, XVI, The 18th NCMR, 2002, pp. 203-208.

[9] Michael S. Sacks, "Biaxial Mechanical Evaluation of Planar Biological Materials", Journal of Elasticity, vol. 61, 2000, p199-246.

[10] M. Tuttle, P. Singhatanadgid and G. Hinds, "Buckling of Composite Panels Subjected to Biaxial Loading", Proceedings of the Society for Experimental Mechanics, INC. Vol. LVI, p191-201, 2000.

[11] K. Buet-Gautier and P. Boisse, "Experimental Analysis and Modeling of Biaxial Mechanical Behavior of Woven Composite Reinforcements",

Proceedings of the Society for Experimental Mechanics, INC. Vol. 41, No. 3, 2002, p260-269.

[12] D. J. Hitt and M. Gilbert, "A Machine for the Biaxial Stretching of Polymers", Journal of Polymer Testing, Vol. 13, No. 3, 1994, pp219-237.

[13] Y. Ma, Y. Qin and R. Balendra, "Clamping design for the biaxial tension test of rubbers", Advances in Manufacturing Technology, XVII, The 1st ICMR and 19th NCMR, 2003, pp. 329-333.

[14] J.A. Haslam, G.R. Summers and D. Willams, "Engineering instrumentation and control", Edward Arnold, A member of the Hodder Headline Group, London Melbourne Auckland, 1981, pp. 1-75.

[15] Annual Book of ASTM Standards, Vol. 09.01, December 1998, pp 37-49.

[16] ABAQUS Manual, Hyperelastic behaviour, 2001, pp 10.5.1-1 to 10.5.1-14.

[17] Y. Qin and R. Balendra, "Optimisation of the lubrication for the extrusion of solid and tubular components by Injection Forging", to appear in the Journal of Materials Processing Technology, 2002.

Appendix 4.1

Biaxial–tension test machine component design

There were 28 different types of non-standard components, from the biggest component (machine frame) to the smallest one (clamp-frame-nut), with different quantities, which were, further individually, designed in details and shown in Figs. 4.1.1 to 4.1.28, respectively.

The main frame design of the machine is shown in Fig. 4.1.1, by which the motor was fixed onto the machine; other three frame designs are shown in Figs. 4.1.2 and 4.1.3, respectively. By assembling these frames and four pairs of (top and bottom) corner plates, as shown in Figs. 4.1.4 and 4.1.5, required stiffness of the machine were achieved. Principal shaft design for transmitting tractive-force from motor to the machine is shown in Fig. 4.1.6; shaft designed for enabling manual operation of the machine and the other two shaft designs are presented in Figs. 4.1.7 and 4.1.8, respectively. Coupling flanges shown in Fig. 4.1.9 were designed to connect all the four lead-screw shafts with the gearbox. As shown in Figs. 4.1.10 and 4.1.11, two plates were designed with a view to improving stability of the gearbox. Fig. 4.1.12 shows another coupling design, by which the motor and the machine were connected. Components shown in Fig. 4.1.13 were designed, to hold 4 pairs of four point angular contact ball bearings (QJ303 SKF) of back to back arrangement, to allow the machine to carry out either compression or tension tests, on the issued materials. The motor frame, which was designed using the weld structure, with a view to achieving the maximum stiffness, and reducing transmission error, from the motor to the machine, is shown in Fig. 4.1.14. Clamp-frame-carriages shown in Figs. 4.1.15 to 4.1.16 were designed, to execute either the backward or forward linear movement along the lead-screw shafts. The clamp-frames, nuts and clamp-plates, shown in Figs.

4.1.17 to 4.1.19, were designed to move linearly and simultaneously with the above carriages to pull the rubber specimen biaxially. The handle components designed, for manual operation of the machine, are shown in Figs. 4.1.20 to 4.1.22, respectively. Components for indicators (1) and (2) are depicted in Figs. 4.1.23 to 4.1.28, respectively, by which the initial positions of the carriages could be adjusted either manually or electrically.

Appendix 4.2

Biaxial-tension test machine construction

A.4.2.1 Standard components bought from the market

Based on the above detailed design, the main standard components, as listed in Table 4.1, were bought from the market. Some of these are shown in Figs. 4.2.1 to 4.2.4 for the gear box, bearings, motor with switches and four linear shafts as well as the linear bearing, respectively.

A4.2.2 Non-standard components fabricated herein

All the designed components (non-standard ones) were carefully manufactured in the Lab M8, (for the construction of the unique biaxial testing machine), at the University of Strathclyde. The components fabricated mainly include four machine frames, four lead-screw shafts, four carriages, four clamp frames, four pairs of clamp plates, a sliding clutch and a motor mounting frame, etc. Some of these fabricated components are presented in Figs. 4.2.5 to 4.2.11, respectively. Figs. 4.2.5 and 4.2.6 show, one of the machine frame and two corner plates fabricated for the machine, respectively. Carriages and motor frame manufactured are presented in Figs. 4.2.7 and 4.2.8, respectively. Bearing lids, clamp frames with some of their accessories, and four screw feet for the machine, are also exhibited in Figs. 4.2.9 to 4.2.11, respectively.

A4.2.3 Assembly of the machine

All the components either bought outside or fabricated inside were subsequently assembled. Some of the assembled parts are shown in Figs. 4.2.12 and 4.2.13: one was the assembled carriage with leads-crew shaft, and another was the carriage with

a linear shaft. The entire machine was assembled in two stages: one was the initial assembly in the metrology Lab to check, adjust and determine some critical dimensions for the final assembly; another was the final assembly conducted in the machine's working place (Lab M3).

A4.2.3.1 Initial assembly

As shown in Fig. 4.2.14, initial assembly of the machine was conducted in the metrology Lab, where four machine frames, four linear shafts and four carriages were assembled first, from which smoothness of the movement of the carriages along the linear shafts was checked initially. Levels of every part of the machine, after the initial assembly, were checked and modified. One of the full assemblies of the machine, in the metrology Lab, is shown in Fig. 4.2.15. Based on these initial checks and modifications, correct location for every component of the machine was determined. Particularly, positions of the holes for both the corner plates and the machine frames were finalised, by which accuracy and stiffness of the machine were guaranteed, after the required dowels were inserted into these holes.

A4.2.3.2 Final assembly

After completing the final fabrication of the holes, on both the machine frames and the corner plates, they were moved to their working place-Lab M3 for final assembly. Three frames with two bottom corner plates were being assembled, as shown in Fig. 4.2.16. Four frames with the four bottom corner plates fixed were waiting to assemble the (four) top corner plates, as depicted in Fig. 4.2.17. Following the whole frame (including the eight corner plates and four screw feet) was placed on its working table, gear box, four linear shafts, four lead-screw shafts and four carriages, were assembled together, as shown in Fig. 4.2.18. After horizontal level check and adjustment for every component as that for every component in the initial assembly (in the metrology Lab), clamps for the four bottom corner plates were assembled to secure the right position of the machine, as shown in Fig. 4.2.19. Subsequently, the sliding clutch and the motor were assembled to the machine, to allow either manual or automatical operation of the machine, as shown in Fig. 4.2.20.

Finally, as shown in Fig. 4.2.21, horizontal level was checked and adjusted again, until the machine was close to its perfect state. Assembly of the entire machine was completed.

Appendix 4.3 Ultimate strain and strength (MPa) computed from the experimental data

Materials		Nitrile641				Nitrile642				Sponge				
Testing Methods	Specimen Number	Ultimate strain tested	mean	Ultimate strength tested	mean	Specimen Number	Ultimate strain tested	mean	Ultimate strength tested	mean	Specimen Number	Ultimate strain tested	mean	Ultimate strength tested	mean
Uniaxial Tension	dumb-s1	3.85	3.30	3.65	3.70	dumb-s1	5.14	4.58	9.14	8.41	dumb-s1	1.82	1.72	0.55	0.63
	dumb-s2	2.86		3.45		dumb-s2	3.56		6.72		dumb-s2	1.91		0.66	
	dumb-s3	3.18		3.99		dumb-s3	5.04		9.36		dumb-s3	1.43		0.67	
	strip12-s1	4.68	4.69	5.14	5.33	strip12-s1	3.67	5.57	6.31	7.49	strip12-s1	2.62	2.60	0.54	0.55
	strip12-s2	4.63		5.24		strip12-s2	5.84		7.77		strip12-s2	2.60		0.56	
	strip12-s3	4.68		5.45		strip12-s3	5.70		7.36		strip12-s3	2.46		0.57	
	strip12-s4	4.78		5.50		strip12-s4	7.08		8.50		strip12-s4	2.72		0.52	
	strip24-s1	5.12	5.06	6.31	6.20	strip24-s1	6.52	6.93	8.33	8.56	strip24-s1	3.36	2.88	0.96	0.94
	strip24-s2	5.16		6.21		strip24-s2	6.80		8.43		strip24-s2	2.64		0.89	
	strip24-s3	4.94		6.09		strip24-s3	7.72		9.31		strip24-s3	2.60		0.91	
	strip24-s4	5.03		6.20		strip24-s4	6.66		8.19		strip24-s4	2.90		1.01	
Uniaxial Compression	wl-s1	0.82	0.78	19.10	17.70	wl-s1	0.79	0.77	19.38	17.83	wl-s1		0.86		5.52
	wl-s2	0.78		19.45		wl-s2	0.75		19.55		wl-s2				
	wl-s3	0.73		14.55		wl-s3	0.78		14.55		wl-s3	0.86		5.52	
	nol-s1	0.57	0.64	7.46	15.05	nol-s1	0.70	0.67	19.17	19.20	nol-s1	0.94	0.97	19.56	19.08
	nol-s2	0.67		18.62		nol-s2	0.66		19.16		nol-s2	0.99		18.60	
	nol-s3	0.69		19.07		nol-s3	0.64		19.26		nol-s3				
Planar Tension	dumb-s1	0.86	1.16	1.27	1.47	dumb-s1	3.00	2.67	3.53	3.84	dumb-s1	1.10	1.04	0.28	0.28
	dumb-s2	1.21		1.47		dumb-s2	2.22		4.09		dumb-s2	1.01		0.24	
	dumb-s3	1.41		1.66		dumb-s3	2.80		3.90		dumb-s3	1.02		0.32	
	strip-s1	1.96	1.82	2.69	2.42	strip-s1	3.48	3.33	6.25	6.14	strip-s1	2.04	1.99	0.33	0.32
	strip-s2	1.98		2.48		strip-s2	3.08		6.20		strip-s2	1.84		0.29	
	strip-s3	1.74		2.32		strip-s3	3.20		5.58		strip-s3	2.10		0.33	
	strip-s4	1.60		2.18		strip-s4	3.56		6.52		strip-s4				
Planar Compression	s1	0.89	0.85	21.98	23.63	s1	0.86	0.87	26.54	26.56	s1	0.93	0.93	2.05	2.05
	s2	0.90		22.90		s2	0.88		26.57		s2				
	s3	0.75		26.00		s3					s3				
Biaxial Tension	s1	1.14	1.13	1.71	1.75	s1	1.97	1.96	2.95	2.65	s1				
	s2	1.12		1.78		s2	1.81		2.30		s2				
	s3					s3	2.11		2.71		s3				

Table 4.1 Main components bought from the market

Part Number	Name of Component	Quantity	Stock Code	Name of Company
1	Reduction gearbox	1	EK60-1	HPC
2	Rolled Leadscrews	1	LFM306	HPC
3	Rolled Leadscrews	1	LFM306	HPC
4	Trapezoidal Nuts	2	KSM306	HPC
5	Trapezoidal Nuts	2	KSM306	HPC
6	Feather Key	8	KK5-40	HPC
7	bearing	4	Q6303-2RS	HPC
8	Linear Shafting	4	Z-30-1000A	HPC
9	Linear Bearing	8	LBE30	HPC
10	PM4CWS motor	1	224-8125	RS
11	16A Insulated switch	1	350-254	RS
12	SPDT Microswitches (level C)	2	398-7865	RS
13	Four point/Angular contact ball bearing	8	QJ303	SKF

Table 4.2 Selection of the bearings

Bearing Designation	Maximum capacity Static C_0 (N)	Load (N)		Factors			Actual total load $P_0 = X_0F_r + Y_0F_a$	Maximum axial load $C_{0a}=S_0P_0$	Capacity check	Conclusions
		F_r	F_a	X_0	Y_0	S_0				
6303-2RS1	6550	2000	20000	0.6	0.5	1	11200	11200	$C_{0a} > C_0$	Capacity not enough
2303	4000	2000	20000	1	1.3	1	28000	28000	$C_{0a} > C_0$	Capacity not enough
21304	18000	2000	20000	1	2.2	1	46000	46000	$C_{0a} > C_0$	Capacity not enough
7203BG	9500	2000	20000	1	0.52	1	12400	12400	$C_{0a} > C_0$	Capacity not enough
3303	15000	2000	20000	1	0.63	1	14600	14600	$C_{0a} < C_0$	Carrying one diretion load only
QJ303	13700	2000	20000	1	0.58	1	13600	13600	$C_{0a} < C_0$	1. Carrying load in both directions 2. Accormodate misalignment 3. Dimensions are suitable 4. Load carrying capacity enough

Table 4.3 Comparison of deflections with different frame sections

Frame section		Maximum load (kN)	Maximum span (mm)	Each frame weight (Kg)	Maximum deflections (mm)	Stiffness rank
Rectangular	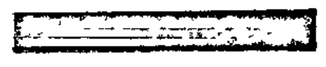	20	410	78.83	2.80	very poor
I-beam		20	410	78.83	0.17	poor
Channel	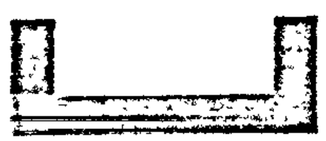	20	410	78.83	0.059	good
Hollow	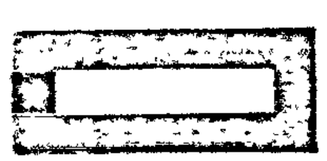	20	410	78.83	0.036	excellent

Table 4.4 Specimens for the tests

Test types	Geometries and Dimensions	Materials	Numbers
Uniaxial Tension	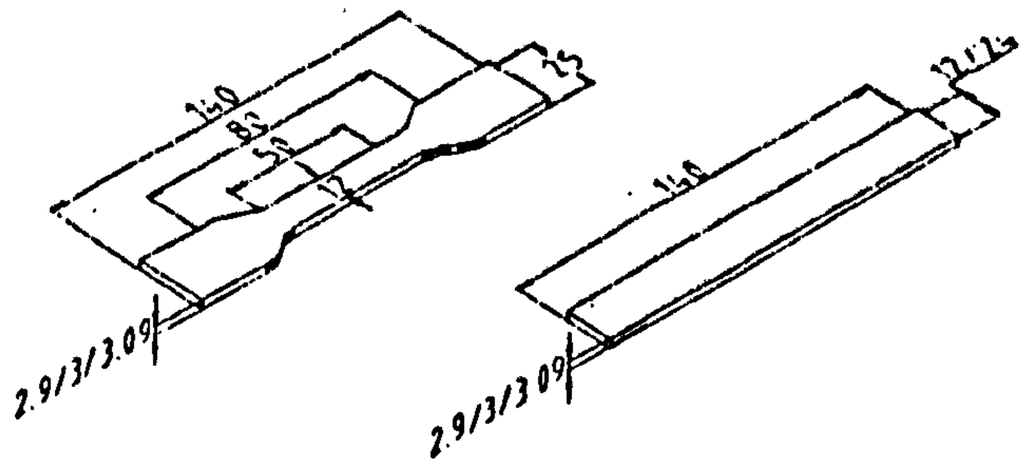	Nitrile641 Nitrile642 Sponge	3-4
Uniaxial Compression	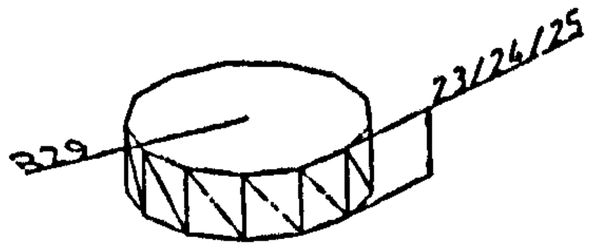	Nitrile641 Nitrile642 Sponge	3-4
Planar Tension	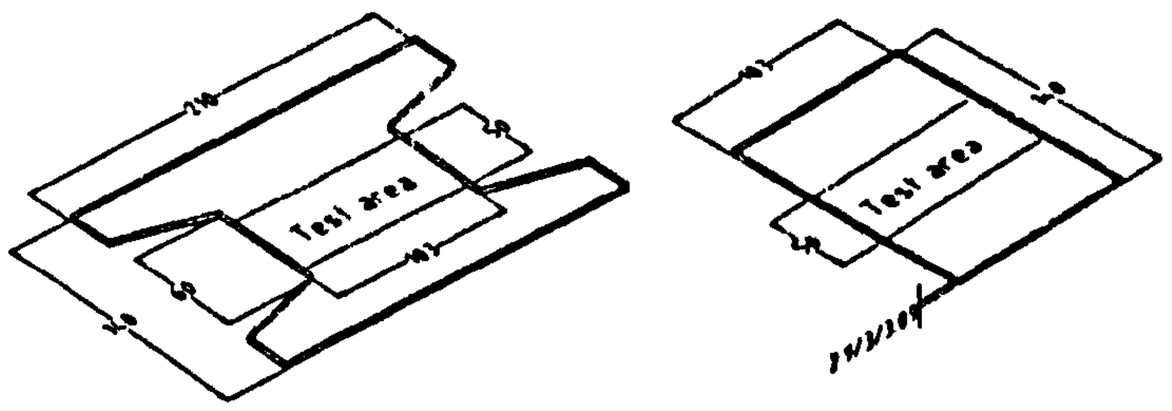	Nitrile641 Nitrile642 Sponge	3-4
Planar Compression	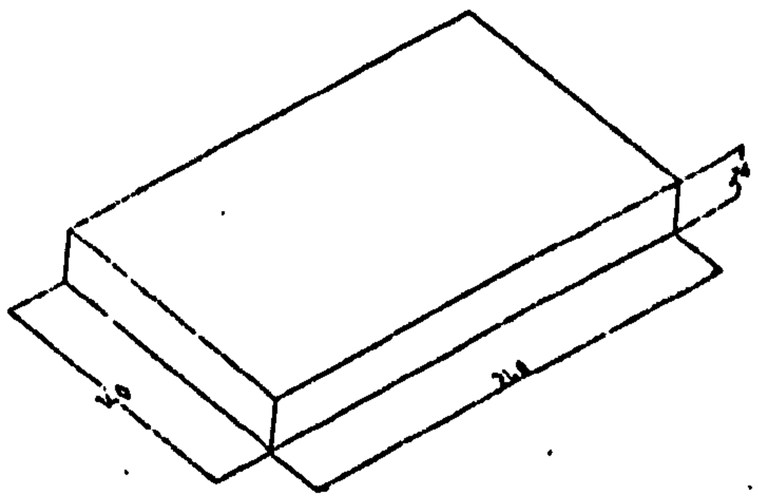	Nitrile641 Nitrile642 Sponge	3-4
Biaxial Tension	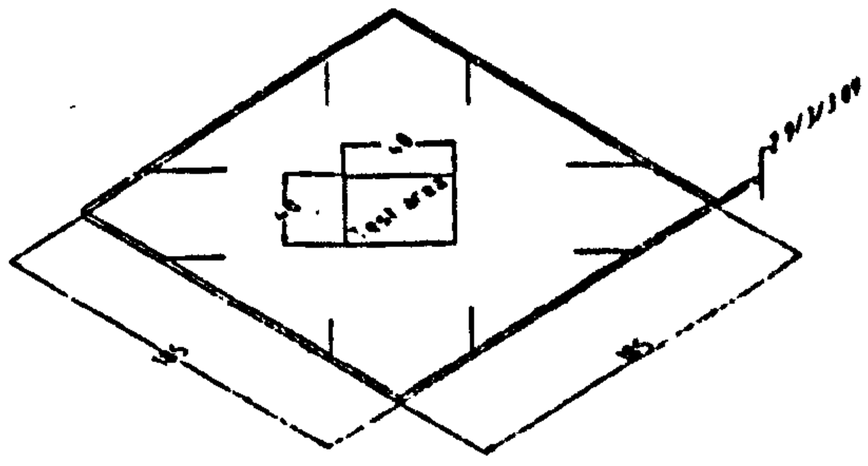	Nitrile641 Nitrile642 Sponge	3-4

Table 4.5 Thicknesses and applications of the Materials

Number	Name of the Materials	Thickness of the materials (mm)	Applications
1	Solid Nitrile641	2.90	Uniaxial tension, Planar tension, Biaxial tension
		25.25	Uniaxial compression, planar compression
2	Solid Nitrile642	3.09	Uniaxial tension, Planar tension, Biaxial tension
		23.48	Uniaxial compression, planar compression
3	Neo Sponge	3.00	Uniaxial tension, Planar tension
		24.31	Uniaxial compression, planar compression

Chapter 5

Upper Bound Analysis of Pressure-Assisted Injection Forging

In this chapter, after the analysis on the needs of an efficient design and analysis procedure in **Section 5.1**, the materials tested, equipment used, and new sets of forming tools developed in particular, are described in **Section 5.2.** Procedures for deriving an upper bound solution for PAIF analysis as well as for experimental validation are introduced in **Section 5.3**. The upper bound solution derived and experimental results are presented in **Section 5.4**, before a discussion is carried out in **Section 5.5**. Conclusions and references are given in **Sections 5.6** and **5.7**, respectively.

Nomenclature

A power dissipation calculation coefficient for W-M, $A = \frac{2\pi\sigma_{ow}\dot{U}}{\sqrt{3}}$;

B power dissipation calculation coefficient for P-M, $B = \frac{2\pi\sigma_{op}\dot{U}}{\sqrt{3}}$;

E_i power dissipation components ($i = I_1, I_2 \ldots I_{p1}, I_{p2} \ldots s_1, s_2 \ldots s_{p1}, s_{p2}, f_1, f_2 \ldots$ and $f_{p1}, f_{p2} \ldots$ respectively; refer to Tables 5.3 to 5.5 for the definition of each component);

h_f height of the flange;

l Length of the tubular billet within the chamber;

m coefficient to measure the friction;

p_{ex89} the pressure applied to the cylindrical surface section 8-9 (refer to the Fig. 5.20) with a radius of r_f by flange ring of the die;

p_{ex910} the pressure applied to the cylindrical surface section 9-10 with a radius of r_f by flange ring of the die.

p_i forming pressure applied by injection punch (refer to Fig. 5.1 and 5.20);

p_p forming pressure applied by pressurising punch (refer to Fig. 5.1 and 5.20);

r, θ, y polar co-ordinate system (refer to Fig. 5.20);

$\bar{r}$ mean radius of the tubular billet ($\bar{r} = \frac{r_i + r_o}{2}$);

r_f outer radius of the flange;

r_i inner radius of the tubular billet;

r_o outer radius of the tubular billet;

t_f thickness of the tubular billet/component ($t_f = r_o - r_i$);

R_1 geometric parameter, $= r_o - r_i$;

R_2 geometric parameter, $= r_f - r$;

R_3 geometric parameter, $= r_f - t_f$;

R_4 geometric parameter, $= t_f - r_f + r$;

R_5 geometric parameter, $= t_f - r_f - r$;

$\dot{U}$ velocity for both punches (refer to Fig. 5.20); also refer to Table 5.1 for the definitions of circumference, radial and vertical velocity components;

$\dot{W}_{il}$ power dissipation due to the internal deformation of the work-material;

$\dot{W}_{ipl}$ power dissipation due to the internal deformation of the pressurising-material;

$\dot{W}_{sl}$ power dissipation due to the internal shear losses along the surfaces of velocity discontinuities within the work-material;

$\dot{W}_{spl}$ power dissipation due to the internal shear losses along the surfaces of velocity discontinuities within the pressurising-material;

$\dot{W}_{fl}$ power dissipation due to the friction between the die and the work-material;

$\dot{W}_{fpl}$ power dissipation due to the friction between the pressurising-material and the work-material;

$\dot{W}_{exf}$ power dissipation due to the external pressure applied through the forming die;

$\dot{W}_{dw}$ power dissipation associated with the work-material;

$\dot{W}_{dp}$ power dissipation associated with the pressurising-material;

$\dot{W}_{id}$ total power dissipation $\dot{W}_{id} = \dot{W}_{dw} + \dot{W}_{dp}$;

$\dot{W}_{ew}$ external power requirement for work-material;

$\dot{W}_{ep}$ external power requirement for pressurising-material;

$\dot{W}_{te}$ total external power requirement;

σ_{ow} flow stress /yield strength of work-material;

σ_{op} flow stress /yield strength of pressurising-material;

τ shear stress/friction stress;

η ratio of the yield strength of work-material to pressurising-material

$\dot{\varepsilon}$ strain rate, refer to Table 5.2 for the definitions of circumference, radial and vertical strain rate components;

5.1 Introduction

As reviewed in the **Chapter 2**, some efforts have been made in the research in Pressure-assisted injection forging. The research conducted so far, for instance, enables a good understanding on the process. Applications of the process to industries would, however, be helped greatly if an efficient design and analysis procedure could be provided. Upper bound method could be a simple and efficient tool for industry.

Based on the upper bound theorem developed by Prager and Hodge [1], an upper bound analysis of injection forging of a solid bar with a solid flange at one of the two ends was conducted [2-3]. Further efforts were made to predict the upper bound loads for similar processes by taking into account of the effect of friction losses [4]. Another progress in the application of the upper bound theorem to the prediction of the upper bound loads for injection forging was the analysis of a tubular billet with a solid flange either at the end of the billet or away from the end [5]. In spite of such efforts, prediction of upper bound loads, using upper bound theorem, for pressure-assisted injection forging of thick-walled tubular components with hollow flanges, has not been attempted. This chapter presents such an analysis. Both, numerical calculations of the upper bound solution and experimental verifications are presented and discussed.

It should be noted that, prior to the development of the upper bound solution for PAIF of thick-walled tubular components with hollow flanges, materials and equipment, particularly new tools developed, for the purpose of validating the upper bound solution experimentally, were prepared and are introduced, firstly, in the following **Section 5.2.**

5.2 Materials and Equipment

5.2.1 Materials

The pure aluminium (E1CM) and five types of polymer rods were used as the work material (for tubular billets) and pressurising materials, respectively, to form the thick-walled hollow flanges with two different flange diameters of 60mm and 85mm. The materials used herein, including the dimensions of their specimens prepared for the tubular billets and pressurising material rods, were similar to those used in the **Chapter 3** and shown in **Table 3.2** and Fig. 3.4. In addition, two groups of cylinder specimens, made of the Solid Nitrile642 (P-M) and pure aluminium (E1CM) (W-M), respectively, were also prepared to determine their mechanical properties by the standard compression tests.

5.2.2 Equipment and development

5.2.2.1 Two existing machines

The 900kN motor driven (TINIUS OLSEN) universal testing machine, which was used for the compression of the compound cylinders in **Chapter 3** (Fig. 3.5) and for the planar compression of the Solid Nitriles in **Chapter 4**, was also used to conduct the compression tests on the pure aluminium cylinders, and to form the thick-walled hollow flanges. The hydraulic driven (Zwick rel 2061 MOW41) universal testing machine, which was used for the qualification of the mechanical properties of the P-Ms under uniaxial compression loading conditions in **Chapter 4** (Fig. 4.1), was also used herein to carry out the compression tests on Solid Nitrile642.

5.2.2.2 Three new sets of tools developed

A new set of forming dies and two sets of punches were designed and fabricated, with a view to carrying out the forming of thick-walled hollow flanges, as well as to validating the upper bound solution to be developed (for PAIF). The design considerations and details are depicted in the following **Sections 5.2.2.2.1** to **5.2.2.2.3**, respectively.

5.2.2.2.1 Design of the forming dies

The set of forming dies, including a lower die, two flange ring dies, an injection chamber, a support ring, a solid punch, two half containers and eight 20mm bolts, were designed to enable the forming of thick-walled tubular components with circular hollow flanges with PAIF. The two flange-ring dies were, particularly, designed to vary the diameters of the hollow flanges. During the test, the assembled die cavity was secured with the two half containers and the eight 20mm bolts. Design details of the forming dies are shown in Figs. 5.2 to 5.8, for lower die, injection chamber, punch, support ring and flange-ring die, respectively.

5.2.2.2.2 Design of the hydraulic punches

The design of hydraulic punches includes two aspects: one was the design of the hydraulic system; another was the design of the injection- and pressurising-punches.

Design of the hydraulic system

More than six types of components were used in the hydraulic system. These include a Hydraulic hand pump (Hi-Force Hydraulics HP110), a Shut off valve (Hi-Force 10000psi HFVS), a Hydraulic pressure gauge (Hi-Force HG1 EN837-1), a gauge mounting block (Hi-Force NGA2) and two high pressure Hydraulic hoses (6B62 B01) as well as a high pressure Hydraulic cylinder (HSS102 AL3047). Among these, the component of shut-off-valve in the system was, particularly, added with a view to obtaining the accurate reading for the load applied to the pressurising material, since the existing valve built in front of the hand pump normally does not work effectively. By adding this additional valve, the pressure level inside the system can be kept still after it reached the expected pressure level, when both valves are closed. In contrast, by opening both valves, the pressure level inside the system can be released.

Calibration of the hydraulic system

After all the above components were assembled, the hydraulic system was calibrated. The calibration results are shown in Fig. 5.9. It was shown that a good linear relationship between the readings of the hydraulic system and the calibration machine was obtained, which ensured that the hydraulic system worked well and properly throughout the tube forming experiments.

Design of the punches

Both inner and outer punches were designed, with a view to applying and controlling the forces onto both the injection- and pressurising-punches separately, by which not only the optimal forming sequences identified previously [6] can be verified experimentally, but also the force displacement characteristics of the forming of thick-walled hollow flanges with PAIF can be studied. The detailed designs of the punches are shown in Figs. 5.10 and 5.11 for the inner and outer punches, respectively.

5.2.2.2.3 Design of the screw punches

Although the hydraulic punches performed satisfactorily during the tests, a set of screw punches, as shown in Fig 3.7(a), was also designed with a view to simplifying the punch system and reducing the costs as well as the potential leakage problems with the hydraulic system. The screw punch mainly includes a lead screw rod, a corresponding nut and two separated punches. By using this set of punches, an initial test was conducted. The results demonstrated that the screw punch, as a simplified forming punch, is feasible to apply the continuous and much more stable load to the pressurising material, as the screw rod was turning downwards for PAIF experiments. In addition, the punches may also be potentially used in the evaluation of material properties under multi-axial loading conditions, in a much simpler manner than those of the conventional methods. Design details of the punches are shown in Figs. 5.12 to 5.19, for the lead-screw shaft, screw punch plate, screw container, compound outer punch, and the others.

After completing the preparation work for experimental validation of the issued upper bound solution in this section, establishment of the upper bound solution for PAIF of the issued components was carried out.

5.3 Procedures

5.3.1 Upper bound analysis

During *PAIF*, the tubular billet, which is supported internally by a pressurising medium and externally by an injection chamber, is injected into the die-cavity to form a required component-form, a hollow flange, in this case. The other component-forms are also possible. The forming of the hollow flange, however, renders general material-flow characteristics of *PAIF*.

5.3.1.1 Assumptions for the analytical model

As shown in Figs. 5.1 and 3.1, both pressurising-material and work-material are deformed sufficiently to convert the compound thick-walled tube into the expected component with a hollow flange. Due to the axial-symmetry of the component, only one quarter of the thick-walled component with its internal pressuring-material and external forming dies were considered. Subsequently an upper bound analytical model was established, as shown in Fig. 5.20.

It was assumed that both injection and pressurising punches were moving downwards with an identical velocity of $\dot{U}$ and therefore imposed forming pressures of p_i and p_p on work-materials and pressurising-materials, respectively. The thick-walled tubular component with hollow flange has the dimensions of an inner radius r_i, an outer radius r_o, wall thickness t_f, flange radius r_f and flange height h_f, which was analytically divided into 6 zones, as denoted as numbers of I to VI, respectively (refer to Fig. 5.20). The internal pressurising-material was also divided

into 3 zones with the series numbers of I_p, II_p and III_p, respectively. In addition, a polar coordinates system (r, θ, y) was used for the analysis. The upper bound theorem [1, 7] was used to estimate the maximum forming force of PAIF of thick-walled tubular component with hollow flange.

The zones of I and I_p were assumed to be rigid bodies and have the same vertical velocity of $\dot{U}$, equivalent to the speed of the ram's as the injection forging progressed. The remaining seven zones were assumed to be perfectly plastic zones. Among them, the materials in the zones of III and III_p were assumed to flow purely radially. That in the zone VI was flowing diagonally towards the top corner of the zone. The zones of II, II_p IV, and V were four turning zones and underwent a 90^0, 90^0, -45^0 and -45^0 turning, respectively, from their starting boundaries to their terminal ones. Seven straight-lines of 3-4, 4-5, 6-7, 7-8, 7-9, 3-13 and 3-12 were assumed to be the boundaries between neighbouring zones, where velocity discontinuities existed. The work-material and pressurising-material in all plastic zones were assumed to be the Mises materials. The friction at the all contact interfaces-between the work-piece/forming-die and work-materials/pressurising-material was described using the following equation [7]: $\tau = \frac{m\sigma_o}{\sqrt{3}}$, where σ_o was defined as the effective flow stresses of σ_{ow} and σ_{op} for both work-material and pressurising-material, respectively. m was the coefficient of friction varying from 0 for a non-friction condition to 1.0 for a maximum friction condition.

It was further assumed that both work-material and pressurising-material were incompressible throughout the PAIF process. Therefore the volume of the intake of the materials due to the downwards movement of both injection and pressurising punches at a velocity of $\dot{U}$ was assumed to be always equal to that of the outlet of the materials from each of the individual zones.

5.3.1.2 Formulas derived for the upper bound solution

Based on above assumptions, the kinematically admissible velocity fields and the corresponding strain-rate fields for all the 9 different deformation zones were deduced and formulated, which are listed in Tables 5.1 and 5.2, respectively. Based on these, power dissipations of forming of the tubular component due to its internal plastic deformation, its shear plastic deformation along the velocity-discontinuity interfaces between any two of the adjacent zones, and the friction losses along friction contact-interfaces were derived, and listed in Tables 5.3 to 5.5, respectively.

Power dissipation due to the horizontal pressure acting on the sidewall of the flange-ring-die on the work-material was also taken into account, which is expressed by equation (1).

$$\dot{W}_{exf} = \frac{2\pi\sigma_o \dot{U}}{\sqrt{3}} m \frac{(r_o^2 - r_i^2)^2}{8 r_f t_f} = \frac{2\pi\sigma_o \dot{U}}{\sqrt{3}} E_{exf} \qquad (1)$$

where $E_{exf} = \dfrac{m(r_o^2 - r_i^2)^2}{8 r_f t_f}$ is a power dissipation factor due to the horizontal external pressure acting on the work-material-surface by the sidewall of the flange-ring-die.

Derivations of the equation (1) and all other equations given in the Tables 5.1 to 5.5 for the work-material are explained in **Appendices 5.1** to **5.5**, respectively. Explanation on the items for pressurising-material is exempted herein, due to their similarities to those for the work material.

5.3.1.3 External power requirements

The external power requirements for PAIF of thick-walled tubular components with hollow flanges are supplied by injection punch with a pressure of p_i and by pressurising punch with a pressure of p_p (Fig. 5.20) with a downward velocity of $\dot{U}$, which can be determined with equations (2) to (4), respectively.

$$\dot{W}_{ew} = p_i \pi (r_o^2 - r_i^2)\dot{U} = P_i \dot{U} \tag{2}$$

$$\dot{W}_{ep} = p_p \pi r_i^2 \dot{U} = P_p \dot{U} \tag{3}$$

$$\dot{W}_{et} = \dot{W}_{ew} + \dot{W}_{ep} = p_i \pi (r_o^2 - r_i^2)\dot{U} + p_p \pi r_i^2 \dot{U} = P_i \dot{U} + P_p \dot{U} \tag{4}$$

where the P_i and P_p are the external total pressure imposed by the injection punch and pressurising punch onto the work-material and the pressurising-material, respectively.

5.3.1.4 The upper bound solution

The external power requirements of $\dot{W}_{ew}$ and $\dot{W}_{ep}$ done by the punch pressures of p_i and p_p should be equal to the power dissipations of $\dot{W}_{dw}$ for the work-material and those of $\dot{W}_{dp}$ for the pressurising-material, respectively, i.e.,

$$p_i \pi (r_o^2 - r_i^2)\dot{U} = \sum_{i=1}^{6} \dot{W}_{Ii} + \sum_{j=1}^{5} \dot{W}_{sj} + \sum_{k=1}^{3} \dot{W}_{fk} + \dot{W}_{exf} \tag{5}$$

$$p_p \pi r_i^2 \dot{U} = \sum_{i=1}^{3} \dot{W}_{Ipi} + \sum_{j=1}^{2} \dot{W}_{spj} + \sum_{k=1}^{3} \dot{W}_{fpk} \tag{6}$$

Substituting the terms on the right side of the equation (5) and (6) with those given in the Tables 5.3 to 5.5 and the equation (1), the follows are obtained:

$$\frac{p_i}{\sigma_{ow}} = \frac{2}{\sqrt{3}(r_o^2 - r_i^2)}(E_{I2} + E_{I3} + E_{I4} + E_{I5} + E_{I6} + E_{s1} + E_{s2} + E_{s3} + E_{s4} + E_{s5} + E_{f1} + E_{f2} + E_{f3} + E_{exf}) \tag{7}$$

$$\frac{p_p}{\sigma_{op}} = \frac{2}{\sqrt{3}r_i^2}(E_{Ip2} + E_{Ip3} + E_{sp1} + E_{sp2} + E_{fp1} + E_{fp2} + E_{fp3}) \tag{8}$$

The maximum forming pressure P_{max} during PAIF of the thick-walled tubular component can be estimated using the upper bound solution:

$$P_{\max} = \pi(r_o^2 - r_i^2)\sigma_{ow}(\frac{p_i}{\sigma_{ow}}) + \pi r_i^2 \sigma_{op}(\frac{p_p}{\sigma_{op}}) \quad (9)$$

The ratio, of effective flow stresses of the work material to those of the pressurising ones at the same level of strain, can be expressed as equation (10)

$$\eta = \sigma_{ow}/\sigma_{op} \quad (10)$$

As a result, equation (8) can be rewritten as equation (11):

$$\frac{p_p}{\sigma_{ow}} = \frac{2}{\eta\sqrt{3}r_i^2}(E_{lp2} + E_{lp3} + E_{sp1} + E_{sp2} + E_{fp1} + E_{fp2} + E_{fp3}) \quad (11)$$

By summing all the terms on the both sides of the equations (7) and (11) correspondingly, the ratio of sum of the both punch-pressures to flow stress of the work-material can be expressed as follows:

$$\frac{p_i + p_p}{\sigma_{ow}} = \frac{2}{\sqrt{3}(r_o^2 - r_i^2)}(E_{l2} + E_{l3} + E_{l4} + E_{l5} + E_{l6} + E_{s1} + E_{s2} + E_{s3} + E_{s4} + E_{s5} + E_{f1} + E_{f2} + E_{f3} + E_{exf}) + \frac{2}{\eta\sqrt{3}r_i^2}(E_{lp2} + E_{lp3} + E_{sp1} + E_{sp2} + E_{fp1} + E_{fp2} + E_{fp3}) \quad (12)$$

5.3.2 Experiments

The experiments were conducted to validate the developed upper bound solution for PAIF of thick-walled hollow flanges. The forming test was performed with the universal testing machine (Fig. 3.5), which was facilitated with an independently-

controlled hydraulic ram mounted against its mechanical platen, as shown in Fig 3.6. Two sets of tools were used in the tube forming tests: the set of dies newly designed (in **Section 5.2**) that enabled the forming of hollow flanges, and the sets of hydraulic/mechanical punches that enabled pressurisation onto the pressurising medium (**Section 5.2** and Fig. 3.7). Both billet/die and polymer/work-material interfaces were lubricated carefully with a hybrid lubrication scheme, as was identified previously [8], to reduce friction at the interfaces and to ease sliding of the work material and polymer along the die and inner surface of the billet. The injection and pressurisation were effected by the tubular injection punch and the solid pressurising punch, respectively. Under the actions of both punches, the specimen was deformed into the thick-walled tubular component with a hollow flange, as shown in Fig. 5.21. The forming pressure and corresponding punch displacement were recorded automatically with the testing machine and the attached transducers.

By using the hydraulic driven universal testing machine (Fig. 4.1), the compression tests were conducted on the cylinder specimens to qualify mechanical properties of the materials.

The experimental results of the compression tests exhibited that the measured true stress-strain curves of the pressuring and work materials can be well fitted with Equations (13) and (14), respectively, as shown in Figs. 5.22 and 5.23.

$$\sigma_{ow} = 135(0.07 + \varepsilon)^{0.33} \text{ MPa} \tag{13}$$

$$\sigma_{op} = 4.7\varepsilon^3 - 4.79\varepsilon^2 + 3.75\varepsilon \text{ MPa} \tag{14}$$

$$\varepsilon = \ln(1 - \Delta L / L_0) \tag{15}$$

where, ΔL is the compression deformation of the specimens (mm), L is the initial height of the specimens. The three constants in each equation were determined experimentally using the measured stress-strain curves.

5.4 Results

The upper bound solution developed is shown in Equations (9) to (12), for predicting the maximum forming force as well as the maximum relative forming pressure (ratio of the applied pressure to the flow stress). Five pressurising materials were also tested (Table 3.2) with PAIF. Some of the specimens produced are shown in Fig. 5.21. Two compression test results, regarding mechanical properties of both work-material and pressurising-material, are presented in Figs. 5.22 and 5.23, respectively. Two billet/component geometries were studied, which are, respectively, defined as Models A and B (Table 5.6), these referring to the changes of billet length and flange dimensions. Initially, forming experiments were conducted to examine the injection-stress and pressurising-stress requirements, with a view to conducting a comparison of the values predicted using the upper bound solution (Table 5.7), for the Models A and B, respectively. A comparison for the Model B is shown in Fig. 5.24.

5.5 Discussion

5.5.1 Validation of the upper bound solution

As shown in Fig. 5.24, the comparison of experimental forming-forces with the analytical ones at different levels of punch displacements was conducted. The analytical pressures were calculated using Equation (9). The flow stresses of σ_{ow} and σ_{op} were determined using Equations (13) to (15). The compression deformation ΔL of the specimen and its height L were taken as the punch displacement and initial length ($160\,mm$) of both rubber rods and tubular billets, respectively. The ratios of both punch pressures to the corresponding flow stresses of both materials- p_i/σ_{ow} and p_p/σ_{op}, defined in Equations (7) and (8) were taken as the upper bound analytical results of 3.8 and 4.19, respectively. These two values were obtained for the specimens shown in Fig. 5.21 and Table 5.6, for the Model B in this case.

As can be seen from the experimental curve in Fig. 5.24, with the increases of the punch displacement from 0 to 5mm during the tube forming, the corresponding forming pressure increased sharply. This was because, at this stage, the work material underwent a transition, from an elastic state to a plastic flow. Bulging of the tube eliminated the clearance between the tube and the injection chamber/die. After this, the punch moved downwards for about 46mm, the hollow flange being formed. The deformation during this stage was a steady process. After the second stage, as the injection of the material continued, the front edge of the flange met the side-wall of the die, due to which the resistance to the material flow increased. As a result, the forming pressure increased sharply again.

Compared with the experimental result (Fig. 5.24), as expected, a big difference exists between the experimental and analytical forming forces, at the initial stage of the forming, as this is a nature of an upper bound analysis. When the die-cavity was almost fully filled, the difference between experimental and analytical forming forces reaches its minimum value. This is because the formed work-piece is mostly similar to the assumed analytical model, as shown in Fig. 5.20. Actually, since it is almost impossible for the material to fill into each corner of the die-cavity perfectly, as that assumed in the analysis, the analytical solution may, therefore always, overestimate the material deformations. The difference between the analytical pressure and the experimental one is, however, less than 5% for the final stage of the forming.

As a result, the upper bound solution presented in this chapter, in deed, predicted the higher forming-force values, which are sufficient, to enable the complete die-filling at the final stage of the tube forming. The difference between the experiments and upper bound solutions, therefore, does not have significant impact on the applications of the method. The solution still gives useful prediction on the forming-pressure requirements for PAIF analysis.

5.5.2 Parametric analysis of tube forming

The analytical results indicate that the forming pressure in the pressure-assisted injection forging of thick walled tubular components varies with mean radius and thickness of the tubular billet, height and radius of the flange of the tubular component, as well as friction at the interfaces, as shown in Figs. 5.25 to 5.27, respectively. Here, the relative forming pressure is expressed with a ratio $(p_i + p_p)/\sigma_{ow}$ of the sum of both punch pressures to the flow stress of the work-material, and is determined with the Equation (12).

Fig. 5.25 shows that the relative forming pressure ratio of $(p_i + p_p)/\sigma_{ow}$ varies with the different mean radii of the tubular billet and the different flange heights substantially, when the thickness of the tubular billet and the diameter of the flange are given. For a given tubular billet with a constant thickness of 9.5 mm and a flange diameter of 60 mm, an increase, of the ratio r_i / r_o of the tube's inner to outer radius, means an increase of its mean radius, which resulted in a decrease of the relative pressure ratio. For example, for the forming of a tubular component with a 10 mm in its flange height, when the radius ratios of r_i / r_o increased from 0.39 to 0.51, the relative pressure ratios of $(p_i + p_p)/\sigma_{ow}$ is reduced from 4.24 to 3.67, with an about 13.4% of reduction in the relative forming pressure. Furthermore, as shown in Fig. 5.25, an increase of flange height h_f increases the relative pressure ratio, due to the increase of amount of the work-material to be deformed. For instance, using the tubular billets with an identical radius ratio of r_i / r_o of 0.39, as the flange height h_f is increased from 7.5 mm to 12.5 mm, the pressure ratio increases by about 2.9%, from 4.16 to 4.28. Obviously, the influence of flange heights on relative pressure is less significant than that the mean radii did.

Fig. 5.26 suggests that the flange radius r_f also affects the relative forming pressure ratio $(p_i + p_p)/\sigma_{ow}$ considerably, when the thickness of the tubular billet and flange height of the tubular component are given. As the flange radius increased, the

relative forming pressure ratio increased significantly. For example, when a tubular billet with a radius ratio of r_i / r_o=0.39 was used to form different radii of the flanges of the components, the increase of the flange radius from 30.0 *mm* to 42.5 *mm* induced an increase in the relative forming pressure ratio from 4.16 to 4.71 with a 13.2% increase. Also, compared with the influence on the relative forming pressure by the flange heights, as shown in Fig. 5.25, influences of the flange radii on the relative pressure ratios were much more significant (Fig. 5.26). This is because an increase of flange radius not only increases the amount of the work-material to be deformed, but also extends the distance for the work-material to flow radially and plastically. Therefore, for a given tube-thickness (9.5 mm in this case), the increases of the flange dimensions (both heights and diameters) led to the increases of the relative forming-pressure requirements.

Fig. 5.27 shows the influences of friction and thickness of the tubular billet on the relative forming-pressure requirement, when the flange dimension (height and radius) is certain. It is clear that an increase of the tube-thickness (ratio of t/r_o) and the friction between the different contacting interfaces (forming die, tubular billet and the pressurising material) resulted in the significant increases of the relative forming-pressure requirement ($(p_i + p_p)/\sigma_{ow}$). This is because increase of tubular thickness and friction increases the amount of the work material to be deformed and the increase of the power required to overcome the friction. Particularly, when the thickness (t_f) is identical, increases of the friction would result in more significant increase of the relative-pressure requirement for larger flanges than that for relatively smaller ones.

5.5.3 Application of the algorithms

Based on above practice in the analysis of PAIF with the algorithm developed, it may be suggested that the upper bound solution developed can be used for the design and analysis of *PAIF* in the following cases:

(a) when the thickness of the tubular billet (t_f) and radius (r_f) of the flange are given, the maximum relative-pressure can be predicted for different mean radii of the tubular billet ($\bar{r}$) and heights of the hollow flanges (h_f).

(b) when the thickness of the tubular billet (t_f) and height (h_f) of the flange are given, the maximum relative forming pressure required for the forming can be predicted for different mean-radii of the tubular billets ($\bar{r}$) and different radii of the hollow flanges (r_f).

(c) when the flange radius (r_f) and flange height (h_f) are given, the maximum relative-pressure can be predicted for different thicknesses of the tubular billets (t_f) and friction conditions.

Therefore, the algorithm developed can be used to produce a reference for the machine selection and tool design for *PAIF* applications.

5.6 Conclusions

From the upper bound analysis of pressure-assisted injection forging of thick-walled tubular components with hollow flanges, following conclusions are drawn:

(1) With reference to the forming configuration of pressure-assisted injection forging of the thick-walled tubular component with a hollow flange, an upper bound solution has been developed and validated experimentally.

(2) The experimental results suggest that maximum forming forces of the forming of thick-walled tubular components can be estimated by the developed upper bound solution with sufficient accuracy.

(3) The experiments and analysis results show that maximum forming pressure decreases with the increase of the mean radius of the tubular billet, but

increases with tubular wall-thickness, flange height and radius as well as the friction between the tube and its surrounding media.

5.7 References

[1] W. Prager and P. G. Hodge, Jr.: "Theory of Perfectly Plastic Solids", Chapman & Hall Ltd., London, 1951.

[2] J. M. Alexander and B. Lengyel, "On the cold extrusion of Flanges Against High Hydrostatic Pressure", Journal of the Institute of Metals, Vol. 93, 1965, pp137-145.

[3] B. Parsons, P. R. Milner and B. M. Cole, "Study of the Injection upsetting of Metals", Journal of Mechanical Engineering Science, Vol. 15, 1973, pp410-421.

[4] W. A. Gordon and C. J. Van Tyne, "Injection Upsetting-An Upper Bound Analysis", NMRCI, 1987, pp278-284.

[5] B. Lengyel, S. A. Shahmoradi and I. A. Chaudhry, "Cold Extrusion of Flanges on Cylindrical Hollows", Proc. 30th Int. MATADOR Conference, 1993, pp227-234.

[6] Y. Qin, "FE and Experimental Analysis of Injection Forging", PhD thesis, Chapter 6, 1997, pp303-368.

[7] B. Avitzur, "Metal Forming Processes and Analysis", Robert E. Krieger Publishing Company, 1979, pp52-64.

[8] Y. Qin and R. Balendra, "Optimisation of the lubrication for the extrusion of solid and tubular components by Injection Forging", Journal of Materials Processing Technology, Vol 135 (2-3), pp 219 – 227, 2003.

[9] B. Avitzur, "Metal Forming: The Application of Limit Analysis", Marcel Dekker, Inc., 1980, pp23-47.

Appendix 5.1

Velocity fields for the work material

On basis of assumptions of both constant volume and incompressibility of the materials during tube forming [7, 9], the strain and strain rate of the materials in all different zones always obey

$$\varepsilon_r + \varepsilon_\theta + \varepsilon_y = 0 \qquad \text{(a5.1.1)}$$

$$\dot{\varepsilon}_r + \dot{\varepsilon}_\theta + \dot{\varepsilon}_y = 0 \qquad \text{(a5.1.2)}$$

Where, ε_r is the radial strain, ε_θ the circumferential/tangential strain, ε_y is the axial strain; $\dot{\varepsilon}_r$, $\dot{\varepsilon}_\theta$ and $\dot{\varepsilon}_y$ are their strain rates in the three directions, respectively.

As shown in Fig. 5.20, both punches were moving downward with same velocity of $\dot{U}$. For the axial-symmetrical analytical model, the circumferential velocities $\dot{U}_\theta$ are always equal to zero for all zones. As a result, only the radial velocity $\dot{U}_r$ and vertical axial velocity $\dot{U}_y$ were derived for each individual zone.

A5.1.1 Zone I

As assumed to be a rigid body and to move vertically downwards, its velocity and strain rate follows below:

$$\dot{U}_{rI} = \dot{U}_{\theta I} = 0 \qquad \dot{\varepsilon}_{rI} = \dot{\varepsilon}_{\theta I} = 0$$

$$\dot{U}_{yI} = -\dot{U} = -1mm/\min \qquad \dot{\varepsilon}_{yI} = 0$$

A5.1.2 Zone II

As assumed to be a perfectly plastic triangle zone and to turn anticlockwise at 90° with its circumferential velocity of

$$\dot{U}_{\theta II} = 0 \qquad \text{(a5.1.3)}$$

From the law of volume constancy, the amount of material flowing into the zone II should be equal to that injected into the zone I i.e.,

$$\pi(r^2 - r_i^2)\dot{U}\,dt = 2\pi r y \dot{U}_{rII}\,dt \qquad \text{(a5.1.4)}$$

from which, the radial velocity component is obtained.

$$\dot{U}_{rII} = \frac{(r + r_i)R_1}{2rt_f} \qquad \text{(a.5.1.5)}$$

According to the law of material incompressibility and equation (a5.1.2), sum of the principal strain rates should be zero within zone II, i.e.,

$$\dot{\varepsilon}_{rII} + \dot{\varepsilon}_{\theta II} + \dot{\varepsilon}_{yII} = 0 \qquad \text{(a5.1.6)}$$

where

$$\dot{\varepsilon}_{rII} = \frac{\partial \dot{U}_{rII}}{\partial r}$$

$$\dot{\varepsilon}_{\theta II} = \frac{\dot{U}_{rII}}{r} + \frac{\partial \dot{U}_{\theta II}}{r\partial\theta}$$

$$\dot{\varepsilon}_{yII} = \frac{\partial \dot{U}_{yII}}{\partial y}$$

Therefore,

$$\dot{U}_{yII} = -\frac{R_1}{2rt_f}\dot{U}\,y \qquad \text{(a5.1.7)}$$

A5.1.3 Zone III

As assumed to be purely radially flowing outwards, correspondingly,

$$\dot{U}_{yIII} = 0 \qquad \text{(a5.1.8)}$$

According to volume constancy,

$$\pi(r_o^2 - r_i^2)\dot{U}\,dt = 2\pi r t_f \dot{U}_{rIII}\,dt$$

The radial velocity component is, therefore, obtained

$$\dot{U}_{rIII} = \frac{r_o^2 - r_i^2}{2rt_f}\dot{U} \qquad \text{(a5.1.9)}$$

A5.1.4 Zone IV

As assumed to be a triangle plastic zone and to turn clockwise at 45^0 from line 6-7 to line 7-8), from the volume constancy

$$\pi[r_o^2 - (r_o - x)^2]\dot{U}\,dt = 2\pi r R_2 \dot{U}_{rIV}\,dt \qquad \text{(a5.1.10)}$$

where $x = \frac{t_f - y}{t_f} R_1$

Therefore, $$\dot{U}_{rIV} = \frac{R_1[2r_o t_f - R_1 R_2]\dot{U}}{2rt_f^2} \qquad \text{(a5.1.11)}$$

and $$\dot{U}_{yIV} = \frac{R_1^2}{2rt_f^2}\dot{U}(y - t_f) \qquad \text{(a5.1.12)}$$

A5.1.5 Zone V

As assumed to be a triangle-plastic flow zone to turn clockwise at 45^0 from the line 7-8 to line 7-9, from the law of volume constancy

$$\pi[(x + r_i)^2 - r_i^2]\dot{U}\,dt = 2\pi r y \dot{U}_{rV}\,dt$$

where $x=\frac{R_1}{t_f}y$, therefore the velocity component for zone V

$$\dot{U}_{rV}=\frac{R_1[2r_it_f+R_1R_4]}{2rt_f^2}\dot{U} \qquad \text{(a5.1.13)}$$

, axial velocity component for zone V is obtained:

$$\dot{U}_{yV}=-\frac{R_1^{\,2}}{2rt_f^2}\dot{U}y \qquad \text{(a5.1.14)}$$

A5.1.6 Zone VI

As assumed to be a perfectly plastic body flowing diagonally towards the corner, from the law of volume constancy

$$\pi[(r_i+x)^2-r_i^2]\dot{U}\,dt=2\pi rh_f\dot{U}_{rVI}\,dt \qquad \text{(a5.1.15)}$$

where $x=\frac{R_1R_4}{t_f}$, from which, the radial velocity component for zone VI is obtained:

$$\dot{U}_{rVI}=\frac{R_1\dot{U}}{2h_ft_f^2}\{\frac{2r_it_fR_4+R_1R_4^{\,2}}{r}\} \qquad \text{(a5.1.16)}$$

Axial velocity component for the zone VI is also obtained:

$$\dot{U}_{yVI}=-\frac{R_1\dot{U}}{2h_ft_f^2r^2}[2r_it_fr+2R_1R_4r]y \qquad \text{(a5.1.17)}$$

After the velocity fields became known, strain-rate fields can be determined from the following and the equation (a5.1.2)

$$\dot{\varepsilon}_r = \frac{\partial \dot{U}_r}{\partial r}$$

$$\dot{\varepsilon}_\theta = \frac{\dot{U}_r}{r} + \frac{\partial \dot{U}_\theta}{r\partial\theta}$$

$$\dot{\varepsilon}_y = \frac{\partial \dot{U}_y}{\partial y}$$

Strain rates for all six zones are listed in Table 5.2.

Appendix 5.2

Internal deformation powers

Internal power rate of plastic deformation is given by

$$\dot{W}_I = \int_v \sigma \dot{\varepsilon} dv = \frac{2\sigma_o}{\sqrt{3}} \int_0^{2\pi} \int_{r_1}^{r_2} \int_{y_1}^{y_2} \frac{1}{\sqrt{2}} \sqrt{\dot{\varepsilon}_r^2 + \dot{\varepsilon}_\theta^2 + \dot{\varepsilon}_y^2} r d\theta dr dy \qquad \text{(a5.2.1)}$$

Where v is the volume of the deformed body; σ is the stress at any point of the deformed body; $\dot{\varepsilon}$ is the corresponding strain rate at any point of the deformed body, and σ_o the effective flow stress of the deformed materials. $\sigma_o = \sigma_{ow}$ for the work material in this case.

A5.2.1 For the zone I

Due to the assumption of a rigid body, its deformation power is expressed as:

$$\dot{W}_{II} = 0$$

Except zone I, all zones including zone II, principal strain rates were involved, when determining the internal-power rate of the material plastic deformation.

A5.2.2 For the zone II

Substituting strain-rates in the equation (a5.2.1), with that given in the Table 5.2 for zone II and performing the integration of θ, r and y, from 0 to 2π, r_i to r_o and 0 to y respectively.

Here y is a function of r and y can be expressed as:

$$y=\frac{(r-r_i)t_f}{r_o-r_i}$$

The internal-power rate for the zone II is obtained:

$$\dot{W}_{12}=\frac{2\pi\sigma_o\dot{U}}{\sqrt{3}}\int_{r_i}^{r_o}(1-\frac{r_i}{r})\sqrt{r_i^2+rr_i+r^2}\,dr \qquad \text{(a5.2.2)}$$

A5.2.3 For the zone III

Substituting strain-rates in the equation (a5.2.1) with that given in the Table 5.2 for zone III, and performing the integration of θ, r and y from 0 to 2π, r_o to R_3, and 0 to t_f, respectively.

The internal power rate for the zone III is derived:

$$\dot{W}_{13}=\frac{2\pi\sigma_o U(r_o^2-r_i^2)}{\sqrt{3}}\ln\frac{R_3}{r_o} \qquad \text{(a5.2.3)}$$

A5.2.4 For the zone IV

Substituting strain rates from Table 5.2 for zone IV into equation (a5.2.1) and performing the integration of θ, r and y from 0 to 2π, r_f-t_f to r_f and y to t_f, respectively.

Here y is a function of r and y is expressed with:

$$y = R_4$$

The internal power rate for zone IV is obtained:

$$\dot{W}_{14} = \frac{2\pi\sigma_o \dot{U}}{\sqrt{3}}\{\frac{R_1}{\sqrt{2}t_f^2}\int_{R_3}^{r_f}\frac{R_2}{r}\sqrt{[r_f R_1 - 2r_o t_f]^2 + [2r_o t_f - R_2 R_1]^2 + r^2 R_1^2}\,dr\}$$

(a5.2.4)

A5.2.5 For the zone V

Substituting strain rates from the Table 5.2 for zone V into equation (a5.2.1) and performing the integration of θ, r and y from 0 to 2π, $r_f - t_f$ to r_f and 0 to y, respectively, here y is the same function of r as that used in the zone IV ($y = R_4$).

The internal power rate for zone V is accordingly deduced:

$$\dot{W}_{15} = \frac{2\pi\sigma_o \dot{U}}{\sqrt{3}}\{\frac{R_1}{\sqrt{2}t_f^2}\int_{R_3}^{r_f}\frac{R_4}{r}\sqrt{[R_1 R_3 - 2r_i t_f]^2 + [2r_i t_f + R_4 R_1]^2 + r^2 R_1^2}\,dr\}$$

(a5.2.5)

A5.2.6 For the zone VI

Similarly, by substituting strain rates from the Table 5.2 into the equation (a5.2.1) and performing the integration of θ, r and y from 0 to 2π, $r_f - t_f$ to r_f and -h_f to 0, respectively.

The internal power rate for zone VI is obtained:

$$\dot{W}_{16}=\frac{2\pi\sigma_o\dot{U}}{\sqrt{3}}\{\frac{R_1}{\sqrt{2t_f^2}}\int_{R_3}^{r_f}\frac{1}{r}\sqrt{[2r_it_fR_3-R_1R_4R_5]^2+[2r_it_fR_4+R_4^2R_1]^2+[2r_it_fr+2rR_1R_4]^2}dr\}$$

(a5.2.6)

Appendix 5.3

Internal shear powers

Internal shear-power rate of the plastic deformation may be expressed as:

$$\dot{W}_s = \int_s \tau |\Delta V| ds = \frac{\sigma_o}{\sqrt{3}} \int_{r_1}^{r_2} \int_0^{2\pi} |\Delta V| r dl d\theta \qquad \text{(a5.3.1)}$$

Where s is the surface of the velocity discontinuity, ΔV the shear velocity difference along the velocity discontinuity surface and dl is a small differential along the velocity discontinuity surface.

A5.3.1 For the velocity discontinuity surface 1 (line 3-4)

$$V_{34}^{It} = \dot{U}_{yI} \sin\alpha = -\frac{t_f}{\sqrt{t_f^2 + R_1^{\,2}}} \dot{U} \qquad \text{(a5.3.2)}$$

where V_{34}^{It} is the tangential velocity within the zone I along the boundary 3-4 and $\sin\alpha = \dfrac{t_f}{\sqrt{t_f^2 + R_1^{\,2}}}$.

The tangential velocity within the zone II along the boundary 3-4 is

$$V_{34}^{IIt} = \dot{U}_{yII}\sin\alpha + \dot{U}_{rII}\cos\alpha = \frac{[(r+r_i)R_1^{\,2} - t_f^2(r-r_i)]}{2rt_f\sqrt{t_f^2+R_1^{\,2}}}\dot{U} \qquad \text{(a5.3.3)}$$

where $\cos\alpha = \dfrac{R_1}{\sqrt{t_f^2+R_1^{\,2}}}$.

Therefore, $$\Delta V_{34}^{I-IIt} = V_{34}^{IIt} - V_{34}^{It} = \frac{(r+r_i)\sqrt{t_f^2+R_1^{\,2}}}{2rt_f}\dot{U} \qquad \text{(a5.3.4)}$$

Also the length of the small differential along the velocity discontinuity surface is expressed as:

$$dl = \frac{\sqrt{t_f^2+R_1^{\,2}}}{R_1}dr \qquad \text{(a5.3.5)}$$

Combining the equations (a5.3.1), (a5.3.4) and (a5.3.5) as well as integrating θ, r from 0 to 2π, and r_i to r_o, respectively, the shear-power rate for the velocity discontinuity surface 1 (line 3-4) is derived:

$$\dot{W}_{s1} = \frac{2\pi\sigma_o\dot{U}}{\sqrt{3}}\{\frac{r_o+3r_i}{4t_f}[t_f^2+R_1^{\,2}]\} \qquad \text{(a5.3.6)}$$

A5.3.2 For the velocity discontinuity surface 2 (line 4-5)

$$V_{45}^{IIt} = \dot{U}_{yII} = -\frac{R_1}{2rt_f}y\dot{U} \qquad \text{(a5.3.7)}$$

where V_{45}^{IIt} is the tangential velocity within the zone II along the boundary 4-5.

Based on the assumption on the zone III, the tangential velocity within the zone III along the boundary 4-5 should be

$$V_{45}^{IIIt} = \dot{U}_{yIII} = 0 \qquad \text{(a5.3.8)}$$

Therefore $$\Delta V_{45}^{II-IIIt} = V_{45}^{IIIt} - V_{45}^{IIIt} = \frac{R_1}{2rt_f} y\dot{U} \qquad \text{(a5.3.9)}$$

The length of the small differential along the velocity discontinuity surface is expressed as

$$dl = dy \qquad \text{(a5.3.10)}$$

Combining equations (a5.3.1), (a5.3.9) and (a5.3.10), as well as integrating θ, y from 0 to 2π, and o to t_f, respectively, the shear-power rate loss due to the velocity discontinuity surface 2 (line 4-5) is obtained:

$$\dot{W}_{s2} = \frac{2\pi\sigma_o \dot{U}}{\sqrt{3}} R_1 \frac{t_f}{4} \qquad \text{(a5.3.11)}$$

A5.3.3 For the velocity discontinuity surface 3 (line 6-7)

Based on the assumption for the zone III,

$$V_{67}^{IIIt} = \dot{U}_{yIII} = 0 \qquad \text{(a5.3.12)}$$

where V_{67}^{IIIt} is the tangential velocity within the zone III along the boundary 6-7. The tangential velocity within the zone IV along the boundary 6-7 is

$$V_{67}^{IVt} = \dot{U}_{yIV}\Big|_{r=r_f-t_f} = -\frac{R_1^2 \dot{U}}{2R_3 t_f^2}(y - t_f) \qquad \text{(a5.3.13)}$$

Therefore, $$\Delta V_{67}^{III-IVt} = V_{67}^{IVt} - V_{67}^{IIIt} = -\frac{R_1^2 \dot{U}}{2R_3 t_f^2}(y - t_f) \qquad \text{(a5.3.14)}$$

Also the relationship of $dl = dy$ (a5.3.10) is applicable herein.

The shear-power rate loss due to the velocity discontinuity surface 3 (line 6-7) is deduced by combining the equations (a5.3.1), (a5.3.10) and (a5.3.14) as well as integrating θ, y from 0 to 2π and o to t_f, respectively.

$$\dot{W}_{s3} = -\frac{2\pi\sigma_o \dot{U}}{\sqrt{3}} \frac{R_1^2}{4} \qquad \text{(a5.3.15)}$$

A5.3.4 For the velocity discontinuity surface 4 (line 7-8)

Tangential velocity within zone IV along boundary 7-8 is

$$V_{78}^{IVt} = \dot{U}_{rIV}\sin\beta + \dot{U}_{yIV}\cos\beta = \frac{r_o R_1}{\sqrt{2rt_f}}\dot{U} \qquad \text{(a5.3.16)}$$

where $\sin\beta = \cos\beta = \frac{\sqrt{2}}{2}$.

Tangential velocity within zone V along the same boundary is

$$V_{78}^{Vt} = \dot{U}_{yV}\sin\beta + \dot{U}_{rV}\cos\beta = \frac{r_i R_1}{\sqrt{2rt_f}}\dot{U} \qquad \text{(a5.3.17)}$$

Therefore, $\Delta V_{78}^{IV-Vt} = V_{78}^{Vt} - V_{78}^{IVt} = \frac{R_1^{\,2}}{\sqrt{2rt_f}}\dot{U}$ (a5.3.18)

The length of small differential along the velocity discontinuity surface here is

$$dl = \frac{dr}{\cos\beta} = \frac{2}{\sqrt{2}}dr \qquad \text{(a5.3.19)}$$

Substituting equations (a5.3.18), (a5.3.19) into (a5.3.1) and integrating θ, r from 0 to 2π, $r_f - t_f$ to r_f, respectively.

The shear power rate loss for velocity discontinuity surface 4 (line 7-8) is derived

$$\dot{W}_{s4} = \frac{2\pi\sigma_o \dot{U}}{\sqrt{3}} R_1^{\,2} \qquad \text{(a5.3.20)}$$

A5.3.5 For the velocity discontinuity surface 5 (line 7-9)

Tangential velocity within zone V along boundary 7-9 is

$$V_{79}^{Vt} = \dot{U}_{rV}\Big|_{y=0} = \frac{R_1[2r_i t_f + R_1 R_4]}{2rt_f^2}\dot{U} \qquad \text{(a5.3.21)}$$

Tangential velocity within zone VI along the same boundary is

$$V_{79}^{VII} = \dot{U}_{rVI}\Big|_{y=0} = -\frac{R_1\dot{U}}{2h_f t_f^2}[\frac{2r_i t_f R_4 + R_1 R_4^{\ 2}}{r}] \qquad \text{(a5.3.22)}$$

Therefore:

$$\Delta V_{79}^{V-VII} = V_{79}^{VI} - V_{79}^{VII} = \frac{R_1\dot{U}(h_f - R_4)[t_f(r_i + r_o) + R_1(r - r_f)]}{2h_f t_f^2 r} \qquad \text{(a5.3.23)}$$

The length of small differential along the velocity discontinuity surface is

$$dl = dr \qquad \text{(a5.3.24)}$$

Substituting equations (a5.3.23), (a5.3.24) into (a5.3.1) and integrating θ, r from 0 to 2π and $r_f - t_f$ o to r_f, respectively.

The shear power rate loss along the velocity discontinuity surface 5 (line 7-9) is obtained:

$$\dot{W}_{ss} = \frac{2\pi\sigma_o U}{\sqrt{3}} R_1 \frac{1}{12h_f}[3h_f(3r_i + r_o) - t_f(5r_i + r_o)] \qquad \text{(a5.3.25)}$$

Appendix 5.4

Friction power rates

Friction energy losses over the die surfaces can be determined by

$$\dot{W}_f = \int_s \tau |\Delta V| ds = \int_s m \frac{\sigma_o}{\sqrt{3}} |\Delta V| ds \qquad \text{(a5.4.1)}$$

A5.4.1 Over the vertical die surface SF1 (line 1-4)

$$|\Delta V|_{14} = \dot{U} \qquad \text{(a5.4.2)}$$

Therefore, by integrating θ and y in the equation (a5.4.1) from 0 to 2π, and t_f to t_f+l, respectively, the friction power loss rate over the die surface 1-4 can be obtained (Table 5.5):

$$\dot{W}_{f1} = \frac{2\pi\sigma_o \dot{U}}{\sqrt{3}} m l r_o \qquad \text{(a5.4.3)}$$

A5.3.2 Over the horizontal die surface SF2 (line 4-8)

There is:

$$|\Delta V|_{48} = |\Delta V|_{46} + |\Delta V|_{68} \qquad \text{(a5.4.4)}$$

where $|\Delta V|_{46} = \dot{U}_{rIII}$ when $r_o \le r \le r_f - t_f$;

$|\Delta V|_{68} = \dot{U}_{rIV}$ when $r_f - t_f \le r \le r_f$.

Combining the (a5.4.1) and (a5.4.4) as well as integrating θ and r from 0 to 2π, r_o to r_f, respectively, the friction power rate loss over die surface 4-8 is deduced (Table 5.5):

$$\dot{W}_{f2} = \frac{2\pi\sigma_o \dot{U}}{\sqrt{3}} m \frac{R_1}{4t_f}[2(r_o + r_i)(r_f - r_o) + t_f R_1] \qquad \text{(a5.4.5)}$$

A5.4.3 For another vertical die-surface SF3 (line 8-10)

There is:

$$|\Delta V|_{810} = |\Delta V|_{89} + |\Delta V|_{910} \qquad \text{(a5.4.6)}$$

where $|\Delta V|_{89} = \dot{U}_{yV}$ when $0 \le y \le t_f$

$|\Delta V|_{910} = \dot{U}_{yVI}$ when $-h_f \le y \le 0$

Combining the (a5.4.1) and (a5.4.6), as well as integrating θ and y from 0 to 2π, 0 to t_f for surface section 8-9 and $-h_f$ to 0 for surface section 9-10, respectively, the friction power loss over die surface 8-10 is obtained (Table 5.5):

$$\dot{W}_{f3} = \frac{2\pi\sigma_o \dot{U}}{\sqrt{3}} m \frac{R_1}{4t_f}[2r_o h_f - t_f R_1] \qquad \text{(a5.4.7)}$$

Appendix 5.5

Power Dissipation due to External Pressures

Power rate dissipation due to overcoming external pressure applied by the side-wall of the ring-die to the cylindrical surfaces 8-9 and 9-10 can be determined by

$$\dot{W}_{exf} = \int_s V p_{exf} ds = \int_0^{2\pi} V_{89} p_{exf}^{89} r_f d\theta \int_0^{t_f} dy + \int_0^{2\pi} V_{910} p_{exf}^{910} r_f d\theta \int_{-h_f}^{0} dy \qquad \text{(a5.5.1)}$$

where

$$V_{89} = U_{rV}\Big|_{r=r_f} = \frac{r_o^2 - r_i^2}{2 r_f t_f}\dot{U} \qquad p_{exf}^{89} = -\frac{\sigma_o m R_1^{\,2}}{4\sqrt{3} r_f t_f} \qquad \text{(a5.5.2)}$$

$$V_{910} = U_{rVI}\Big|_{r=r_f} = \frac{r_o^2 - r_i^2}{2 r_f h_f}\dot{U} \qquad p_{exf}^{910} = \frac{\sigma_o m R_1 r_o}{2\sqrt{3} r_f t_f} \qquad \text{(a5.5.3)}$$

Combining the (a5.4.6), (a5.5.1) and (a5.5.2), and integrating θ from 0 to 2π for both surfaces, y from 0 to t_f for surface 8-9, and -h$_f$ to 0 for surface 9-10, respectively, the power rate losses over flange surface are obtained.

$$\dot{W}_{exf} = \frac{2\pi\sigma_o \dot{U}}{\sqrt{3}} m \frac{(r_o^2 - r_i^2)^2}{8 r_f t_f} \qquad \text{(a5.5.4)}$$

It should be noted that, power losses due to overcoming the exterior pressure, for instance, the pressure applied through the side-wall of the die to the workpiece surface 8-10 in this study, are usually negligibly small, compared with the internal power losses due to the internal deformations. Therefore, when deducing equations of (a5.5.2) and (a5.5.3), some simplifications were made, i.e., constant velocity $\dot{U}$ was used, rather than using $\dot{U}_{yV}\big|_{r=r_f}$ for the flange surface section 8-9 and $\dot{U}_{yVI}\big|_{r=r_f}$ for the flange surface section 9-10.

Table 5.1 Velocity fields of the deformation zones

Materials	Zone no. and deformation features	Circumfere-nce velocity $\dot{U}_o$	Radial velocity $\dot{U}_r$	Vertical velocity $\dot{U}_y$
Work-material (W-M)	I, Vertically downwards	0	0	$-\dot{U}$
	II, Turning anticlockwise 90^0	0	$\frac{(r+r_i)R_1\dot{U}}{2rt_f}$	$-\frac{R_1\dot{U}y}{2rt_f}$
	III, Purely radially outwards	0	$\frac{(r_o^2-r_i^2)\dot{U}}{2rt_f}$	0
	IV, Turning clockwise 45^0	0	$\frac{R_1[2r_ot_f-R_1R_2\dot{U}]}{2rt_f^2}$	$\frac{R_1^2\dot{U}}{2rt_f^2}(y-t_f)$
	V, Turning clockwise 45^0	0	$\frac{R_1[2r_it_f+R_1R_4]\dot{U}}{2rt_f^2}$	$-\frac{R_1^2\dot{U}}{2rt_f^2}y$
	VI, Flowing diagonally towards top right	0	$\frac{R_1\dot{U}}{2h_ft_f^2}\{\frac{2r_it_fR_4+R_1R_4^2}{r}\}$	$-\frac{R_1\dot{U}}{2h_ft_f^2r^2}[2r_it_fr+2R_1R_4r]y$
Pressurising-material (P-M)	I_p, Vertically downwards	0	0	$-\dot{U}$
	II_p, Turning anticlockwise 90^0	0	$\frac{r_i\dot{U}}{2h_f}$	$\frac{r_i\dot{U}}{2rh_f}(h_f-y)$
	III_p, Purely radially outwards	0	$\frac{r_i^2\dot{U}}{2rh_f}$	0

Table 5.2 Strain-rate fields of the deformation zones

Materials	Zone no. and deformati-on feature	Circumference strain rate $\dot{\varepsilon}_o$	Radial strain rate $\dot{\varepsilon}_r$	Vertical strain rate $\dot{\varepsilon}_y$
Work-material (W-M)	I Vertical downward	0	0	0
	II Turning anticlock-wise 90^0	$\frac{(r+r_i)R_1}{2r^2t_f}\dot{U}$	$-\frac{r_iR_1}{2r^2t_f}\dot{U}$	$-\frac{rR_1}{2r^2t_f}\dot{U}$
	III Purely radially outwards	$\frac{r_o^2-r_i^2}{2r^2t_f}\dot{U}$	$-\frac{r_o^2-r_i^2}{2r^2t_f}\dot{U}$	0
	IV Turning clockwise 45^0	$\frac{R_1[2r_ot_f-R_2R_1]}{2r^2t_f^2}\dot{U}$	$\frac{R_1[R_1r_f-2r_ot_f]}{2r^2t_f^2}\dot{U}$	$-\frac{R_1^2}{2rt_f^2}\dot{U}$
	V Turning clock wise 45^0	$\frac{R_1[2r_it_f+R_1R_4]}{2r^2t_f^2}\dot{U}$	$\frac{R_1[R_1R_3-2r_it_f]}{2r^2t_f^2}\dot{U}$	$-\frac{R_1^2}{2rt_f^2}\dot{U}$
	VI Flowing diagonally top right	$\frac{R_1[2r_it_f(R_4+R_1R_4^2]}{2h_fr^2t_f^2}\dot{U}$	$-\frac{R_1\{2r_it_fR_3-R_1[R_3^2-r^2]\}}{2h_fr^2t_f^2}\dot{U}$	$-\frac{R_1[2r_it_f+2R_1R_4]}{2h_frt_f^2}\dot{U}$
Pressurising-material (P-M)	I_p Vertical downward	0	0	0
	II_p Turning anticlock-wise 90^0	$\frac{r_i}{2h_fr}\dot{U}$	0	$-\frac{r_i}{2h_fr}\dot{U}$
	III_p Purely radially outwards	$\frac{r_i^2}{2h_fr^2}\dot{U}$	$-\frac{r_i^2}{2h_fr^2}\dot{U}$	0

Table 5.3 Power dissipations due to the internal deformations

Materials	Zone no. and deformation features	Power dissipation $\dot{W}_{Ii}$ $i=1, 2, 3, 4, 5, 6$ / $\dot{W}_{Ipi}$ $i=1, 2, 3$
Work-material (W-M)	I Vertical downward	$\dot{W}_{I1} = 0$
	II Turning anticlockwise 90^0	$\dot{W}_{I2} = A * E_{I2} = A\int_{r_i}^{r_0}(1-\frac{r_i}{r})\sqrt{r_i^2 + rr_i + r^2}\,dr$
	III Purely radially outwards	$\dot{W}_{I3} = A * E_{I3} = A(r_o^2 - r_i^2)\ln\frac{R_3}{r_o}$
	IV Turning clockwise 45^0	$\dot{W}_{I4} = A * E_{I4}$ $= A*\{\frac{R_1}{\sqrt{2}t_f^2}\int_{R_3}^{r_f}\frac{R_2}{r}\sqrt{[r_f R_1 - 2r_o t_f]^2 + [2r_o t_f - R_2 R_1]^2 + r^2 R_1^2}\,dr\}$
	V Turning clockwise 45^0	$\dot{W}_{I5} = A * E_{I5}$ $= A\{\frac{R_1}{\sqrt{2}t_f^2}\int_{R_3}^{r_f}\frac{R_4}{r}\sqrt{[R_1 R_3 - 2r_i t_f]^2 + [2r_i t_f + R_4 R_1]^2 + r^2 R_1^2}\,dr\}$
	VI Flowing diagonally top right	$\dot{W}_{I6} = A * E_{I6} =$ $A\{\frac{R_1}{\sqrt{2}t_f^2}\int_{R_3}^{r_f}\frac{1}{r}\sqrt{[2r_i t_f R_3 - R_1 R_4 R_5]^2 + [2r_i t_f R_4 + R_4^2 R_1]^2 + [2r_i t_f r + 2rR_1 R_4]^2}\,dr\}$
Pressurising material (P-M)	I_p Vertical downward	$\dot{W}_{Ip1} = 0$
	II_p Turning anticlockwise 90^0	$\dot{W}_{Ip2} = B * E_{Ip2} = \frac{2\pi\sigma_{op}\dot{U}}{\sqrt{3}} * r_i^2$
	III_p Purely radially outwards	$\dot{W}_{Ip3} = B * E_{Ip3} = \frac{2\pi\sigma_{op}\dot{U}}{\sqrt{3}} r_i^2 \ln\frac{R_3}{r_i}$

Table 5.4 Power dissipations due to the velocity discontinuities

Materials	Velocity discontinuity surface no.	Power dissipation $\dot{W}_{si}$ $i=1, 2, 3, 4, 5$ / $\dot{W}_{spi}$ $i=1, 2$
Work-material (W-M)	S1 (line 3-4)	$\dot{W}_{s1} = \frac{2\pi\sigma_{ow}\dot{U}}{\sqrt{3}}\{\frac{r_o + 3r_i}{4t_f}[t_f^2 + R_1{}^2]\}$
	S2 (line 4-5)	$\dot{W}_{s2} = \frac{2\pi\sigma_{ow}\dot{U}}{\sqrt{3}} R_1 \frac{t_f}{4}$
	S3 (line 6-7)	$\dot{W}_{s3} = -\frac{2\pi\sigma_{ow}\dot{U}}{\sqrt{3}} \frac{R_1{}^2}{4}$
	S4 (line 7-8)	$\dot{W}_{s4} = \frac{2\pi\sigma_{ow}\dot{U}}{\sqrt{3}} R_1{}^2$
	S5 (line 7-9)	$\dot{W}_{s5} = \frac{2\pi\sigma_{ow}\dot{U}}{\sqrt{3}} R_1 \frac{1}{12h_f}[3h_f(3r_i + r_o) - t_f(5r_i + r_o)]$
Pressurising-material (P-M)	S_p1 (line 3-13)	$\dot{W}_{sp1} = \frac{2\pi\sigma_{op}\dot{U}}{\sqrt{3}} \frac{(r_i^2 + 3h_f^2)r_i}{4h_f}$
	S_p2 (line 3-12)	$\dot{W}_{sp2} = \frac{2\pi\sigma_{op}\dot{U}}{\sqrt{3}} \frac{3r_i h_f}{4}$

Table 5.5 Power dissipations due to the friction between dic/work-piece and W-M/P-M

Materials	Friction surface no.	Power dissipation $\dot{W}_{fi}$ $i=1, 2, 3$ / $\dot{W}_{fpi}$ $i=1, 2, 3$
Work-material (W-M)	F1 (line 1-4)	$\dot{W}_{f1} = \frac{2\pi\sigma_{ow}\dot{U}}{\sqrt{3}} m l r_o$
	F2 (line 4-8)	$\dot{W}_{f2} = \frac{2\pi\sigma_{ow}\dot{U}}{\sqrt{3}} m \frac{R_1}{4t_f}[2(r_o + r_i)(r_f - r_o) + t_f R_1]$
	F3 (line 8-10)	$\dot{W}_{f3} = \frac{2\pi\sigma_{ow}\dot{U}}{\sqrt{3}} m \frac{R_1}{4t_f}[2r_o h_f - t_f R_1]$
Pressurising-material (P-M)	F_p1 (line 3-5)	$\dot{W}_{fp1} = \frac{2\pi\sigma_{op}\dot{U}}{\sqrt{3}} m R_1 (\frac{r_o^2 + 2r_i r_o - 3r_i^2}{4t_f} - \frac{r_i^2}{2h_f})$
	F_p2 (line 5-7)	$\dot{W}_{fp2} = \frac{2\pi\sigma_{op}\dot{U}}{\sqrt{3}} \frac{m}{2t_f h_f}[r_i^2 t_f - (r_o^2 - r_i^2)h_f](r_f - t_f - r_o)$
	F_p3 (line 7-11)	$\dot{W}_{fp3} = \frac{2\pi\sigma_{op}\dot{U}}{\sqrt{3}} \frac{m R_1 r_i h_f}{2t_f}(-1)$

Table 5.6 Definition of the Models A and B for analysis (Length unit: mm

MODEL	d_o	d_i	d_f	t_f	$2h_f$	L_t
A	35	16	85	9.5	35	230
B	35	16	60	9.5	35	160

Table 5.7 Comparison of the ratios of applied pressures to flow stress of the work material

(Aluminium, $\sigma_{ow} = 84.2MPa$, m=0.0025 for both Models)

Process Modelling Methods	Ratios of applied pressure to yield strength	
	Model A	Model B
Upper bound solution	4.37	3.85
Experimental	4.15	3.66

Chapter 6

Failure Modes and Forming Limits of Pressure-Assisted Injection Forging

In this chapter, following an identification of the inadequacy in investigation of the failure modes and forming limits for PAIF in **Section 6.1**, the materials and equipment used for new experimental investigation are introduced in **Section 6.2.** Procedures, for preparing specimens, conducting forming-limit experiments and FE simulations, are depicted in **Section 6.3.** The experimental and FE simulation results are presented in **Section 6.4,** followed by the discussions on the results in **Section 6.5**. Conclusions are drawn in **Section 6.6.** The references used in this Chapter are listed in **Section 6.7.**

Nomenclature

$2h_f$	free gap height of the die cavity
d	diameter of the polymer rod
d_i	inner diameter of the tubular billet
d_o	outer diameter of the tubular billet
h	height of the tubular billet
h_r	height of the polymer rod
T	aspect ratio $T=2h_f/d_o$
t_f	wall thickness of the tubular billet
t_f/d_o	ratio of wall thickness to the outer diameter of the tubular billet

6.1 Introduction

In order to extend the process ranges and forming limits of injection forging of solid billets (Fig. 2.9(a)), efforts were made through years [1-11] to identify various failure-forms, either experimentally or computationally, with reference to different process parameters. Based on these, measures were searched to prevent the initiation of failures, and hence, to extend the process-ranges. As a result, a procedure was developed to extend effective aspect ratios of the solid flanges formed from 1.2 [7] to 1.64 [11] successfully. Efforts were also made to investigate the failure forms with injection forging of tubular billets with a mandrel (Fig. 2.9(b)) used for supporting the inner surface of the tube; a pre-forming procedure was introduced to extend the solid-flange aspect ratios from 1.8 to 3.6 without folding defects [12]. A number of experiments and FE simulations were also conducted with reference to different forming sequences for PAIF (refer to Fig. 2.9(c)) [13-14]. These were, however, not sufficient for producing a systematic definition on the process-ranges for process design applications. Previous studies were also limited, due to only smaller ranges of pressurising materials being investigated. The studies also did not address the stability of the tubular billets, which is a function of the pressurising-material parameters and pressure-levels applied.

Further to the previous research results, an experimental and EF investigation on the failure modes and process ranges of PAIF was carried out. The results drawn from the study are presented and discussed in this **Chapter**.

6.2 Materials and Equipment

To enable observation of the initiation of typical defects during injection forging, injection forging of the tubular components with hollow flanges was used as a process model for the study. The material deformations at the injection-chamber exit and in the die-cavity in this process represent typical material-flow patterns of the

injection forging of the tubular components. Therefore, the failure models and forming limit diagrams established through this study are of general significance for the design of injection forging of the tubular components.

The work material used throughout the tests was commercially-used pure aluminium E1CM, which had an initial Yield Strength of 84.2MPa. Pressurising materials used were Polyethylene and Nitrile642, which were selected after a series of tests on six groups of polymers, (refer to **Chapters 3** and **5**).

Two sets of tools were developed (refer to Fig. 3.7 and **Section 5.2.2**) for the forming experiments: one was a set of forming dies, which mainly consists of a lower die, an injection chamber and two half containers (Fig. 3.7 (c)), to enable the forming of the hollow flanges; another was a set of hydraulic punches-consisting of a hydraulic pump, cylinder, gauge and two punches, to enable pressurisation onto the pressurising medium (Fig. 3.7 (b)). 3 pairs of spacers with different heights of 19mm, 53.5mm and 88.3mm, were also used, with a view to varying the aspect ratios, from 0.54 to 1.523 and 2.52, respectively.

Similarly, the 900kN TINIUS OLSEN universal testing machine (Fig. 3.5), which was used in the studies described in the **Chapters 3** to **5,** was also used for the experiments herein. Both, pressurising and injection punches' displacements were measured with a DCT1000A LVDT transducer and a PT-101-0010 Wire wound transducer, which are connected to an PC for automatic data-processing. The pressurising punch's load was measured with the hydraulic gauge and the total load was measured with a force transducer, which was also connected to an PC. The injection punch's load was deduced from these values. The experimental set-up is shown in Fig. 6.1.

6.3 Procedure

6.3.1 Preparation of the specimens

All tubular specimens, as shown in Fig. 6.2, were machined from the standard aluminium bar with a diameter of 38 mm. The outer diameter of 35mm for all tubular billets was deigned to fit both the existing lower die's and injection chamber's dimensions. The specimens' inner diameters of 12.4mm and 16.1mm were designed to allow polymer rods to be fitted in with a 0.1mm clearance, so that the influence of different thicknesses of tubular billets on the failure forms could be studied. The heights of 110mm, 120mm and 130mm of the specimens were used to investigate the effects of different aspect ratios on the failure modes. 3 groups (12 specimens in each group), were designed with a view to studying the influences of different loading paths on the failure modes. Specifications of one of the 3 groups of the specimens are listed in Table 6.1.

6.3.2 Considerations for experiments

6.3.2.1 Overall loading path design

3 loading paths, as shown in Fig. 6.3, were designed for testing each group of the specimens (quantity of 12, similar geometries and materials), with a view to qualifying their influences on the initiation of the forming defects. The three loading paths represent the pressures-time histories applied onto the pressurising punch during the forming. The loading path 1 was designed to implement a linear pressurisation throughout the process. The loading path 2 was for a larger initial pressurisation, then sharply increasing the pressure at the 1st stage of the forming; slow increase of the pressure at its second stage. The loading path 3 was designed in contrarily to the loading path 2 (apart from a similar larger initial pressurisation used), i.e., it had a linear increase of the pressure at its 1st stage; a steep increase of the pressure at the 2nd stage. Those three loading paths were used to achieve the

different levels of the stability of the tubular work-piece and different effectiveness' in assisting in material-flow into the die cavity.

6.3.2.2 Specification of the loading path design

For all loading paths, after the injection punch slightly touching the tubular billet, initial pressurisations were applied to the pressurising material to eliminate the initial clearance between the pressurising material and the tubular billet. An initial pressure level of 9.75MPa for loading path 1 was applied, while a pressure level of 24MPa was imposed for both loading path 2 and 3 (Fig. 6.3) with a view to comparing their test results. A constant loading speed of 10 mm/min for loading path 1 (for both punches) was used until each of the 12 specimens reached their final position of 10mm from the exit of the injection chamber.

For loading path 2 and 3, besides a much higher initial pressurisation (24MPa) used, the subsequent tests were conducted in two stages, which referred to the different pressure and time/displacement combination, as well as different loading speeds, (rather than a single stage and a constant loading speed for loading path 1 by which a linear increase of the pressure from 9.75MPa to 28.8MPa was created (Fig. 6.4)). Namely, for loading path 2's 1^{st} stage (refer to Fig. 6.3), a much higher pressurisation up to 67.9MPa was used and a much slower speed of 1 mm/min was chosen for the injection of the tube, with a view to observing the deformation of the tube during the first stage. The displacement for this stage was designed to be one fifth of the total length of the injected tube of each specimen. For loading path 2's 2^{nd} stage, pressurisation rate was reduced, only increasing from 67.9MPa to 101.8MPa, but the rate of injection of the tubular billet was increased from 1 mm/min to 10 mm/min, with a view to supplying enough work-material for the final die filling during this stage. The displacement for the 2^{nd} stage was correspondingly designed to be four fifth of the total length of the injected tube of each specimen.

For loading path 3's 1st stage, a much lower pressurisation of only up to 44MPa was used, but a much faster speed of 10 mm/min was set for the injection of the tube, with a view to quick supplying enough work material during this stage and observing the differences of the deformation processes between this stage and the loading path 2's 1st stage. The displacement for the 1st stage herein was designed to be four fifth of the total length of the injected tube of each specimen. For loading path 3's 2nd stage, pressurisation was speed up from 44MPa to 101.8MPa, but speed for injection of the tubular billet was slow down from 10 mm/min to 1 mm/min. Such a slow rate was used herein with a view to reducing the work material injected and identifying the differences of the deformation processes between this stage and the loading path 2's 2nd stage. The displacement for the 2nd stage herein was correspondingly used to be one fifth of the total length of the injected tube of each specimen.

Specifications of the loading paths for the experimental and FE investigation of the failure modes are shown in Fig. 6.3, in which all the pressure levels and displacement values were designed to be achievable, under the issued forming-limit-test conditions.

It should be noted that the values of the loading paths may be different (higher) from (than) the values shown in Fig. 6.3 for an actual tube-forming test, in which a much higher pressure levels will be involved, rather than the pressure levels, under the relative "free-forming-limit" tests herein. Also, although two stages were involved for loading path 2 and 3, only a single stroke was used to form the tubular component.

6.3.2.3 Specimen arrangements

For each of the loading paths, 12 specimens were used and arranged in such a way, that 3 groups of 4 specimens with the similar height in each group were tested, to study the failure modes under different aspect ratios (0.54, 1.523 and 2.52). Also, within each group's 4 specimens, 2 different thicknesses of tubular billets and 2

different pressurising materials were involved, so that under an identical aspect ratio, the influences of the issued factors (tubular thicknesses and materials) on the failure forms could also be investigated.

6.3.3 Forming-limit experiments and FE simulations

Initially, an optimal lubrication scheme [15] was applied to the interfaces between the pressurising materials/tubular billets and tubular billets/die surfaces. 3 pairs of spacers with different heights (19mm, 53.5mm and 88.3mm) were used to make up of 3 different aspect ratios of T=0.54, 1.523 and 2.52, respectively. Then following the test procedures designed, forming experiments and FE simulations were conducted for each combination of the loading paths, billet geometries, die-cavities geometries and pressurising materials. The formed specimens were sectioned for assessing the deformations of the materials. Initiation of the forming defects was also identified through FE simulation.

6.4. Results

Experimental failure modes, for the given 3 aspect ratios and 3 loading paths were produced and shown in Fig. 6.4. Some close views for the larger aspect ratios T>1.5 are also shown in Fig. 6.5. A comparison of an experimental result and a simulated deformation is presented in Fig. 6.6. The observed deformations/defects were classified into several standard forms, as depicted in Fig. 6.7, which were further used for developing the forming limit diagrams for pressure-assisted injection forging of tubular components.

6.5 Discussion

6.5.1 Experimental results

As shown in Figs. 6.4 and 6.5, for the given two different pressurising materials (Solid Nitrile642 and Polyethylene) and two different tube-thicknesses (t=9.45 mm and t=11.3 mm), various failure forms were observed for the different loading paths (1 to 3), and particularly for the different aspect ratios (T=0.54, 1.523 and 2.52). With reference to the variation of aspect ratios only, the failure forms may be further classified as three main categories:

a). buckling or bending when the high aspect ratios (flange-height/tube-thickness ratio) $T > 1.5 - 2.5$;
b). folding or folding plus material accumulated at the injection-chamber exit when the aspect ratios $0.7 < T < 1.5$);
c). folding or fracture plus weakened section when the aspect ratio $T < 0.7$.

With reference to the different loading paths, failure forms also occurred differently. For example, for a given aspect ratio (T=2.52), refer to Fig. 6.5 (a), although bending and buckling occurred for all three loading paths, the extents of the bending/buckling were different, i.e., loading path 1 produced the severe failure forms; the loading path 2 resulted in the least extent of failure forms; and loading path 3 showed the moderate extent of failure forms. The reason may be that, when a small pressurisation onto the pressurising material was maintained throughout the forming (Fig. 6.3 and loading path 1), extra stability of the tube, which could be created by the pressurisation, was less significant. As a result, extent of the buckling/bending is larger, compared with a higher, internal pressurisation, as utilised in the loading path 2 (Fig. 6.3).

The influences of the different thicknesses of the tubular billets and the different pressurising materials on the failure forms were also studied. The results showed that

the thicker the tubular billets were, the more stable the tubular billets were. Therefore, the extent of the failure forms of buckling or bending for the thickness of t_f=9.45 mm were larger than the ones with a thickness of t_f=11.3 mm. The tendency of producing a failure form with pressurising material-Polyethylene was bigger than that with Solid Nitrile642, particularly, when the aspect ratio T > 0.7. It may be interpreted by the different characteristics of the mechanical properties of the pressurising materials. For instance, under a same value of strain, the hardness with Solid Nitrile642 was much lower than that with Polyethylene. Solid Nitrile642, therefore, might function better as a hydrostatic medium to the work material (E1CM tube) than Polyethylene did, particularly under the relative "free-forming-limit" testing conditions.

The experimental results, however, also suggested that when the pressurisation became a dominant factor, compared with the initial yield strength of the pressurising medium, the type of the pressurising medium was no longer a significant factor, in terms of the prescription of the global failure-forms of the work-piece. The damage of the pressurising material and its follow ability under high pressures do prescribe the local deformation of the work-piece, and hence, have effects on the forming of sound component-forms.

As shown in Fig. 6.6, a good agreement was reached, from a comparison of the experimental result with FE simulation result, which may verify that the specimen preparation, the testing procedures designed and facilities used, as well as the experimental results, are reliable and applicable.

6.5.2 Standard failure modes

Based on both the experimental and FE simulation results, the different standard failure modes for different aspect ratios and loading paths are depicted in Fig. 6.7, most of which, (apart from failure form "H", due to the limitation of the stroke (57mm) with the hydraulic cylinder used), were observed experimentally. It is a

general indication of the process ranges of injection forging of the tubular components. For example, when tube forming was conducted under loading path 1, failure forms A to G will occur inevitably. Under loading path 2, although the initial pressure (24MPa) applied to the P-M as well as pressurisation throughout the forming was higher than that for loading path 1 and failure form C was therefore avoided, the pressure levels were not high enough to eliminate the failure forms D to G. Also it indicates that though the loading path pattern for loading path 3 was different from the one for loading path 2, failure forms occurred were almost identical, due to the insufficient pressurisation levels for the loading path 3, during the forming-limit tests.

6.5.3 Forming limit diagrams

Based on the above standard failure modes produced experimentally and computationally, it was, therefore, deduced that if the same loading-path pattern (pattern for the loading path 3 in Fig. 6.3) was used, by applying much higher initial pressure and pressurisation levels for the forming, the tendency of initiation of the failure forms might be reduced. That is, failure forms D to G might be eliminated, for which another *loading path* was designed and shown in Fig. 6.8. Based on these analysis and also by taking the influences of the tubular thicknesses and pressurising materials into account, three forming limit diagrams were further proposed, as shown in Figs. 6.9 to 6.11, for three loading paths (loading paths 1, 2 in Fig. 6.3 and loading path in Fig. 6.8) respectively, with a view to establishing the optimal forming sequences for PAIF of thick-walled tubular components.

Forming limit diagrams 1 and 2 (Figs. 6.9 and 6.10) were established based on the experimental results for loading paths 1 and 2 used in this experimental investigation, as shown in Fig. 6.3. Forming limit diagram 3 (Fig. 6. 11) was proposed based on the above both experimental and analytical results for loading path shown in Fig. 6.8. Although the pressure levels designed for the loading path shown in Fig. 6.8 was impossible to be achieved experimentally with the free forming limit tests herein, due

to the limitations of the facilities (tools and hydraulic cylinder) used, a similar loading path, similar loading-path pattern to the one shown in Fig. 6.8, but with much higher pressure levels (from 60MPa to 471MPa), as shown in Fig. 6.12, was designed for the tube forming experiments, with a view to examining the loading path pattern and forming sequences designed, as well as completing the forming limit diagram 3. This is because pressure levels shown in Fig. 6.12 could be achieved when a flange ring-die was used, rather than the spacers in the free-forming-limit tests.

In the tube forming tests, an aspect ratio of T=1.0, tubular thickness of t_f =9.45 mm and two types of pressurising materials (Solid Nitrile642 and Polyethylene) were used.

Using the results as a design guideline (standard failure modes in Fig. 6.7, forming limit diagram 3 in Fig. 6.11 and loading path in Fig. 6. 12), some sound tubular component-forms have been produced, two of which as well as their sectioned views are shown in Fig. 6.13. These results not only verified the testing procedures designed, but also facilitated the completion of the forming limit diagrams.

It should be noted that although both the standard failure-modes (Fig. 6.7) and the forming limit diagrams (Figs. 6.9 to 6.11) have been created, influences of the forming sequence in some aspect-ratio ranges have not been experimentally defined yet, such as failure form "H" in Fig. 6.7. Also in the forming limit diagrams (Fig. 6.9 to 6.11), only limited experimental data were available to define some ranges. Further experiments and FE simulations, therefore, need to be conducted to complete these failure modes and forming limit diagrams completely.

6.6 Conclusions

From the experimental and analytical investigations on the failure forms with pressure-assisted injection forging of thick-walled tubular components, following conclusions may be drawn:

(1) With reference to the different aspect ratios and loading paths, failure-forms of the workpiece during PAIF of thick-walled tubes were identified.

(2) Forming limit diagrams have been produced, which can be used as the guidelines during the design of the injection forging process.

(3) Failures for the thinner tube (t_f=9.45 mm) were severer than that for the thicker tube (t_f=11.3 mm).

(4) Failures with Polyethylene were severer than that with Solid Nitrile642, when $T > 0.7$.

(5) Further efforts will be made to design "optimal" forming sequences, through an optimisation procedure, either to extend the forming limits of the process or to improve the quality of the formed components.

6.7 Reference

[1] "Some aspects of the cold extrusion of steel", NEL Report 196, Staff of Plasticity Division, Department of Industry, UK, 1965.

[2] J.C. Henry, "An investigation of the injection upsetting of six steels", NEL Report 494, Department of Industry, UK, 1971.

[3] R. Balendra, "Process mechanics of *injection upsetting*", International Journal of Machine Tools Manufacture, Vol. 25 (1), 1985, pp63-73.

[4] Y. Qin and R. Balendra, "Development of the flaws during injection forging", Proceedings of the 10th NCMR, Loughborough, UK, 1994, pp587-591.

[5] R. Balendra and Y. Qin, "FE simulation of the development of flaws during injection forging", Int. J. Mach. Tools Manuf. Vol. 34 (8), 1994, pp1091-1101.

[6] Y. Qin, "Limiting aspect ratio of the PDZ", Chapter 4, PhD thesis, Strathclyde Unversity, 1997, pp178-250.

[7] Y. Qin and R. Balendra, " The limiting aspect ratio of the PDZ in injection forging, Proc. 32nd Int. MATADOR Conf. Manchester, UK, 1997, pp349-354.

[8] R. Balendra, "Material-flow considerations for the design of injection forging", Trans. ASME, J. Manuf. Sci. Eng. Vol. 119, 1997,pp350-357.

[9] Y. Qin and R. Balendra, "Preform design for eliminating folding defects during injection forging of engineering components", Proc. 14th Int. Conf. on CAPE, 1998, pp307-312.

[10] R. Balendra and Y. Qin, "Identification and classification of flow-dependent defects in the injection forging of solid billets", J. Materials processing technology", Vol. 106, 2000, pp199-203.

[11] Y. Qin and R. Balendra, "An approach for the forming of large-thickness-flange components by Injection forging", J. Mater. Proces. Technology, Vol. 145, 2004, pp153-162.

[12] S. B. Petersen, et al, "Extended formability limits for tubular components through combined injection forming/upsetting-a finite element analysis", Proc. Mech. Engrs, Part B Vol. 209 (B2), 1995, pp107-114.

[13] D. Colla, et al, "An investigation into the performing of tubes", Int. J. Mech. Sci. Vol. 39, No. 5, 1997, pp507-521.

[14] Y. Qin and R.Balendra, "Simulation of forming sequence of Pressure-assisted injection forging of thick-walled tubes", Trans. NAMRI/SME, Vol. XXIII, 1995, pp27-32.

[15] Y. Qin and R. Balendra, "Optimisation of the lubrication for the extrusion of solid and tubular components by Injection Forging", Journal of Materials Processing Technology, Vol. 135/2-3 2003, pp 219 – 227.

Table 6.1 Specifications of the specimens

Specimen Number/code		work material	Dimensions of tubular billets (mm)			pressurising materials	Dimensions of polymer rods (mm)	
			d_i	d_o	h		d	h_r
1	NL1	aluminium	16.1	35	130	Nitrile642	16	130
2	HL1	aluminium	16.1	35	130	Polyethylene	16	130
3	NL2	aluminium	12.4	35	130	Nitrile642	12.3	130
4	HL2	aluminium	12.4	35	130	Polyethylene	12.3	130
5	NL3	aluminium	16.1	35	120	Nitrile642	16	120
6	HL3	aluminium	16.1	35	120	Polyethylene	16	120
7	NL4	aluminium	12.4	35	120	Nitrile642	12.3	120
8	HL4	aluminium	12.4	35	120	Polyethylene	12.3	120
9	NL5	aluminium	16.1	35	110	Nitrile642	16	110
10	HL5	aluminium	16.1	35	110	Polyethylene	16	110
11	NL6	aluminium	12.4	35	110	Nitrile642	12.3	110
12	HL6	aluminium	12.4	35	110	Polyethylene	12.3	110

Chapter 7

Forming of an Engineering Component with Pressure-Assisted Injection Forging

In this chapter, after the insufficiency with the manufacture of engineering components, like gears, is revealed in **Section 7.1,** materials and equipment used for experimental investigation are described in **Section 7.2.** Procedures, for preparing specimens and producing the preforms of hollow-gear-shafts, are introduced in **Section 7.3.** Experimental results are presented in **Section 7.4,** followed by the discussion on the results in **Section 7.5.** Conclusions are drawn in **Section 7.6** and all references used in this chapter are given in **Section 7.7.**

Nomenclature

L	displacement of either inner/pressurising punch or outer/injection punch
p	pressure applied by either inner/pressurising punch or outer/injection punch

Subscripts

i	initial, inner/pressurising punch
o	current, outer/injection punch
1	forming stage 1
2	forming stage 2

7.1 Introduction

Gears are well known, the most important types of engineering components widely used by industry, particularly by automotive and aerospace industry. Gears can be manufactured in many ways, such as casting, forging, rolling, cutting, blanking, powder metallurgy and so on [1]. Although cutting has been a predominating means for manufacturing gears for many decades up to now, after insufficiencies, such as long production lead-time, complex tooling, expensive machinery, material waste, and particularly, the reduced strength of the gears produced, had been identified [2-3], hot die forging, as an alternative means, was used to produce this type of components, for more than two decades [4], due to its ability to achieve complex component-forms and to improve component-strength. It was reported that a bevel gear was hot-die forged successfully, using 7 operational sequences [4]. Although this process resulted in a 25% material savings due to its flashless, compared with conventional hot forging of the same part (with flash), the multi-operational stages and the post forging process requirements, namely, post heat treatment and machining still cost a lot.

In order to minimise the drawbacks with the hot die forging of gears, cold die forging was subsequently employed to achieve the near-net-shape forging of gears. Kondo [5], for instance, produced hollow gears satisfactorily, using cold die forging plus post machining, in which a Divided flow method (flow relief-hole principle and flow relief-axis principle) was initially proposed and used effectively. A bevel gear was also formed with success, by using a way so called Forging with Fully Enclosed Dies (FED Forging) [6], though the tooling and machinery were quite complex.

From the development of forging processes for producing gears point of view, advantages with cold die forging, may be summarized as:

(1) Gears produced with excellent tolerances and surface finish, since thermal expansion, associated with hot forging is eliminated.

(2) Material waste and post machining are reduced, since the near-net shape of

gears can be achieved.

(3) Gears cold-forged are strengthened, since the better grain flow and strain hardening can improve the mechanical properties of the gears.

On the other hand, cold die forging also has some typical problems. These may include:

(1) high performances with cold forging dies are required to withstand the much higher pressure levels of up to 2.07GPa [7].
(2) Several preforming stages are required in the conventional cold forging. Tooling costs are, therefore, increased.
(3) Strain hardening associated with cold forging, on the other hand, results in the loss of formability of the material.
(4) Efficient lubricants/special coatings are needed to reduce the friction throughout the cold forging processes.

Pale [7] also pointed out that "Recent developments for forming complex shapes such as bevel gears and trunions require 2 or 3 independent tool motions, achieved at an additional cost."

Injection forging/radial extrusion, as an extrusion process, which is suitable for production of precise component with complex geometry, has, therefore, been paid more attention by many researchers [4, 7-8]. This is because injection forging has both, the advantages with cold die forging and the potential merits with injection forging itself, as mentioned in **Section 2.7**. Toothed components were attempted with injection forging/radial extrusion with a view to overcoming the drawbacks with cold die forging. For example, "wheels with helical gears can be produced" [9] and "In the laboratory, quality class IT 6-7 is attainable for planetwheels for automatic transmissions, by lateral extrusion." [9].

"However, this quality is not sufficient enough for gear wheels of car gear boxes where accuracies up to IT5 are requested due to quietness." [8] and "For the use of

the net-shape production in practice, the cold forging of running gears is not perfect yet" [9]. Prof. Geiger further concluded that "A concluding outlook on the next years in cold forging technology does not suggest any revolutionary new technologies. Optimization and improvement of existing procedures and process combinations is standing in the foreground." [9].

Significant efforts were devoted to both, the modification of the existing processes and the development of the computer-aided design systems, for either injection forging or cold, warm and hot die forging of gears [2-3, 10-13] recently, with both powerful FEM and experimental method, from which, optimal geometries of the gears were achieved and the final die filling forces were reduced.

Further to the above achievements in the forming of gears, Pressure-assisted Injection Forging, was used to form a hollow-gear with hollow shaft. The findings from the 1st stage of this research are reported and discussed in this chapter.

7.2 Materials and Equipment

7.2.1 Materials

The commercially pure aluminum (E1CM), with a characteristics of the mechanical properties of $\sigma_{ow} = 135(0.07 + \varepsilon)^{0.33}$ MPa, was selected as the work-material. There were two reasons for this choice:

(a) its good ductility and formability under room temperature; (b) the pressure level produced during the forming is affordable with the existing forming facility within the laboratory.

The Solid Nitrile642 and Polyethylene were used as the pressurising materials for the preform of the hollow-gear-shafts with Pressure-assisted injection forging. Both Solid Nitrile642 and Polyethylene were chosen based on a series of tests, which confirmed that they are the mostly suitable pressurising materials for PAIF.

Such selection of the materials would, therefore, facilitate the experimental investigation on the preforming of the hollow-gear-shafts.

7.2.2 Equipment

The 900kN motor driven (TINIUS OLSEN) universal testing machine (Fig. 3.5) and an independently controlled hydraulic ram (Fig. 3.6), which are the same as that used for the study described in the **Chapters 3** to **6**, were also used in the forming of the hollow-gear-shaft (preform) herein. Similarly, the total load and pressurising punch's loads were recorded using a built-in load cell and a high pressure hydraulic gauge, respectively, from which the injection punch's load was deduced. Both, the built-in load cell and the high pressure hydraulic gauge, were connected to a PC based data acquisition system for data processing. The injection and pressurising punches' displacements were measured with a PT-101-0010 Wire wound transducer and a DCT1000A LVDT transducer, respectively. Both transducers were also connected to the PC for automatic data acquisition.

The two sets of tools described in **Sections 5.2.2.1** and **5.2.2.2** were also used for the forming of the hollow-gear-shafts. One set (Fig. 3.7(c)) enabled the forming of hollow flange, another (Fig. 3.7(b)) enabled the pressurisation during the forming. In order to form the hollow flanges with secondary elements – preforming of an integral hollow-gear-shaft, a forming die with tooth elements was further designed and shown in Fig. 7.1. The outer diameter (85mm) of the forming die was designed to allow it to slide into the existing flange ring-die with a 0.08mm clearance. The top and root diameters of the tooth elements within the forming die were designed to be 50mm and 60mm, respectively. The forming die fabricated is shown in Fig. 7.2.

7.3 Procedures

7.3.1 Preparation of the specimens

Specimens were designed and fabricated from the standard pure aluminum bars with a diameter of 38 mm. The outer diameter of 35mm for all tubular billets was used to fit the existing forming dies' geometries (lower die's and injection chamber's dimensions). The specimens' inner diameters of 16.1mm were designed to allow the polymer (Solid Nitrile642 and Polyethylene) rods to be fitted in with a 0.1mm clearance, so that the optimal lubrication scheme identified previously [14] could be applied onto the contact interface between the tubular billet and the polymer rod. The height of 160mm was used for all specimens with a view to forming a hollow-gear-flange with a hollow shaft. The diameter for the hollow gear-flange and the length for the hollow shafts were designed to be 60mm and 35mm, respectively. Two different pressurising materials were used with a view to comparing the differences in their performance in the assisting in the forming of the hollow-gear-shafts. Specimens prepared and specifications of the two groups of the specimens are shown in Fig. 7.3 and Table 7.1, respectively.

7.3.2 Design of the testing procedures

Two aspects were considered in the design of the testing procedures: one was the pattern of loading; and another was the magnitude of loading.

7.3.2.1 Pattern of loading

The loading pattern for the forming of the hollow-gear-shafts, were determined based on the forming limit diagrams developed in **Chapter 6** for PAIF of thick-walled

tubular components. The loading pattern for loading path 3 shown in Fig. 6.3 was chosen, with a view to producing the tubular components with secondary elements flawlessly, and simultaneously *verifying the forming* limit diagrams developed once again. The loading path used herein, for the preforming of the hollow-gear-shafts, is shown in Fig. 7.4. The loading path used in **Chapter 6** (Fig. 6.12) for the tube forming is also presented in Fig. 7.4, with a view to comparing the differences between their magnitudes.

7.3.2.2 Magnitudes of loading

After the injection punch slightly touched the tubular billet, an initial pressure (p_i) of 46.7MPa was applied onto the pressurising material, with a view to adding the extra stability to the compound tube, when pressurising punch was moved downwards from 0 to 15mm (L_i). During the first stage of the forming, the tubular billet was injected into the die cavity, for a length of 46mm (L_{o1}), at a speed of 10mm/min, with a view to quick supplying enough work material for the purpose of subsequent stage's (second stage's) die filling use. Simultaneously, the pressurising punch was moved downwards from 15mm to 19.13mm (L_{i1}) at a rate of 1mm/minute. A slow deformation rate was used herein, with a view to observing the deformation process and increasing the pressurisation levels, from the initial pressure level of 46.7MPa (p_i) to a pressure level of 271MPa (p_{i1}), at the end of the 1st stage of the forming, by which the collapse of the tube was prevented and the forming force was transmitted from the pressuresing punch to the work-material. During the second stage, the rate of the injection of the tubular billet was reduced from 10mm/min to 2mm/min, while the pressurisation rate was increased from 1mm/min to 5mm/min, with a view to facilitating and completing the final die filling. The lengths of the injected tube and the pressurising material (polymer rod), during the second stage, were (46+7.2=) 53.2mm (L_{o2}) and (19.13+14.87=) 34mm (L_{i2}), respectively, from which an increase of the pressure level from 343.3MPa (p_{o1}) to 523.5MPa (p_{o2}) for the tubular billet and an increase of the pressurisation level from 271MPa (p_{i1}) to 611MPa (p_{i2}) within the

pressurising material were achieved, by which the final die-filling, particularly for the tooth elements, was completed.

7.3.3 Forming experiments

Initially, forming dies, particularly the die with tooth elements, were lubricated with light oil (Mobile Vacuoline 1405). Then the tubular billet and polymer rod were well lubricated with the optimal lubrication scheme identified previously [14]. As shown in Fig. 3.6, after the specimen and the forming dies were assembled, the expected die cavity was firmly secured with eight 20mm diameter screw rods. Subsequently, forming of the hollow-gear-shaft was conducted, following the testing procedures described above. During the test, loads on both punches were applied, as the crosshead of the testing machine moved downwards. Simultaneously, the pressurisation was imposed with the hydraulic cylinder. As a result, each of the compound tubular specimens with a length of 160mm (Fig. 7.3 and Table 7.1) was deformed sufficiently into the hollow-gear-shaft, as shown in Fig. 7.5.

7.4 Results

Hollow-gear-shafts were achieved, following the procedures mentioned above, two of which are presented in Fig. 7.6. A plain, hollow flange formed is also presented with a view to effecting a comparison. The axial sectioned views of these components are also shown in Fig. 7.6 (b). The radial sectioned views of the gear-shafts formed are exhibited in Fig. 7.7.

7.5 Discussion

7.5.1 Overall evaluation on the components formed

7.5.1.1 General dimensional and defect check

The 12 teeth-hollow-gear-shafts are shown in Fig. 7.6. The hollow flange has an outer/top diameter of 60mm, root diameter of 50mm, an inner diameter of about 40mm and a height of 34.2mm, respectively (Figs. 7.6 and 7.8). The hollow shaft has an outer diameter of 35mm, inner diameter of 16mm and a length of 35mm approximately and respectively (Figs. 7.5 and 7.6). The geometrics of the components formed were achieved as expected. Also the overall check shows no defects, such as cracks, folding, weakened sections and chips within the components produced. This may verify that both, Solid Nitrile642 and Polyethylene, which were qualified previously (**Chapters 3** to **5**) as the most suitable pressurising materials for PAIF, can be used to form the hollow flanged components with secondary elements, i.e., the hollow-gear-shafts efficiently and economically.

7.5.1.2 General profile check

Profiles (sectioned) of the hollow-gear-shafts produced are shown in Figs. 7.6 and 7.7, from which it can be seen that, with Pressure-assisted injection forging, the profiles of the teeth (Fig.7.7) are clear, axial-symmetric and fully filled with the work-material. The hollow-gear-shafts also demonstrated the even pitch width and wall thickness etc. In other words, the hollow-gear-shafts were formed successfully using the designed procedures and dies with PAIF. It is, therefore, may be deduced that, when a forming die with the final teeth-form is used, the hollow-gear-shaft with the corresponding final teeth-form may be formed with PAIF, though it is not tested yet.

7.5.1.3 Forming load requirement

It was obtained that a total maximum forming force of about 493 kN was used to form the 12 teethed hollow-gear-shafts (Figs. 7.5 to 7.7) satisfactorily. Such a load level requirement using PAIF seems much lower than those using cold, warm even hot die forging of the similar components (a 12-teethed-bevel-gear, for example, was hot closed-die forged under a maximum load level of 700 kN [10] and a 27-teethed-spur-gear was warm closed-die forged under a maximum force level of 15000 kN [13] respectively). This may be the desired feature of the PAIF, namely, the combined movements between both the work- and the pressurising-materials may not only apply the loads to facilitate the deformation of the materials, but also transfer the forming environment, from the deformed material with solid mandrel [10, 13] to the deformed material with rubber like medium (PAIF). The maximum forming load was, therefore, reduced and the hollow-gear-shafts may, therefore, be formed more efficiently and economically.

7.5.2 Effect of the process parameters

As can be seen from Fig. 7.4, although the loading patterns for both, forming of the hollow-gear-shafts and forming of the plain, hollow flanges, were identical to that of the loading pattern 3 shown in Fig. 6.3, the loading magnitudes were different. For example, when an initial pressure (p_i) of 60MPa was required for the forming of the plain hollow flanges, a pressure of 47.6MPa was used for the forming of the hollow-gear-shafts; a 20.7% difference between these values existed. This was because of the reductions of the dimensions of the forming die (for the forming of the hollow-gear-shafts) from a diameter of 60mm (for the top diameter of the tooth elements) to a diameter of 50mm (for the root diameter of the tooth elements). The initial pressure of 47.6MPa was large enough to secure the stability of the compound tube for the forming of the hollow-gear-shafts. Similarly, during the first stage of the forming, a length of 46mm of the injected tube was required for the forming of the hollow-gear-shafts, while a 7mm extra length, which made up a length of 53mm, was needed for

the forming of the plain, hollow flanges. The pressurisation required at the end of this stage of the forming (hollow-gear-shaft) was 271MPa. It was higher than that for the forming of the plain, hollow flanges (261MPa). Such characteristics were, particularly, exhibited during the second stage of the forming. For instance, although a similar length, (about 7mm) of the injected tube was required for either the forming of the hollow-gear-shafts or the forming of the plain, hollow flanges, the pressurisation level for the forming of the hollow-gear-shafts was much higher (611MPa) than that for the forming of the plain, hollow flanges (471MPa). This may be due to the increased resistance and friction, resulted from the increase of the contact surfaces between the work-material and the forming die with tooth elements. A much higher pressurisation level was, therefore particularly, required to overcome the resistance and to complete the final die filling.

7.5.3 Effect of the pressurising materials

The experimental results also showed that the different pressurising materials performed differently during the forming of the hollow-gear-shafts. For instance, at the beginning of the forming, as the pressurising punch was moved downwards for a similar displacement (5mm), pressures of 56.87MPa and 53.36MPa were required for Polyethylene and Solid Nitrile642, respectively. The difference between these values was not significant, it might, however, reflect difference in material characteristics, i.e., the elastic modulus of Solid Nitrile642 is smaller than that of Polyethylene. The experimental results shown in Fig. 7.7 and Fig. 7.6 (b) also suggested that Solid Nitrile642 exhibited a better force transmission ability than Polyethylene did, particularly at the final stage of the die filling, since a better internal profile was formed with the Solid Nitrile642. For example, small arcs with a radius of 4.6mm were clearly formed with Solid Nitrile642 (Figs. 7.7 and 7.8), while the arcs were almost hardly to be seen with the inner profile formed with Polyethylene (Figs. 7.7 and 7.8). These might be because the Solid Nitrile642 functions better as a hydrostatic medium during the forming, particularly during the late stage. Such results also coincide with the research results shown in **Chapter 6**. This may indicate

that the specimen preparation, testing tools, procedures used in this study, and particularly, the forming-limit diagrams proposed in **Chapter 6**, are proved again to be reliable and applicable.

It is evident that although the geometry of the hollow-gear-shaft is somewhat more complex than those of the plain, hollow flange, as compared in Fig. 7.6 (a), the forming procedure for the forming of the hollow-gear-shaft was as simple as those used in the forming of the plain, hollow flanges. For example, the identical loading patterns (Fig. 7.4) and a single stroke, were used for both. The results may also verify that, with PAIF, the integral, hollow-gear-shafts can be formed with a single stroke, rather than the conventional multiple processes. In conventional manufacture, i.e., the gear and the shaft normally are manufactured separately, then these parts may be assembled together, with the subsequent welding or key way processes. Obviously, with PAIF, a hollow-gear-shaft may be produced in such a manner that the material waste can be reduced, the subsequent assembly processes can be eliminated, and the manufacturing cost can, therefore, be reduced.

The research conducted so far has only addressed the forming of a simplified hollow-gear-shaft. Further efforts will need to be made in the forming of the hollow-gear-shafts with certain levels of precision. Particularly, efforts should also be devoted to the FE simulation of the process with a view to verifying the experimental results as well as optimizing the processing parameters.

7.6. Conclusions

From the exercises in the preforming of the hollow-gear-shafts with Pressure-assisted injection forging, following conclusions may be drawn:

(1) Hollow-gear-shafts have been produced successfully by means of the PAIF with the selected pressurising materials.

(2) A much higher pressurisation is needed at the final stage of the forming of the hollow-gear-shafts.

(3) Solid Nitrile642 functioned better as a pressurisng medium for PAIF of the hollow-gear-shafts than Polyethylene did.

(4) Further efforts are needed in achieving higher precision of the components, which needs substantial reduction of the forming pressure at the final stages.

(5) Ejection of the component after the completion of the forming of the hollow-gear-shafts is also needed to be considered. A special arrangement should be given to this type of components.

7.7 References

[1] S. Kalpakjian and S. R. Shmid, "Manufacturing Processes for Engineering Materials", Fourth Edition, Prentice Hall, 2003, pp. 480-481.

[2] B.I. Tomov and V.I. Gagov, "Modelling and description of the near-net-shape forging of cylindrical spur gears", Journal of Materials Processing Technology, Vol. 92-93, 1999, pp 444 – 449.

[3] Y.K. Lee, S.R. Lee, C.H. Lee and D.Y. Yang, "Process modification of bevel gear forging using three-dimentional finite element analysis", Journal of Materials Processing Technology, Vol. 113 2001, pp. 59 –63.

[4] T.A. Dean, "Concepts and practice in precision forging", Proc. 7th Int. cold Forging Cong., Birmingham. UK, 1985, pp15-23.

[5] K. Kondo, "Developments of new precision cold die forging processes", Proc. Advanced Technology of Plasticity Conf., Tokyo, Japan, Vol. 2, 1984, pp. 878-887.

[6] T. Nakano, "Modern applications of complex forming and multi-action forming in cold forging", Journal of Materials Processing Technology, Vol. 46, 1994, pp. 201 –226.

[7] J. A. Pale, " Recent developments in tooling, machines and research in cold forming of complex parts", Journal of Materials Processing Technology, Vol. 33 1992, pp. 1 –29.

[8] R. Geiger, "State of the art and development trends in cold forging technology", Proc. of the 2nd ICTP, 1987, pp. 469-477.

[9] R. Geiger, K. H. A. GmbH, M. Hansel and P. Stanzwerk AG, "Form near-net-shape to net-shape cold forging – state of the art", Proc., 9th Intern. Cold Forging Congress, Solihull, UK, 22-26 May, 1995, pp. 59-75.

[10] A. G. Mamalis, D. E. Manolakos and A. K. Baldoukas, "Simulation of the precision forging of bevel gears using implicit and explicit FE techniques", Journal of Materials Processing Technology, Vol. 57, 1996, pp. 164 – 171.

[11] E. Doege and B.-A. Behrens, "Reduce process chains due to the precision forging of gears-effect on the conventional forging technology", Journal of Materials Processing Technology, Vol. 71, 1997, pp 14–17.

[12] J. S. Song and Y. T. Im, "Development of a computer-aided-design system of cold forward extrusion of a spur gear", Journal of Materials Processing Technology, Vol. xxx, 2004, pp xxx– xxx (article in press).

[13] J. Cai, T. A. Dean and Z. M. Hu, "Alternative die designs in net-shape forging of gears", Journal of Materials Processing Technology, Vol. xxx, 2004, pp xxx– xxx (article in press).

[14] Y. Qin and R. Balendra, "Optimisation of the lubrication for the extrusion of solid and tubular components by Injection Forging", Journal of Materials Processing Technology, Vol. 135/2-3 2003, pp 219 – 227.

Table. 7.1 Material geometries for the forming of the gear-shafts

Pressurising material No.	Pressurising materials		Work materials(Aluminium)		
	Names of polymer rods	Diameter d_r (mm)	Inner diameter d_i (mm)	Outer diameter d_o (mm)	Height (mm)
1	Polyethylene/HDPE	16.04	16.12	35	160
2	Solid Nitrile642	16.00	16.08	35	160

Chapter 8

Suggestions to the Future Work

In this chapter, after the achievement from the research is summarised in **Section 8.1**, suggestions for the future work, regarding process configuration development, forming equipment development, design/analysis-related issues as well as engineering-application related issues, are given in **Section 8.2**.

8.1 Summary of the Achievement from the Research

Possible pressurising materials (P-Ms) for pressure-assisted injection forging (PAIF) were tested under confined compression conditions, for which a simplified configuration was proposed and used effectively. Solid Nitrile642 and Polyethylene were identified to be the best P-Ms, among the available materials. The identified P-Ms for PAIF were further qualified under five loading conditions, namely, uniaxial tension, uniaxial compression, planar tension, planar compression and biaxial tension. For the purpose of carrying out the biaxial tension tests, a unique biaxial tension test machine was developed and used successfully. In order to produce a simple and efficient tool for industrial application of PAIF technology, an upper bound analysis of pressure-assisted injection forging of thick-walled tubular components with hollow flanges was conducted and an upper bound solution for PAIF was derived, by which maximum forming-force requirements for different specimen geometries, component geometries and friction conditions were predicted, with sufficient accuracy (less than 5% difference between the predicted values and the experimental values). With reference to different loading paths and aspect ratios, failure modes for pressure-assisted injection forging of thick-walled tubular components were observed either experimentally or computationally, based on which, eight failure forms were classified and three forming limit diagrams were established. Using the developed knowledge and technologies, including upper bound solution, forming limit diagrams, the approach for synthesising concurrent design and manufacture etc., an engineering component – hollow gear shaft, was produced satisfactorily.

8.2 Suggestions for Future Work

Although significant progresses have been made in the development of the pressure-assisted injection forging technology, further work needs to be done subsequently on the following aspects.

8.2.1 Process configuration development

Most of the existing process configurations of injection forging either solid billets or tubular billets have only been used to produce symmetric components, including the ones rotationally-symmetrical or symmetrical about a face, with success. More efforts should, therefore, be devoted to the development of process configurations of injection forging of asymmetrical and more complex components, such as cam-shaft and multi-branches at different stages/levels, at a reduced forming force requirement, reduced number of operations and therefore a reduced cost, which may be achieved by the combination of injection forging with other metal forming processes, or by different die designs/arrangements and different die movements.

8.2.2 Forming equipment development

To facilitate the development of the proposed technology – Pressure-assisted injection forging, apart from three sets of forming tools (Fig. 3.7) developed and used in the forming of thick-walled hollow flanges, a unique biaxial testing machine was particularly developed (Fig. 4.21) for the qualification of the mechanical properties of the pressurising materials, under biaxial tensile loading condition effectively. More efforts, however, need to be made to explore the potential applications of the machine. Namely, by modifying the existing clamps, biaxial compression tests on the materials, and particularly, the biaxial tension of the thin sheet metal materials may be carried out for the purpose of further research use.

8.2.3 Design/analysis-related issues

8.2.3.1 Selection and qualification of the pressurising materials

To date, more than 7 types of polymers were initially examined under confined compression conditions, using the simplified configuration (Fig. 3.8). Pure aluminium (E1CM) was also tested using an identical tube forming procedure for

their feasibility and suitability, as a pressurising medium for PAIF application. As a result, the best P-Ms were identified from the available materials. A material, which is able to fully recover to its original shape from its final deformed state after unloading, would be an ideal pressurising medium for PAIF application and has not been found yet. How such types of materials may behave during PAIF of thick-walled tubular components was not known yet. More attention should, therefore, be paid to find and to test these materials, if they were available, in a rod form, from the market. The testing (for further involved P-Ms) should include not only the initial tests, but also the qualification under different loading conditions, with a view to providing supporting information for process design and optimisation, since the pressurising materials, which were identified to be "optimal" for the PAIF application in this study, only represent the relatively optimal solutions, among the currently available pressurising materials.

8.2.3.2 Process ranges and forming limit diagrams

Process ranges, of injection forging of solid billets and the injection forging of tubular billets with the support of mandrel, were well defined and extended, using either a pre-from design procedure for injection forging of solid billets (Fig. 2.20) or a procedure developed to extend the effective aspect ratio of injection forging of tubular billet with mandrel (Fig. 2.21) significantly. Failure modes and process ranges for PAIF of thick-walled tubular components were investigated and three forming limit diagrams were developed recently, with reference to different loading paths, different aspect ratios and different pressurising materials. More experimental and FE simulation work should be carried out, with a view to further validating the forming limit diagrams, and to extending the process ranges, as well as improving the quality of the components produced.

8.2.3.3 Forming of engineering components

Numerous engineering components were produced using injection forging either solid billets or tubular billets successfully. Thick-walled tubular components with hollow flanges were subsequently attempted with PAIF. The latest achievement of PAIF of engineering components, is the preform of a hollow-gear-shaft satisfactorily (Figs. 7.5 and 7.6). More efforts should be made to form the hollow-gear-shafts with certain level of precision. Attention should also be paid to reduce the final die filling force requirement and to eject the component out of the forming die easily, for which new designs or devices may be needed.

8.2.3.4 Process modelling

In order to provide more reliable supporting information for process design and analysis, both numerical and physical process modelling techniques should progress further to be able to model more complex component forms, for instance the hollow-gear-shafts.

8.2.4 Other research and engineering-application related issues

8.2.4.1 Approach for synthesising concurrent design and manufacture

Development of the approach for synthesising concurrent design and manufacture of thick-walled tubular components with PAIF (Fig. 3.22), is a significant progress towards the engineering-application of the technology developed. More details, however, need to be defined for this approach.

8.2.4.2 Dissemination and exploitation

Concept of PAIF of thick-walled tubular components and some of the research results (such as simplified configuration for confined compression test, clamping

design for biaxial tension of rubbers, process range definition of PAIF tubular components and the approach for synthesising concurrent design and manufacture of thick-walled tubular components with PAIF) from this study, have already been presented at international conferences. Further promotion of the technology to be applied to industry should be continued. Efforts should also be made to produce a brochure, providing an overview of the theory and application prospects of PAIF. A seminar, disseminating and exploitating the technology to industry should also be organised shortly.